Study of the Instability and Dynamics of Detonation Waves using Fickett's Analogue to the Reactive Euler Equations

by

Justin Tang

Thesis submitted to the
Faculty of Graduate and Postdoctoral Studies
In partial fulfillment of the requirements
For the M.A.Sc. degree in
Mechanical Engineering

The Ottawa-Carleton Institute for Mechanical and Aerospace Engineering
Faculty of Engineering
University of Ottawa

Abstract

The instability behaviour of detonation waves are studied using Fickett's model with a 2-step reaction model with separately controlled induction and reaction zones. This model acts as a simplified toy-model to the reactive Euler equations allowing for more clarity of the detonation phenomenon.

We numerically simulate a 1D self-supported detonation and investigate the pulsating instability behaviour. We are able to clarify the governing mechanism behind the pulsations through a characteristic analysis describing the coupling that takes place between the amplification of the compressions waves and the alteration to the induction timing. We examine the acceleration phase of the pulsations and determine an analytical solution to describe the strength of the amplification. Fickett's model is as well shown to reproduce the same period doubling bifurcation with increasing sensitivity of the induction rate, and route to chaos as seen in the full reactive Euler equations.

Acknowledgements

NSERC and H2CAN sponsorship was much appreciated. The time, finances, effort, and guidance provided by research supervisor Dr. Radulescu were of immeasurable assistance and he has my sincere gratitude.

I would also like to thank my colleagues from the Detonation & Reactive Dynamics Laboratory at the University of Ottawa for their assistance and cooperation.

Finally I'd like to thank my friends and family for their support and goodwill.

Contents

List of Figures

Nomenclature

Latin Letters:

a: Acceleration of the path of the onset of reaction.

D_{CJ}: The Chapman-Jouguet (CJ) detonation velocity.

$H()$: The Heaviside function.

$\tilde{K}$: Nondimensional constant representing the ratio of induction to reaction times.

K_i: Induction rate constant.

K_r: Reaction rate constant.

p: Pressure analogue used in the model.

Q: Heat release parameter.

$\tilde{Q}$: Nondimensional Heat release parameter.

r: Reaction rate.

t: Time variable.

$\tilde{t}$: Nondimensionalized time variable.

$t^*(x)$: Path of the onset of the reaction. zone

x: Position following a fluid element.

$\tilde{x}$: Nondimensionalized position following a fluid element.

Greek Letters:

α: The induction reaction rate sensitivity parameter.

$\tilde{\epsilon}$: The inverse activation energy

ρ: Density analogue used in the model.

$\tilde{\rho}$: Nondimensional density analogue used in the model.

ρ_{CJ}: A constant representing the density for the Chapman-Jouguet case.

$\rho_{s,CJ}$: A constant representing the shock front density for the Chapman-Jouguet case.

λ_i : The progress variable for the induction zone which ranges from 1 to 0 marking the onset of reaction.

λ_r : The progress variable for the reaction zone which ranges from 0 (unreacted) to 1 (completely reacted).

ν: Reaction order.

ζ: Position coordinate in steady Chapman-Jouguet detonation frame.

Chapter 1

Introduction

The focus of this work is to clarify the instability mechanism of pulsating detonations. The dynamics of detonation waves in 1D are modeled using Fickett's mathematical model, which serves as a simplified model to the 1D reactive Euler equations. The model is augmented by a 2-step induction-reaction model for the material decomposition. The mechanisms controlling the pulsating instability and transient behaviour of detonations are clarified using this simplified model.

1.1 Study of detonations

Detonation waves are self-sustained supersonic reaction waves. While deflagrations rely on heat and mass diffusion for their propagation, detonations rely on compression wave dynamics. It is the coupling of the chemical energy release and the resulting compression or expansion waves that is the main mechanism behind detonation propagation. The basic detonation structure is composed of a front shock followed closely by a zone of reacting material as seen in Fig. 1.1.

Detonation propagation and behaviour has been the subject of study for many years. Fickett & Davis (2000) provides a good overview of the detonation theory and experimentation. Lee (2008) provides an overview of the dynamics of unstable detonation waves one encounters in gaseous media. Detonations can be sustained in various media, such as: reactive gases (Shepherd, 2012), explosives or energetic materials in condensed form (Bdzil & Stewart, 2007), the combustion of dust particles in air (Zhang, 2009), and in thermonuclear reactions (as in the astrophysical phenomenon of supernovae (Fickett, 1979)). The study of detonations are thus of interest in many different applications, such as for propulsion applications and in industrial safety where the large forces that are generated

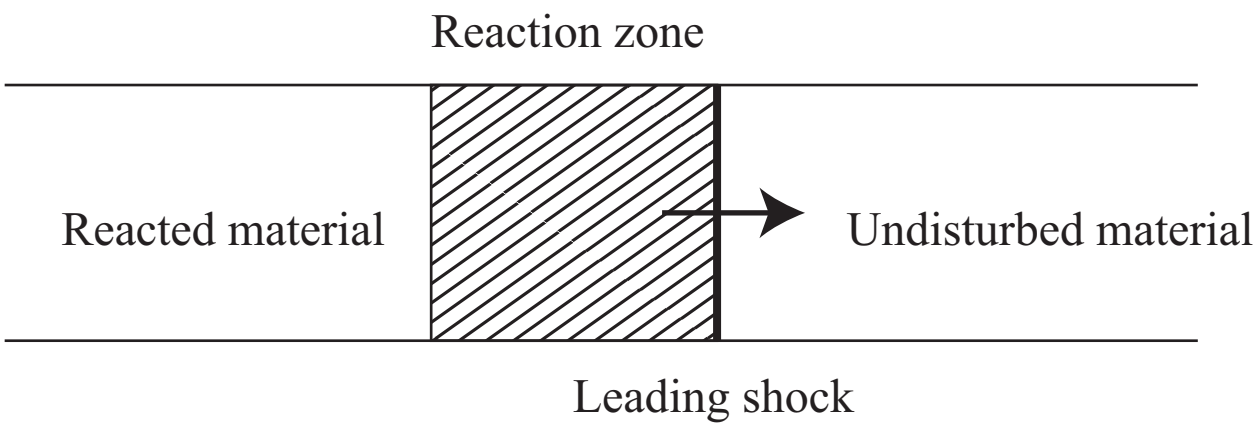

Figure 1.1: Sketch of 1D detonation structure.

by detonations can cause damage. Detonation theory can as well be used to model other self-sustained wave propagation phenomena such as traffic jams (Flynn *et al.*, 2009) or shallow water waves (Kasimov, 2008).

The study of detonations is complicated by the fact that they are such a highly unstable phenomenon. The coupling of the gas dynamics and reactive dynamics behind detonation propagation are not well understood. The equations governing detonation behaviour are also complex, making the main dynamics and mechanism of propagation difficult to describe. It is thus our aim to explore and improve the understanding of unstable detonation waves.

1.2 Detonation structure

The existence of a steady detonation wave solution has been posed, which has led to more insight into the propagation mechanism of detonations (Chapman, 1889; Jouguet, 1904, 1905). The detonation velocity can be predicted through the conservation laws and thermodynamic properties. The minimum admissible wave velocity is known as the Chapman-Jouguet (CJ) condition. The CJ condition requires that a sonic surface exist behind the detonation preventing it from being affected by following perturbations and allowing it to propagate undisturbed. This formulation requires treating the whole detonation shock and reaction zone structure as a whole unit and does not take into account the internal reaction kinetics. A description of the internal structure of a detonation in 1D has been postulated by Zel'dovich, von Neumann, and Dowering (ZND) to follow that of a lead shock front sustained by a trailing finite chemical reaction zone (Fickett & Davis, 2000). It is the internal coupling of the reaction chemistry and the compression wave hy-

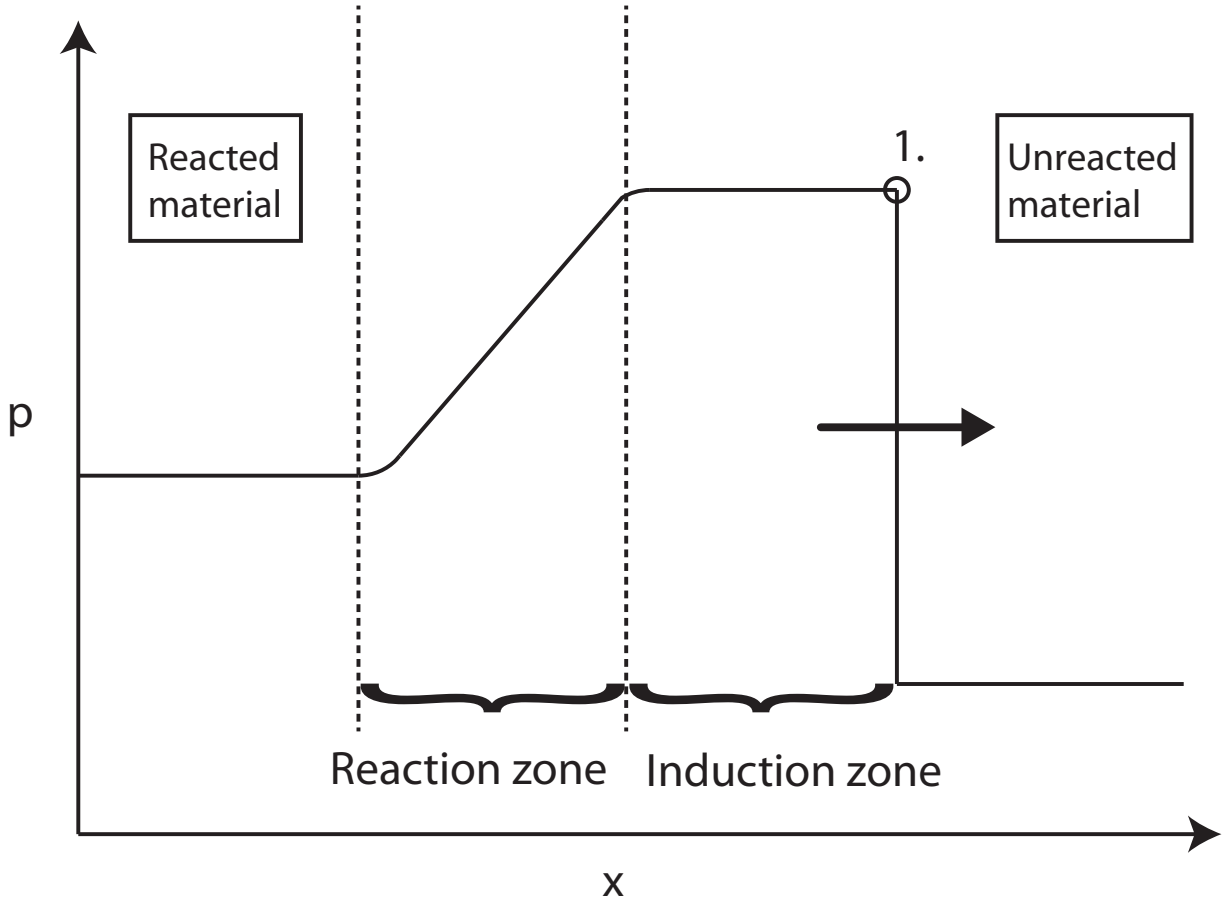

Figure 1.2: A description of the ZND detonation profile showing the variation in pressure over position across the detonation. The circled point 1 is the von Neumann state which is located just after the front shock before the reactions begin.

drodynamics which describes detonation propagation. This coupling is the focus of study in the present thesis, with a particular emphasis on cases where this structure is unstable and prone to periodic or chaotic oscillations (Ng *et al.*, 2005*a*).

The ZND structure is headed by a shock front which initiates the chemical reaction. After the shock there is a period of slow reaction known as the "induction zone" in which there is little heat release. This period is followed by a rapid acceleration of the reaction rates to their completion known as the "reaction zone" where the bulk of the exothermicity occurs. A sketch of the steady ZND structure is shown in Fig. 1.2 showing the pressure profile across a detonation propagating to the right.

1.3 Detonation instability

Detonations are a very unstable and complex phenomenon. Even so, they have been shown to exhibit certain regular behaviour. When studied experimentally in two or three dimensions, detonations have been shown to admit multiscale cellular patterns formed from transverse wave interactions (Fickett, 1979). A characteristic dominant dimension of these cells, known as the cell size, has been used to characterize the detonability of a given mixture (Lee, 1984).

Detonation instability has as well been studied numerically using the Euler equations, which are the inviscid form of the Navier-Stokes equations for fluid flow, with added reaction. As detonations travel supersonically, viscous forces become negligible, and the main dynamics are described through the compression wave hydrodynamics coupled with the chemical energy release of the reactions. This makes the reactive Euler equations an appropriate system to study detonation behaviour. In 1D numerical simulations, detonations have been shown to admit a behaviour in which the detonation front regularly oscillates. The 1D unstable detonation behaviour is characterized by the whole detonation structure regularly accelerating and decelerating, and is known as a pulsating instability (Edwards & Morgan, 1977), which is the focus of the present thesis.

The stability of detonations has been shown to be closely controlled by the reaction parameters governing the chemical energy release (Sharpe & Falle, 2000). A pulsating instability develops from a stable solution after a threshold value is reached in the activation energy (E_a), a parameter that controls the sensitivity of the induction rate to temperature. The activation energy basically alters how closely linked the induction time (t_i) is to changes to temperature following: $t_i \propto e^{E_a/RT}$ (with R the gas constant, and T temperature). Further studies have shown that a range of dynamical states occur beyond the single period oscillation cycle (Short & Sharpe, 2003; Ng *et al.*, 2005*a*; Henrick *et al.*, 2006). The 1D pulsation behaviour can be shown by tracking the pressure at the von Neumann point (Fig. 1.2) with time. The pressure oscillation cycles for a range of activation energies are shown in Fig. 1.3. The different oscillation modes are shown, in which an increase in the activation energy causes the period of oscillation to regularly double. This regular period-doubling behaviour can be plotted with increasing activation energy in a bifurcation diagram. Figure 1.4 shows such a bifurcation diagram, generated numerically from the 1D reactive Euler equations, with the activation energy plotted against D_{max}, the peak amplitude/s of each oscillation cycle; these peaks are indicated in Fig. 1.3 by the dashed lines. In the bifurcation diagram (Fig. 1.4) we can see that for low activation energy we have a stable solution, but at a certain activation energy the solution becomes

oscillatory. With increasing activation energy D_{max} increases, signifying an increase in the oscillation amplitude. Then, at certain activation energies, the period of oscillation doubles and we can see a split, or bifurcation, in the D_{max} representing the two peaked oscillation cycle. These period doubling bifurcations are seen to occur regularly at increasingly smaller intervals of the activation energy, and then transition into a chaotic solution where there is no longer a set period of oscillation. This bifurcation sequence follows Feigenbaum's scaling, a phenomenon shared by other simpler nonlinear systems (Feigenbaum, 1983) such as the logistic map, demonstrating the universality in the wave dynamics found in detonations. Though this pulsation behaviour is well documented (Sharpe & Falle, 2000; Short & Sharpe, 2003; Ng *et al.*, 2005*a*,*b*; Leung *et al.*, 2010), a clear description of the evolution and dynamics of the instability has been difficult due to the nonlinearity of the system. The mechanisms governing the pulsating instability are also unclear.

Along with the activation energy E_a, the ratio of induction to reaction time has been identified to play a large role in governing detonation dynamics (Sharpe & Short, 2003). The induction time to reaction time ratio controls the energy release period compared with the induction delay period. Increasing values of this ratio have been correlated with larger instability in detonations (Ng *et al.*, 2005*b*). Together, both the activation energy and ratio of induction to reaction time have been seen to have a coherent effect on the 1D pulsation dynamics of detonations (Short & Sharpe, 2003; Ng *et al.*, 2005*b*; Leung *et al.*, 2010). They have been posed as the product of the ratio of the induction to reaction time $\frac{t_i}{t_r}$ and the nondimensional activation energy $\frac{E_a}{RT}$. Though these factors have been seen to affect detonation instability, the complexity of the Euler equations used to study this problem has made it difficult to get a clear description of the exact mechanism at work behind the controlling effect of these parameters. We address this problem using a simpler analogue to the Euler equations.

1.4 Fickett's model

To study the 1D instability of detonations we have applied Wildon Fickett's detonation analogue as a simplified toy model of the 1D reactive Euler equations in order to allow for a more transparent description of the physics and dynamics of unstable detonation behaviour.

Fickett constructed a simple model, similar in form to the inviscid Burgers' equation for wave propagation, as a mathematical analog to the reactive Euler equations. Fickett's model is seen to admit shocks and rarefactions and can also describe detonation behaviour.

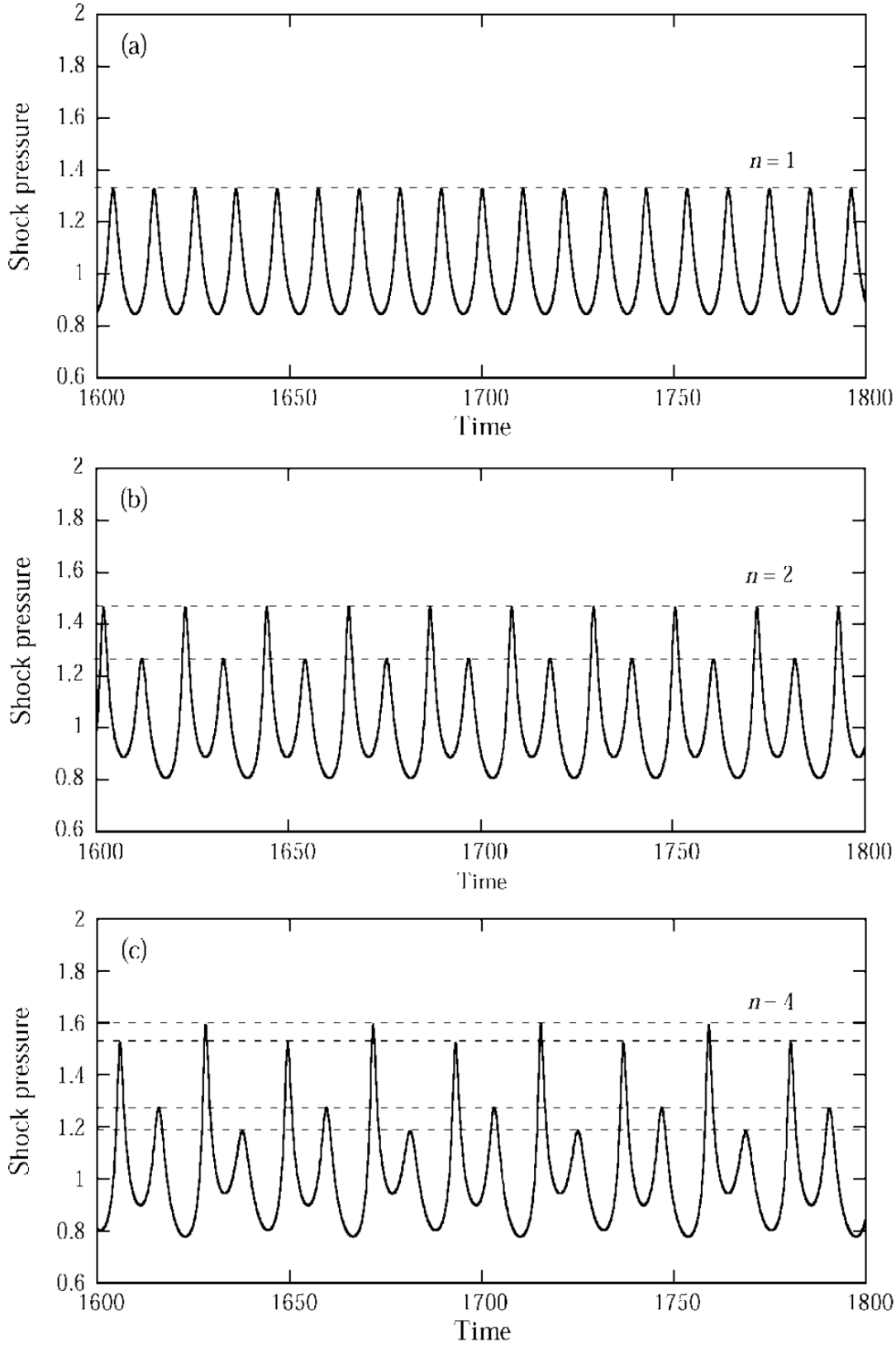

Figure 1.3: Front shock pressure history showing different modes of oscillation for varying activation energies: (a) $E_a = 27.00$; (b) $E_a = 27.40$; (c) $E_a = 27.80$. (Taken from Ng *et al.* (2005*a*)).

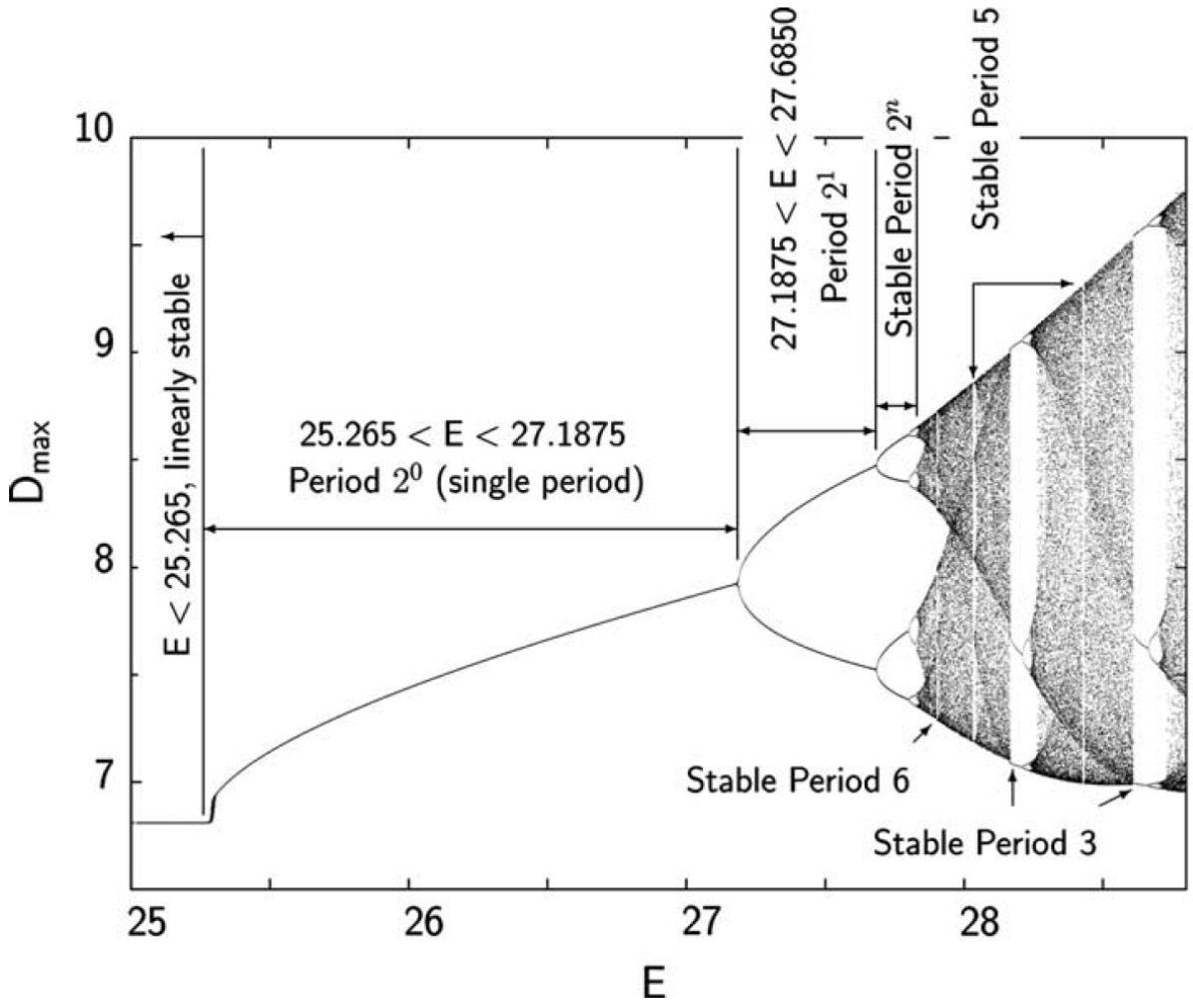

Figure 1.4: Bifurcation diagram for 1D detonation behaviour using the Euler equations with a 5th order accurate numerical modeling scheme, plotting peak detonation strength (D_{max}) with activation energy (E), taken from Henrick *et al.* (2006). A stable, as well as multiple unstable oscillatory solutions are described.

It is able to qualitatively reproduce many traits and dynamics of chemical detonations, such as the structure of the stable self-sustained wave, initiation transients, and response to boundary loss (Fickett, 1979, 1985a).

In the past, Fickett's model has been used as a tool to describe the stable behaviour of detonations. It was only in 1985 that Fickett addressed the stability of the traveling wave solution through the use of a square wave reaction model (Fickett, 1985b). In the square wave model the reaction zone that trails behind the shock front in a detonation is represented by a finite induction delay time followed by instantaneous heat release (Fickett, 1985b). For the duration of the induction delay there is no heat release, representing the initial slower exothermicity period in real reactions, after which all the energy release occurs at once. In this study Fickett was able to show the existence of an unstable solution both analytically and numerically using his simplified model. Detonation instability in Fickett's model was further explored by Hall & Ludford (1987) where they used a generalized reaction model, which had a finite gradual heat release, and from which the square wave model could be recovered as a limiting case. They were able to predict instability through a linear stability analysis and characterize the stability boundary point with one of their reaction parameters.

We continue to explore detonation instability through Fickett's model using a characteristic analysis. While the reactive Euler equations admit three characteristic paths, the simpler model developed by Fickett has only two families of characteristics (Fig. 1.5). This allows us to describe the system dynamics in terms of the forward C+ pressure wave characteristics and the particle path characteristics, along which the chemical reaction proceeds. Together, it is the coupling of the pressure waves amplifying through the reaction zone and their effect on the reaction rates along the particle paths which describes the detonation dynamics. The reduction to a two characteristic system gives us a more transparent depiction of the interaction between the hydrodynamics and chemical kinetics.

1.5 Present study

In the present thesis we seek to clarify the 1D detonation instability. Our approach to this problem is to investigate the detonation dynamics from a sufficiently simple standpoint in order to clearly demonstrate the governing mechanisms behind the detonation behaviour. We thus choose to use Fickett's model in order to clarify detonation instability.

We modify the original square wave Fickett model by assuming a 2-step induction-reaction model, which has finite independently controlled induction and reaction phases. In the 2-step model a zero heat release induction delay time is initiated by the front

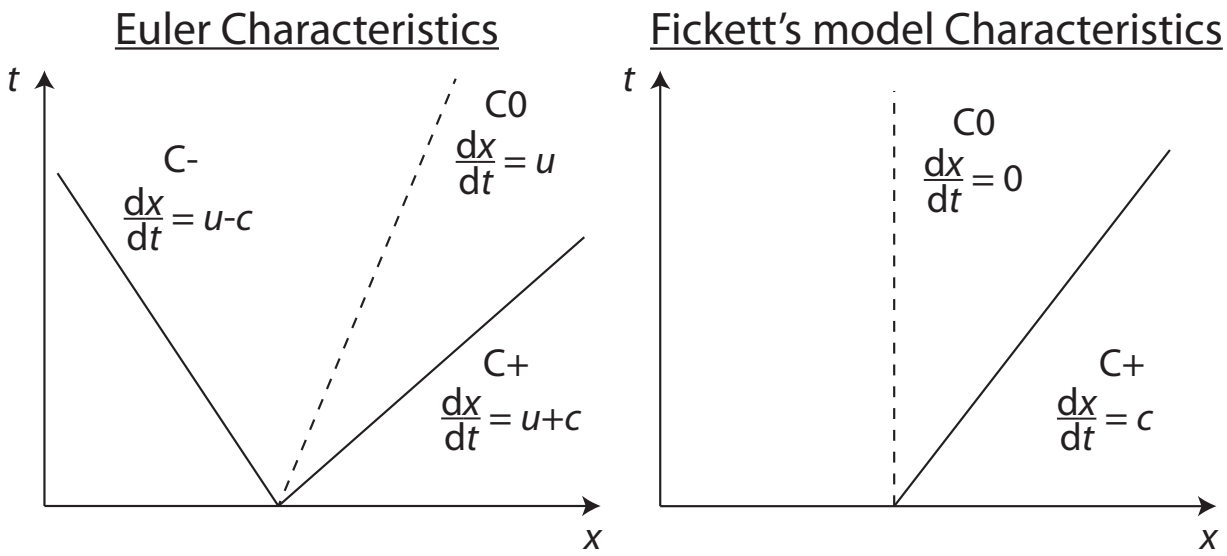

Figure 1.5: Sketch of the characteristics admitted by the Euler equations and Fickett's model.

shock, after which the energy release occurs over a finite amount of time. The induction delay duration in the 2-step model depends on the strength of the shock, which is an excellent assumption for activated chemical reactions (Fickett & Davis, 2000). The finite reaction zone of this model resolves the singularity which occurs in the square wave model, which had an instantaneous heat release (Fickett, 1985*b*). The 2-step model also allows us to independently control each reaction period and investigate the effect of the ratio of the induction time to the reaction time, and of changing the sensitivity of the induction reaction rate. Previously the 2-step model has been useful in studying 1D detonation instability (Ng *et al.*, 2005*b*; Short & Sharpe, 2003). Leung *et al.* (2010) were able to gain insight into the pulsating instability through a characteristic analysis using the reactive Euler equations and 2-step reaction model. We continue to explore the 1D pulsating behaviour using characteristic analysis from the simpler framework of Fickett's model with the 2-step induction-reaction model. We investigate the onset of instability, the period doubling bifurcation behaviour, as well as the instability mechanism driving the 1D pulsations.

The layout of the present thesis is organized as follows. Chapter 2 is a description of Fickett's model, which we use to model detonation behaviour. We detail the governing equations, the characteristics, our reaction model, and the main dynamics seen in Fickett's model. Chapter 3 outlines the numerical technique used to obtain the transient solutions of the proposed model. In Chapter 4 we investigate the 1D pulsating instability behaviour of detonations. We identify the onset of instability as controlled by our reac-

tion parameters α, the sensitivity of the induction rate, and $\tilde{K}$, the ratio of induction to reaction time. We then describe the governing mechanism behind the unstable pulsation behaviour through a characteristic analysis. In Chapter 5 we investigate the transient pulsation dynamics. We study the acceleration phase amplification through modeling a piston-induced shock initiated detonation. The shock initiation problem demonstrates the same amplifying process as in the acceleration phase during the pulsations. We investigate the effect of the ratio of induction to reaction times ($\tilde{K}$) and the inverse activation energy ($\tilde{\epsilon}$) on the amplification process and detonation dynamics. We then analytically identify the relation governing the amplification process. In Chapter 6 we examine the various modes of oscillation our model admits, and determine whether our model shares the same period-doubling bifurcation route to chaos behaviour seen in the 1D Euler equations. We identify the series of even-numbered period doubling bifurcation modes, and identify an odd numbered period-three mode signifying the transition to chaos (Ng *et al.*, 2005*a*). We build a bifurcation diagram of the resulting peak shock strength during oscillation with increasing sensitivity of the induction rate, and compare it with the same diagram captured using the Euler equations. We identify the galloping mode of instability, characterized by the formation of internal shocks, as well as a quenching behaviour, in which the reactions are seen to decouple from the shock front leaving an inert piston-supported shock. Chapter 7 is a discussion of our results and the significance of our findings. Chapter 8 is our conclusion and summary of our findings along with future areas of study. Parts of the results and analysis available in Chapters 4, 5 and 6 have already appeared in the literature: Radulescu & Tang (2011) and Tang & Radulescu (2012).

Chapter 2

Extension to Fickett's Model

2.1 Main dynamics of Fickett's model

In our study we use Wildon Fickett's detonation analogue. Fickett's analogue is a simple mathematical model, which shares many of the same dynamics as the reactive Euler equation for fluid flow and can be applied to study detonation behaviour. One of the key simplifications of Fickett's model is that its characteristic form, which describes the fluid dynamics in terms of wave dynamics, is reduced when compared with the Euler equations.

The reactive Euler equations can describe fluid flow by the interaction of its three families of characteristics: the particle path or entropy wave (C0), the forward (C+) and backwards (C-) waves (Fig. 1.5). The particle paths travel at the fluid velocity following a fluid element and along which the chemical reaction proceeds. The forward and backwards wave paths travel at the fluid velocity plus or minus the speed of sound, and become amplified by the chemical reaction occurring along the particle paths. Through the characteristics, the dynamics of the system can be described through the interaction between the hydrodynamic waves motion and the energy release occurring along the particle paths. However, the Euler equations are highly nonlinear and the dynamics are difficult to describe in a clear and concise manner. Fickett's model, which does not include backwards characteristics, reduces the system enough to allow for a more transparent description of the mechanisms governing the detonation process.

2.2 Governing Equations

The system described by Fickett's model has many of the same properties as the reactive Euler equations but its form is significantly simpler. It follows the form of the inviscid

Burgers' equation for wave propagation (Whitham, 1974), but with an added amplification term for the energy releasing reaction process. The inviscid Burgers' equation ($\frac{\partial u}{\partial t} + u\frac{\partial u}{\partial x} = 0$) allows for wave propagation like the generic advection equation, but the wave speed is dependent on the state of the material (u) instead of being constant. This allows for the formation of shock wave solutions. Fickett's model describes 1D inviscid reactive compressible flow in the Lagrangian frame of reference (Fickett, 1985*b*). Shown below are the conservation equation (Equation 2.1), the equation of state (Equation 2.2), and the reaction rate equation (Equation 2.3):

$$\frac{\partial \rho}{\partial t} + \frac{\partial p}{\partial x} = 0 \tag{2.1}$$

$$p = \frac{1}{2}\left(\rho^2 + \lambda_r Q\right) \tag{2.2}$$

$$\frac{\partial \lambda}{\partial t} = r(\rho, \lambda) \tag{2.3}$$

where x is the Lagrangian material coordinate, t is the time, ρ represents density in our model, p has the meaning of pressure, λ is a reaction progress variable tracking the completion of the reaction, and Q is the heat release parameter representing the available energy in the excitable material (Fickett, 1979, 1985*b*). The equation of state applied here (Equation 2.2) is a generic formulation proposed by Fickett and chosen for simplicity. It demonstrates how pressure increases with density, or with the release of energy due to the reaction. The reaction rate equation (Equation 2.3) describes the progress of the energy release along each particle with Lagrangian coordinate x, and is dependent on the current progress of the reaction and the local density.

2.3 Characteristics

As the governing equations for our analogue are hyperbolic and admit a traveling wave solution, they can be solved in characteristic form. The use of characteristics allows us to solve the system of partial differential equations (PDE's) by expressing them as ordinary differential equations (ODE's) along certain paths. This simplifies the system and is useful in the study of wave propagation as the characteristic paths describe the motion and amplification of waves by the chemical reaction. Fickett's model has the advantage of being described by the interactions between only two characteristics paths, the C+ forward wave characteristics and the particle path characteristics.

The characteristics for Fickett's model can be developed by inspection following a form similar to the characteristics for the reactive Euler equations in Lagrangian form.

First, by combining the conservation equation (Equation 2.1) and equation of state (Equation 2.2), we find that we recover the inviscid Burgers' equation with an amplification term appearing on the right-hand-side:

$$\frac{\partial \rho}{\partial t} + \rho \frac{\partial \rho}{\partial x} = -\frac{1}{2} Q \frac{\partial \lambda_r}{\partial x} \tag{2.4}$$

We notice that the left-hand-side of Equation 2.4 becomes the total derivative of density with time ($\frac{d\rho}{dt} = \frac{\partial \rho}{\partial t} + \frac{dx}{dt}\frac{\partial \rho}{\partial x}$) along the characteristic curve given by $\frac{dx}{dt} = \rho$. Along this characteristic, Equation 2.4 becomes:

$$\frac{d\rho}{dt} = -\frac{1}{2} Q \frac{\partial \lambda_r}{\partial x} \tag{2.5}$$

We can rewrite this in terms of pressure and the reaction rate by rearranging the terms and using Equations 2.2 and 2.3.

$$\frac{dp}{dt} = \frac{1}{2} r Q \tag{2.6}$$

So along lines of $\frac{dx}{dt} = \rho$ we have pressure vary based on the reaction rate r and heat of release Q. This is the first family of characteristics, where compression and expansion waves propagating through the material are amplified according to Equation 2.6.

The second family of characteristics, the particle paths, are found from the reaction rate equation (Equation 2.3). As we are in the Lagrangian frame of reference, we have stationary particle paths of $\frac{dx}{dt} = 0$. Along these particle paths the partial derivative with time becomes a total derivative. Thus along $\frac{dx}{dt} = 0$ we have:

$$\frac{d\lambda}{dt} = r \tag{2.7}$$

In summary, the two characteristic paths for Fickett's model are:

$$\frac{dp}{dt} = \frac{1}{2} r Q \quad \text{along} \quad \frac{dx}{dt} = \rho \tag{2.8}$$

$$\frac{d\lambda}{dt} = r \quad \text{along} \quad \frac{dx}{dt} = 0 \tag{2.9}$$

The C+ forward wave characteristics (Equation 2.8) carry values of pressure and travel only in the positive x direction. They travel at the speed of sound in our analogue which

is equal to the local density ($\frac{dx}{dt} = \rho$). Along these wave paths the pressure becomes amplified when they are in the presence of energy release along the particle paths. The amount of amplification they undergo is based on the rate of energy release r, the heat of release of the material Q, as well as the amount of time the waves spend in phase with the energy release.

The particle path characteristics (Equation 2.9) show the motion of the material and track the progress of the reactions. In the Lagrangian frame of reference the particle paths in our model do not move in x and are stationary. Along the particle paths the progress of the reactions for each path is described by the reaction rates set by the system (r).

Together, the detonation dynamics can be described by the coupling of these two characteristics, in which the forward pressure waves amplify through the reaction zone and travel forward to alter the energy releasing reaction occurring along the particle paths.

We can demonstrate how the characteristics interact together to form the basic stable structure of the 1D detonation. This interaction is described in the time-space characteristic diagram sketch in Fig. 2.1 where the various shock and characteristic paths are shown. At $t = 0$ a stable detonation structure is set, which is left to propagate steadily down a 1D channel in position x over time t. The detonation structure is shown by the paths for the shock front, the end of the induction zone, and the end of the reaction zone positions. A few characteristics paths for our system are plotted, both the forward pressure wave paths and the particle path, to demonstrate their behaviour. The particle paths are stationary vertical paths. The pressure wave paths travel forward at a constant rate equal to the local density ρ, and only become amplified as they pass through the reaction zone where the characteristic paths accelerate and slope forward.

In our diagram we can follow one of the undisturbed particle paths in the channel ahead of the initial stable detonation numbered "1.". As the shock passes over the material at that point (where the shock intersects the particle path) the reaction begins along the particle path. As each particle of the channel is successively activated by the shock, a trailing reaction zone is formed behind the shock. At this point, any of the pressure wave paths that become exposed to the reaction zone (2.) become amplified and slope forward. They travel forward to eventually amplify the shock and keep it propagating forward at a constant rate. Behind the shock (3.) we can see how the pressure waves are parallel with the detonation structure, which indicates a sonic point behind the detonation. This restricts the detonation from being affected by any disturbances in the following flow.

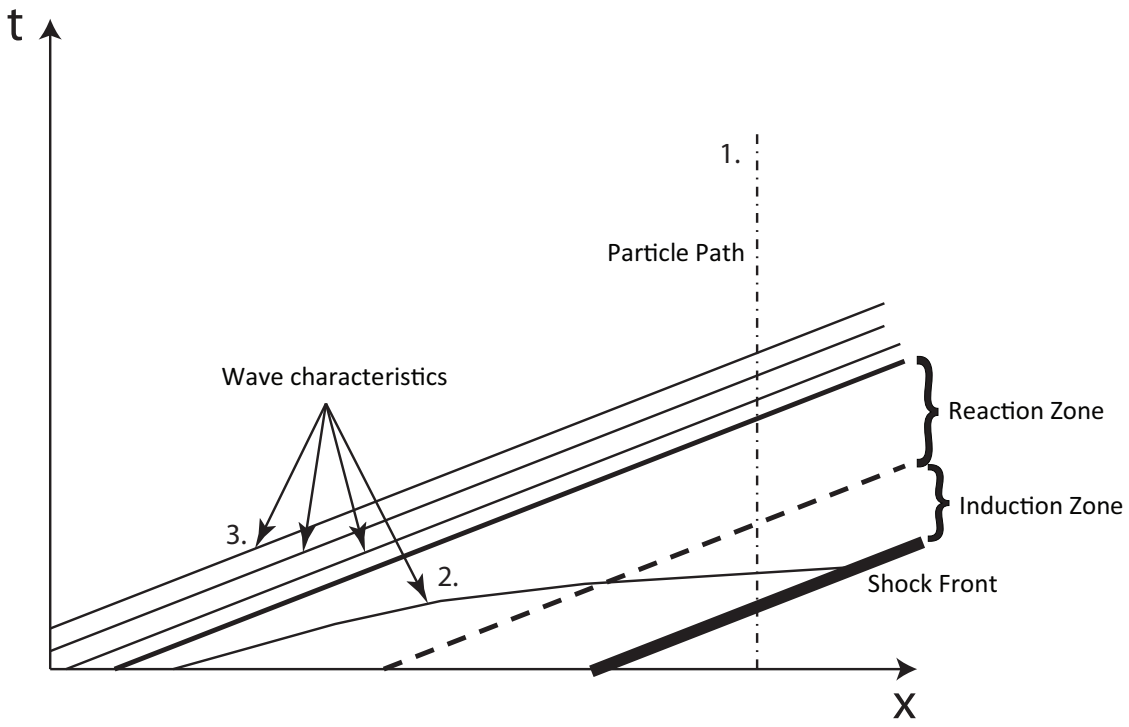

Figure 2.1: Characteristic diagram sketch of a propagating stable detonation structure. Only a selection of characteristic paths is illustrated. The forward pressure wave characteristics are shown as solid lines (2. & 3.), and the particle paths are the dot-dashed vertical lines (1.). The paths describing the detonation structure are shown as well.The shock front path is shown in thick bold, the end of the induction zone is in dashed bold, and the end of the reaction zone is in solid bold.

2.4 Reaction Model

To model the chemical reaction we use a 2-step induction-reaction model. This model has independently controlled induction and reaction periods, which allows us to investigate the effect of both the induction and reaction zones on the instability behaviour of detonations, yet remains relatively simple. A thermally neutral induction period proceeds after the leading shock, whose duration depends on the material's local compression. Following the induction zone is the reaction zone, characterized by a reaction rate chosen to be state independent, for simplicity. During the reaction period, energy is released to amplify pressure. The resulting induction-reaction model we propose is thus:

$$\partial_t \lambda_i = r_i = -K_i H(\lambda_i) e^{\alpha(\frac{\rho}{2\rho_{CJ}}-1)} \tag{2.10}$$

$$\partial_t \lambda_r = r_r = K_r[1 - H(\lambda_i)]H(1-\lambda_r)(1-\lambda_r)^\nu \tag{2.11}$$

where K_i and K_r are reaction constants, ρ_{CJ} is a constant based on the CJ case, λ_i is the induction zone progress variable, λ_r is the reaction zone progress variable, ν is the reaction order, $H()$ is the Heaviside function, and α is the reaction rate sensitivity parameter. The progress variables track the completion of each of the reaction periods. In the unreacted state we have $\lambda_i = 1$ and $\lambda_r = 0$. The reactions are then activated by the passage of a shock, which begins the induction reaction and starts the λ_i progress variable counting down to zero (marking the end of the induction zone) based on the induction reaction rate (Equation 2.10). After which, the reaction zone begins and λ_r counts up based on the reaction zone rate (Equation 2.11) to unity. In the fully burnt state we would then have $\lambda_i = 0$ and $\lambda_r = 1$. The Heaviside function $H()$ is used as a switch to control the timing of the onset of the second reaction. The parameter α, which we vary in our study, controls the sensitivity of the induction rate to changes in density. Higher values of α causes the induction reaction rate to increase more (and shorten the induction zone length) when exposed to increases in density. With this reaction model description applied to Fickett's model, we now have a full description of the system.

2.5 Stable solution structure

Our system is seen to admit a coherent self-propagating traveling wave solution having the properties of a detonation (Fickett, 1985*a*). We can analytically derive the structure of the stable solution for our given system to begin our study of the unstable dynamics

of detonations. The details of the development are available in Fickett's "Introduction to Detonation Theory" (Fickett, 1985a).

The study of detonation propagation builds on the Chapman-Jouguet (CJ) model theory (Fickett & Davis, 2000). This has long been established as a method of predicting the detonation speed based on the conservation laws and thermodynamic properties. It treats the detonation structure, both the shock and reaction zone, as a whole unit removed from disturbances downstream. This implies that the CJ wave is followed by a sonic surface which isolates it from waves from the rear.

To define the traveling wave solution for our system given by Equations 2.1-2.3 we assume a steady wave speed D of a detonation traveling into an undisturbed unreacted material, while trailing behind it is fully reacted material. To simplify the description, we develop the detonation structure from the frame of reference of the stable detonation since the system is constant with time relative to the stable detonation. First, we find the wave speed D in terms of the unreacted state (ρ_0, λ_{r0}) in front of the wave, and the reacted state (ρ_2, λ_{r2}) behind the wave. For simplicity, and without any loss of generality, we set $\rho_0 = 0$ and $\lambda_{r_0} = 0$ ahead of the detonation, and behind it we have $\lambda_{r2} = 1$. We also let ρ_2 vary (i.e., the piston problem; see Fickett & Davis (2000)). To denote the changes across the wave we use the following notation $[y] = y_2 - y_0$. We can now describe the wave speed for our single conservation equation, which follows the form of the the wave speed solution for Burgers' equation (Whitham, 1974) as:

$$D = \frac{[p]}{[\rho]} \tag{2.12}$$

$$D = \frac{(\rho_2^2 + Q)}{2\rho_2} \tag{2.13}$$

We now invoke the CJ condition, which predicts the wave speed assuming a sonic boundary behind the wave structure. In the CJ case the forward propagating characteristics trailing the wave cannot penetrate the wave structure. The speed of this so-called "limiting characteristic" needs to be equal to the detonation speed. This special case is denoted with the subscript CJ, and in our model requires that $\rho_2 = \rho_{CJ} = D = D_{CJ}$. Making this substitution in Equation 2.13 we then obtain the CJ speed of the steady detonation:

$$D_{CJ} = \sqrt{Q} \tag{2.14}$$

We can now develop the density (ρ) and reaction progress variables' (λ_i, λ_r) distribution across the steady wave structure. The detonation wave is headed by an inert shock jump discontinuity, across which there is no energy release and the density and pressure exhibit step change. We denote the state just behind the shock in the induction zone with a subscript "ind". In front of the shock we have $\rho_0 = 0, \lambda_r = 0$ while after the shock we have some density ρ_{ind} and $\lambda_r = 0$. For a nonreactive shock satisfying the weak form of the inert inviscid Burgers' equation, we can again apply Equation 2.12 across the shock to describe the state in the induction zone, in which case we get: $\rho_{ind} = 2D = 2D_{CJ}$.

We can now integrate the governing equations to develop the detonation structure. We now make the formal change of coordinates to a fixed system traveling with the steady detonation where we have: $(\zeta = x - D_{CJ}t - x_0, \quad t' = t)$. The partial derivatives then become:

$$\frac{\partial}{\partial t} = -D_{CJ}\frac{\partial}{\partial \zeta} + \frac{\partial}{\partial t'} \quad , \tag{2.15}$$

$$\frac{\partial}{\partial x} = \frac{\partial}{\partial \zeta} \tag{2.16}$$

Applying these to the governing equations (Equations 2.1 and 2.10 and 2.11) and setting the time derivatives equal to zero in order to obtain the steady solution, we arrive at:

$$\frac{d}{d\zeta}(\frac{1}{2}\rho^2 - D_{CJ}\rho + \frac{1}{2}\lambda_r Q) = 0, \tag{2.17}$$

$$-D_{CJ}\frac{d\lambda_i}{d\zeta} = -K_i * H(\lambda_i), \tag{2.18}$$

$$-D_{CJ}\frac{d\lambda_r}{d\zeta} = [1 - H(\lambda_i)]H(1 - \lambda_r)K_r(1 - \lambda_r)^\nu \tag{2.19}$$

This system is then integrated from the shock at $\zeta = 0$ across the detonation reaction zone structure. The induction zone equation (Equation 2.18) is integrated from $\zeta = 0$ and $\lambda_i = 1$ to the completion of the induction zone at $\zeta = \zeta_{ind}$ and $\lambda_i = 0$ to solve for the variation in λ_i and induction zone length ζ_{ind}:

$$\lambda_i = \frac{K_i}{D_{CJ}}\zeta + 1, \tag{2.20}$$

$$\zeta_{ind} = -\frac{D_{CJ}}{K_i} \tag{2.21}$$

The reaction zone equation (Equation 2.19) can now be integrated from the beginning of the reaction zone at $\zeta = \zeta_{ind}$ and $\lambda_r = 0$ to some point in the reaction zone ζ and some λ_r. This gives us the distribution of λ_r in the reaction zone, which we can evaluate at $\lambda_r = 1$ to find the end of the reaction zone and the entire steady detonation structure ζ_{CJ}:

$$\lambda_r = 1 - [1 + (1-\nu)\frac{K_r}{D_{CJ}}(\zeta - \zeta_{ind})]^{\frac{1}{1-\nu}}, \tag{2.22}$$

$$\zeta_{CJ} = \zeta_{ind} - \frac{D_{CJ}}{K_r(1-\nu)} \tag{2.23}$$

The steady frame conservation equation (Equation 2.17) is then integrated from just after the shock at $\rho = \rho_{ind}$ and $\lambda_r = 0$, to some point in the detonation at some ρ and λ_r. This allows us to solve for the density throughout the detonation structure, with a constant density in the induction zone (where $\lambda_r = 0$ and we have $\rho = 2D_{CJ}$), and we can find the density in the reaction zone using Equation 2.22. The density is given by:

$$\rho = D_{CJ}(1 + \sqrt{1 - \lambda_r}) \tag{2.24}$$

This results in a complete description of the steady detonation structure. To summarize, ahead of the detonation is quiescent material, for $\zeta > 0$, where we have:

$$\rho = 0, \tag{2.25}$$

$$\lambda_i = 1, \tag{2.26}$$

$$\lambda_r = 0 \tag{2.27}$$

The detonation structure is lead by a shock front at $\zeta = 0$. Behind the shock front is the induction zone, which continues for $\zeta_{ind} < \zeta < 0$ (where $\zeta_{ind} = -\frac{D_{CJ}}{K_i}$) . In the induction zone we have (where D_{CJ} is given by Equation 2.14):

$$\rho_{ind} = 2D_{CJ}, \tag{2.28}$$

$$\lambda_i = \frac{K_i}{D_{CJ}}\zeta + 1, \tag{2.29}$$

$$\lambda_r = 0 \tag{2.30}$$

Following the induction zone is the reaction zone, for $\zeta_{CJ} < \zeta < \zeta_{ind}$ (where $\zeta_{CJ} =$

$\zeta_{ind} - \frac{D_{CJ}}{K_r(1-\nu)}$), and with the following distribution of properties:

$$\rho = D_{CJ}(1 + \sqrt{1 - \lambda_r}), \tag{2.31}$$

$$\lambda_i = 0, \tag{2.32}$$

$$\lambda_r = 1 - [1 + (1 - \nu)\frac{K_r}{D_{CJ}}(\zeta - \zeta_{ind})]^{\frac{1}{1-\nu}} \tag{2.33}$$

The density profile for the steady structure of a CJ detonation for our model along with a characteristic diagram sketch of the steady solution is shown in Fig. 2.2. The characteristic solution (a) shows the steady path of the detonation which is headed by a constant velocity shock, behind which are the paths for the end of the induction and reaction zones. Below the characteristic diagram is a diagram showing the variation in density across our steady solution (b). We have a detonation speed of $D_{CJ} = \sqrt{Q}$ which corresponds to the inverse of the slope of the shock front path in the t-x characteristic diagram. The density and pressure jump after the shock front, and are constant in the induction zone in the steady solution. The density then steadily decreases through the reaction zone to the burnt flow following behind at CJ conditions. Figure 2.2 c) shows the locations of the end of the induction and reaction zones in the ζ frame of reference fixed to the shock at $\zeta = 0$.

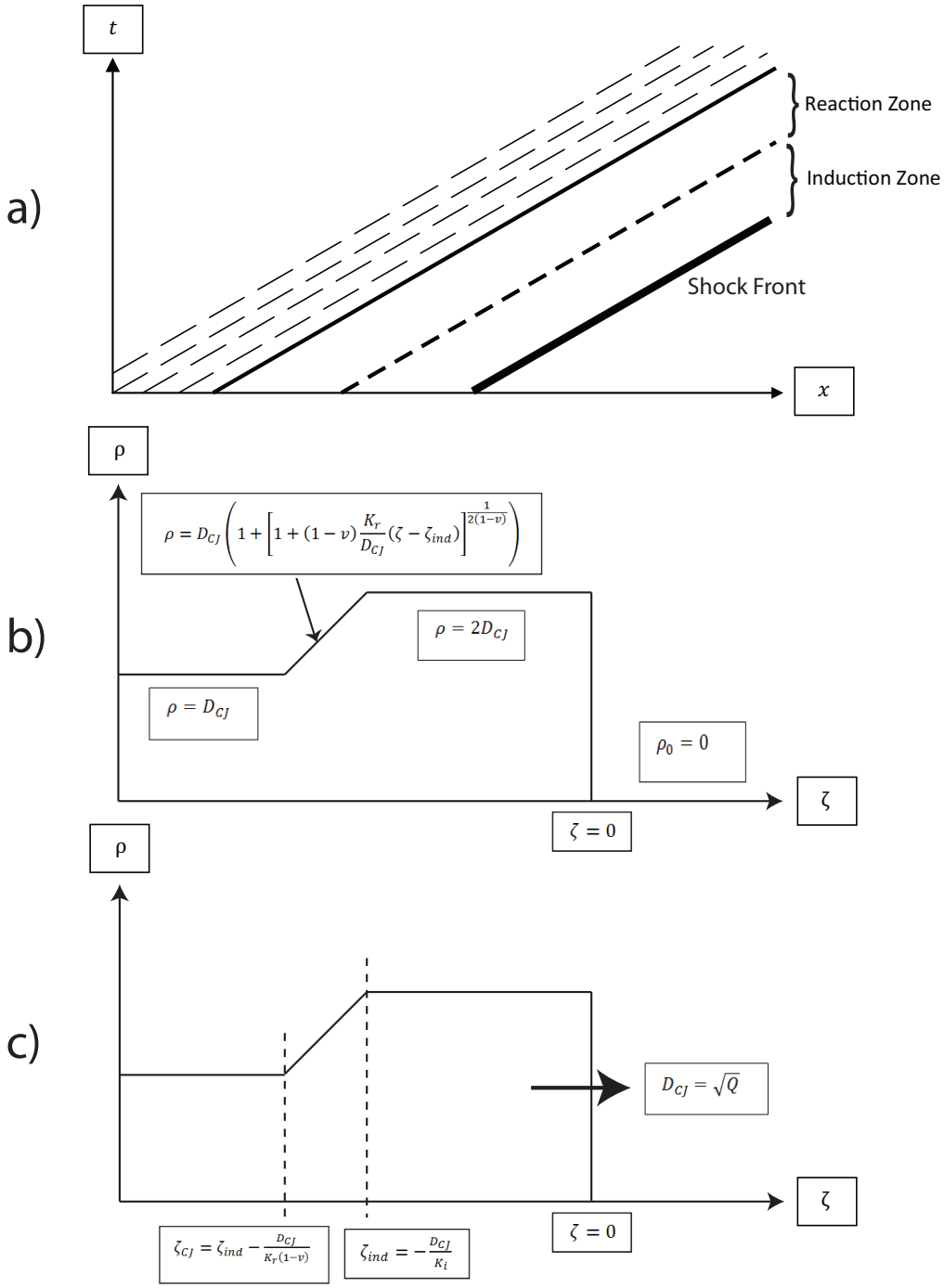

Figure 2.2: Description of the steady detonation structure. a) The $t-x$ diagram sketch showing the paths of the shock front in thick bold, the end of the induction zone in dashed bold, and the end of the reaction zone in solid bold. b) A sketch of the density profile showing the density distribution across the induction and reaction zone, as well as in the following flow. c) A sketch of the detonation structure in the ζ frame of reference following the shock, with the position of the end of the induction and reaction zones labeled. D_{CJ} is the steady CJ detonation speed.

Chapter 3

The Numerical Technique

3.1 Numerical model

To seek unstable, time varying solutions to the model problem (Equations 2.1, 2.10, 2.11), we solve these equations numerically. The numerical technique uses the fractional step method, whereby the non-reactive hydrodynamics and reactive dynamics can be decoupled during an integration time step. We use the C++ programming environment with the code provided in Appendix B. The present chapter details the numerical procedure used and its verification.

The system of equations we wish to model can be given together in conservative form as:

$$\frac{\partial}{\partial t}\begin{bmatrix} \rho \\ \lambda \end{bmatrix} + \frac{\partial}{\partial x}\begin{bmatrix} p \\ 0 \end{bmatrix} = \begin{bmatrix} 0 \\ r \end{bmatrix} \tag{3.1}$$

For the fractional step method the flux and source terms (the second and third terms respectively in Equation 3.1) are sequentially evaluated during separate half-steps at each time-step. The hydrodynamic half-step first evaluates the flux term with the reactions frozen, which is then followed by the reaction half-step, which evaluates the reaction source term separately from the flux.

3.1.1 Hydrodynamic step

The hydrodynamic half-step is evaluated by an exact first-order Riemann solver which we develop below.

In the hydrodynamic half-step we evaluate the flux term only, with the reactions frozen:

$$\frac{\partial}{\partial t}\begin{bmatrix}\rho\\ \lambda\end{bmatrix}+\frac{\partial}{\partial x}\begin{bmatrix}p\\ 0\end{bmatrix}=\begin{bmatrix}0\\ 0\end{bmatrix} \tag{3.2}$$

The first linear equation of Equation 3.2 requires that a change in a conserved quantity (ρ) be equal to the change in the flux (p) (given by Equation 2.2) at constant λ. The second equation shows that λ remains constant during the hydrodynamic step at a given location. We can numerically solve our equation given in conservative form (Equation 3.2) as a finite volume problem. We discretize our domain into finite volume cells which hold piece-wise constant cell-averaged values of density (Fig. 3.1). At each cell boundary the flux (F) between cells is evaluated over time to calculate the change in each cell's contents. Through this discretization, the updated density values of any cell ρ_i^{n+1} is equal to the initial density plus the difference in the numerical flux through each of the cell boundaries:

$$\rho_i^{n+1}=\rho_i^n+\frac{\Delta t}{\Delta x}(F_{i-1/2}-F_{i+1/2}) \tag{3.3}$$

To evaluate the flux we apply an exact Riemann solver which calculates the flux through each cell interface based on solving the Riemann problem across each cell boundary. The Riemann problem is a special initial value problem where two constant states are separated by a contact discontinuity. The Riemann problem can be initialized in several ways, which are shown in Fig. 3.2. In our system we consider the physical case of only positive density.

In Fig. 3.2 the density is initialized on the left (1) and right (2) across $x = 0$, a point which represents the cell boundary ($i \pm 1/2$) through which the flux ($F_{i\pm1/2}$) occurs. In case a) we have $\rho_1 > \rho_2$, while in case b) we have $\rho_1 < \rho_2$.

In Fig. 3.2 a), in the bottom figure, we have a characteristic diagram showing the development of a shock wave into the right cell as the faster moving material on the left compresses the material in the right cell. In Fig. 3.2 b), in the bottom figure, we have a rarefaction occurring between the slower moving left material, and faster moving right material. In either of these cases the flux occurring through the boundary at $x = 0$ is simply the material brought forward from the left state.

Thus, we can evaluate the numerical flux at the interfaces ($i + 1/2$ and $i - 1/2$) in Equation 3.3 by the upwind flux values (p_{i-1}^n and p_i^n) in order to solve the Riemann problem exactly:

$$\rho_i^{n+1}=\rho_i^n+\frac{\Delta t}{\Delta x}(p_{i-1}^n-p_i^n) \tag{3.4}$$

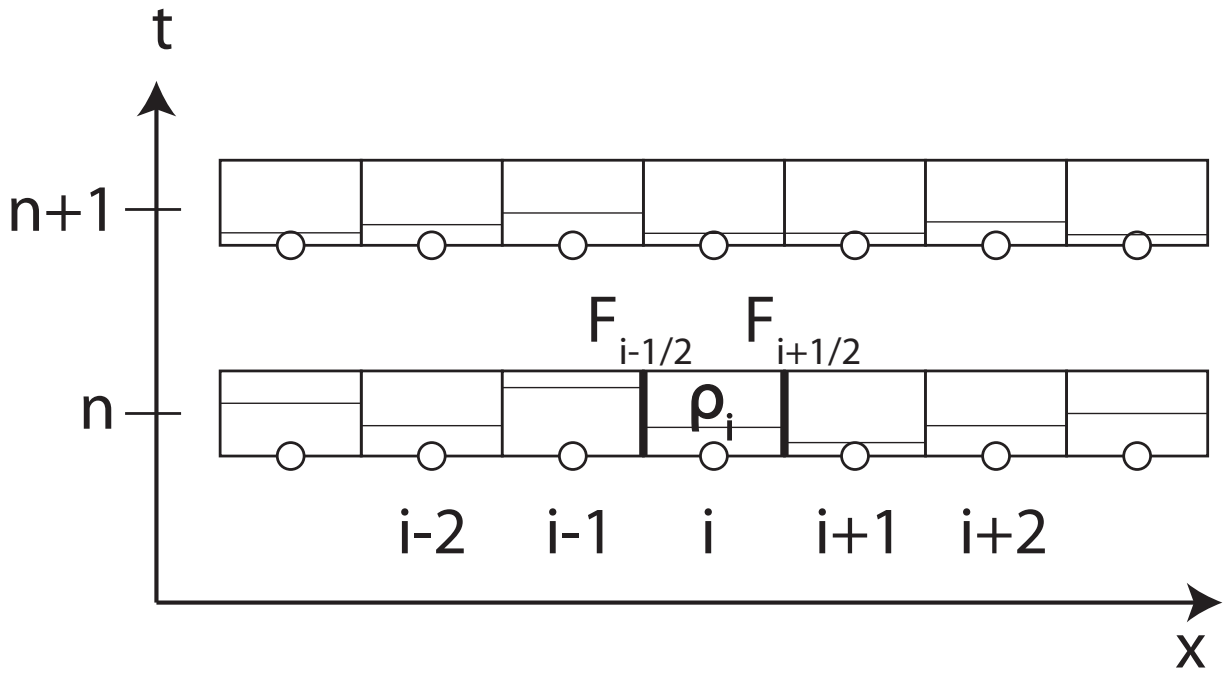

Figure 3.1: Diagram of the discretization of the domain into cells (i). Cells contain piece-wise constant cell-averaged values of density. The contents of each cell is updated at every new time step (n+1) based on the flux (F) through the boundaries of each cell.

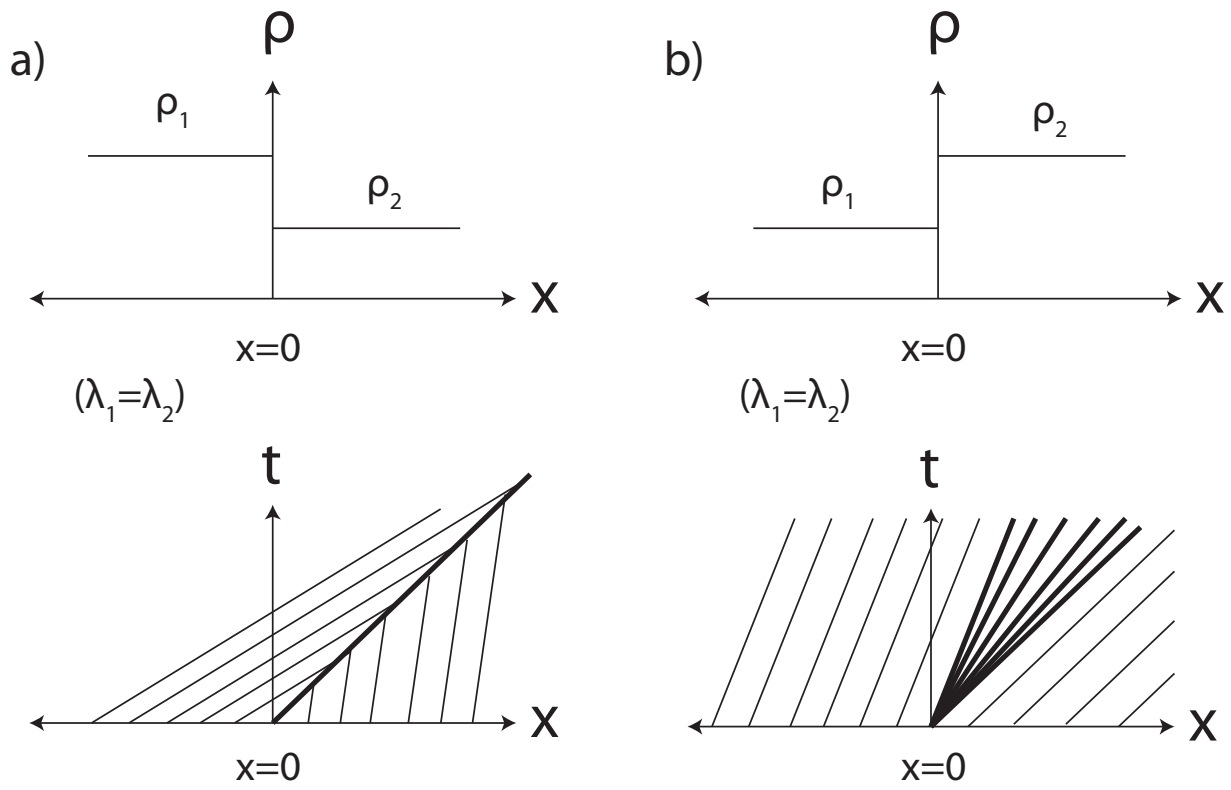

Figure 3.2: The special initial-value case, the Riemann problem. Two constant states are separated at x=0. For case a) the left state has greater density: $\rho_1 > \rho_2$. For case b) the right state has greater density: $\rho_1 < \rho_2$. The bottom figures for each case are the equivalent characteristic diagrams showing the wave paths of the flux "p".

With the equation of state (Equation 2.2) this equation allows us to discretize the hydrodynamic step as follows:

$$\rho_i^{n+1} = \rho_i^n + \frac{\Delta t}{2\Delta x}((\rho_{i-1}^n)^2 - (\rho_i^n)^2 + Q(\lambda_{r_{i-1}}^n - \lambda_{r_i}^n)) \tag{3.5}$$

where the subscript i is the current space nodal position in x, the superscript n is the current time step data, Δt and Δx represents the difference between time steps and position nodes respectively.

3.1.2 Reaction step

The reaction half-step is solved analytically, where we evaluate the reactions only:

$$\frac{\partial}{\partial t}\begin{bmatrix} \rho \\ \lambda \end{bmatrix} = \begin{bmatrix} 0 \\ r \end{bmatrix} \tag{3.6}$$

where r is given by Equations 2.10 and 2.11. The induction and reaction progress variables at each half-step are solved analytically by direct integration, while the density is kept constant. The progress variables become discretized as follows:

$$\lambda_{i_i}^{n+1} = \lambda_{i_i}^n - K_i * H(\lambda_{i_i}^n) * H(\rho_i - \rho_{act}) e^{\alpha(\frac{\rho_i}{(2\rho_{CJ})}-1)}\Delta t \tag{3.7}$$

$$\lambda_{r_i}^{n+1} = 1 - [(1-\lambda_{r_i}^n)^{1-\nu} - (1-\nu)[1 - H(\lambda_{i_i}^n)]H(1-\lambda_{r_i})K_r\Delta t]^{\frac{1}{1-\nu}} \tag{3.8}$$

where ρ_{act} is a threshold value of density which, when exceeded, marks the activation of the chemical reaction by the leading shock. The term ρ_{CJ} is the CJ value of density, which is equal to the CJ detonation speed $\rho_{CJ} = D_{CJ}$ (where D_{CJ} is given by Equation 2.14).

3.2 Initial conditions

Two different problems are addressed in Chapters 4 and 5. In Chapter 4 we address the stability of the traveling wave ZND solution outlined in the previous chapter. The numerical domain is thus initialized as a stable ZND detonation wave which is left to propagate through a 1D channel of unreacted material. The channel has inlet boundary conditions set to reacted CJ conditions of $\rho = \sqrt{Q}, \lambda_i = 0, \lambda_r = 1$, while the undisturbed state of the channel is set to zero density unreacted material which assumes the strong

shock limit with $\rho = 0, \lambda_i = 1, \lambda_r = 0$. The parameters we used for the simulations were: $Q = 5$,$K_i = 1$,$K_r = 2$, $\nu = 0.5$. We kept a CFL value of 0.8 for all simulations. We report our results in terms of the nondimensionalization described in Appendix A, with ρ_s taken as the post shock density in the CJ case: $\rho_s = \rho_{s,CJ} = 2\rho_{CJ}$.

For the transient detonation acceleration study in Chapter 5 we simulate a piston-initiated shock-induced ignition problem. The governing equations are nondimensionalized and discretized as seen in Appendix A in order to describe the effect of the ratio of the induction to reaction time ($\tilde{K}$) and the sensitivity of the reaction rates (inverse activation energy $\tilde{\epsilon}$) in a scaled system. Simulating the piston path in Lagrangian coordinates corresponds to a constant piston position at $\tilde{x} = 0$. To model a steady piston compressing the material we set $\tilde{\rho}(\tilde{x} = 0, \tilde{t}) = 1$. In front of the piston is unreacted quiescent material of zero density: $\tilde{\rho} = 0, \lambda_i = 1, \lambda_r = 0$. During the simulation an inert shock propagates down the channel initiating a reaction, which then amplifies the shock into a detonation simulating the amplification that takes place during the normal cycles in the pulsating instability behaviour. We use the parameters $\tilde{Q} = 1, \nu = 0.5$ and vary the nondimensional ratio of induction to reaction time $\tilde{K}$, as well as the inverse activation energy $\tilde{\epsilon}$, in order to identify the role these factors play in controlling the amplification process and to clarify their effect on the instability dynamics. For the transient detonation acceleration study in Chapter 5 we simulate a piston-initiated shock-induced ignition problem. The governing equations are nondimensionalized and discretized (Appendix A) in order to describe the effect of the ratio of the induction to reaction time ($\tilde{K}$) and the sensitivity of the reaction rates (inverse activation energy $\tilde{\epsilon}$) in a scaled system. Simulating the piston path in Lagrangian coordinates corresponds to a constant piston position at $\tilde{x} = 0$. To model a steady piston compressing the material we set $\tilde{\rho}(\tilde{x} = 0, \tilde{t}) = 1$. In front of the piston is unreacted quiescent material of zero density: $\tilde{\rho} = 0, \lambda_i = 1, \lambda_r = 0$. During the simulation an inert shock propagates down the channel initiating a reaction, which then amplifies the shock into a detonation simulating the amplification that takes place during the normal cycles in the pulsating instability behaviour. We use the parameters $\tilde{Q} = 1, \nu = 0.5$ and vary the nondimensional ratio of induction to reaction time $\tilde{K}$, as well as the inverse activation energy $\tilde{\epsilon}$, in order to identify the role these factors play in controlling the amplification process and to clarify their effect on the instability dynamics.

3.3 Diagnostics

We model the characteristics of the system together in a space-time characteristic diagram describing the system dynamics. We create this diagram by reconstructing a discrete set

of pressure waves, which are evaluated from integrating the forward characteristic path (Equation 2.8) starting from arbitrary locations. We used the Euler method to discretize the forward characteristics which follow paths given by:

$$\tilde{x}_{i+1} = \tilde{x}_i + \Delta\tilde{t}\tilde{\rho}_i \tag{3.9}$$

An example case of the characteristic diagram that can be generated from our numerical model for the stable detonation solution is seen in Fig. 3.3. This diagram is taken in the stable CJ detonation frame of reference (ζ). The detonation structure is in coloured lines (refer to figure caption) and the characteristics for the pressure paths are in solid black for the C+ pressure wave characteristics, and dashed gray for the particle paths. The pressure wave characteristics are seen to slope forward as they amplify through the reaction zone. The particle paths are sloped backwards in this frame of reference. Again, they are straight linear paths as this model is in the Lagrangian frame of reference following a fluid element.

3.4 Numerical verification

We performed a resolution convergence study to determine a satisfactory level of accuracy in our simulation. We measured the resolution as the number of grid points across the stable detonation structure. For varying resolution we found the critical α value at which the solution became oscillatory (Fig. 3.4). With increasing resolution the stability point measured by α begins to decrease. Beyond a resolution of 192 points the value of α does not change to 2 significant digits. Taking this as a criterion for convergence, we thus determine that 256 points across the detonation structure is sufficient to have a converged solution.

We measured the change in the stability point (at which the solution becomes unstable) for varying resolution values as seen in Fig. 3.4. The stability point begins to asymptote to a constant value at higher resolution. We therefore choose a resolution of 256 points across the whole detonation structure to accurately capture the onset of stability for alpha values to within ± 0.1.

To observe how well the stable structure is captured by our numerical model we simulate a stable detonation at 256 resolution and allow it to propagate through a channel for long times and observe how well the structure is retained. We observe minor rounding at the front of the shock and at the end of the reaction zone in our long term solution as seen in Fig. 3.5. This can be attributed to the inherent dissipative errors in the first order scheme used. The rest of the structure stays very consistent with the initial profile, and

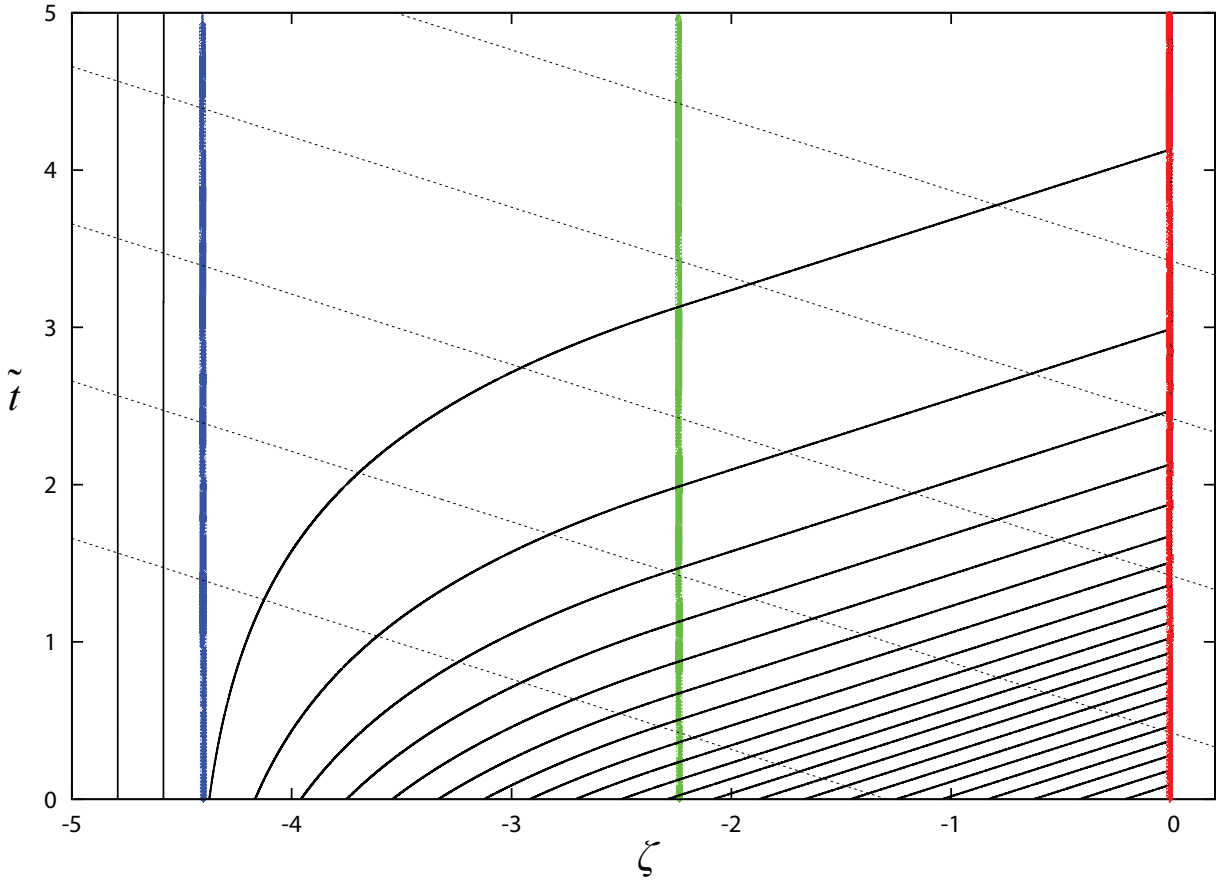

Figure 3.3: Numerically generated characteristic plot for the stable detonation structure plotted in the stable CJ detonation frame of reference (ζ). The path of the shock front is in red, the end of the induction zone is in green, and the end of the reaction zone is in blue. An arbitrary set of pressure characteristics are plotted as black lines across the detonation structure. The particle paths are shown as dashed gray lines.

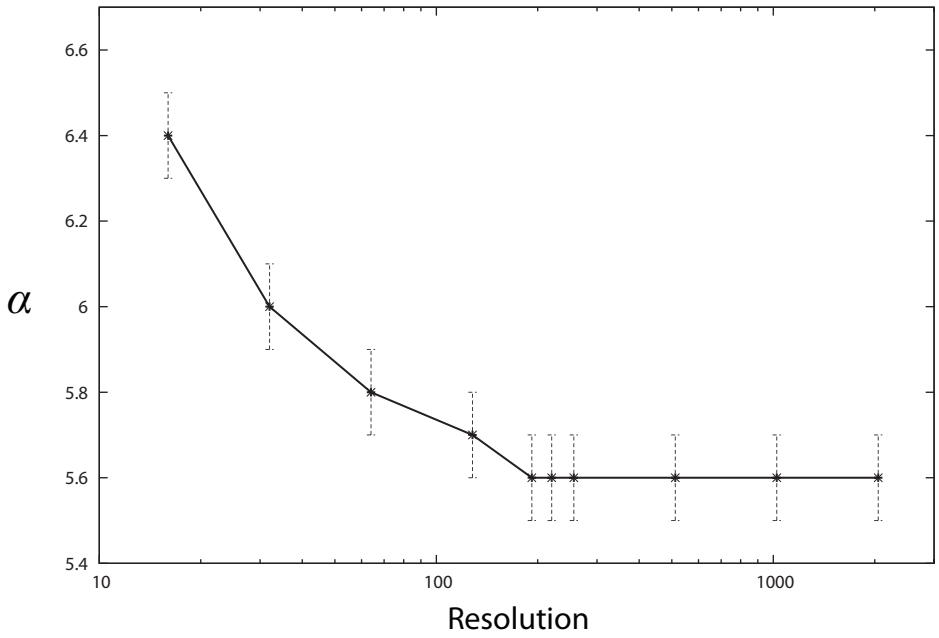

Figure 3.4: A plot of the effect of numerical resolution on the stability point. On the y-axis is the α value for the onset of instability. Along the x-axis is the resolution used in the simulation as measured by the number of nodes describing the entire stable detonation structure, plotted logarithmically.

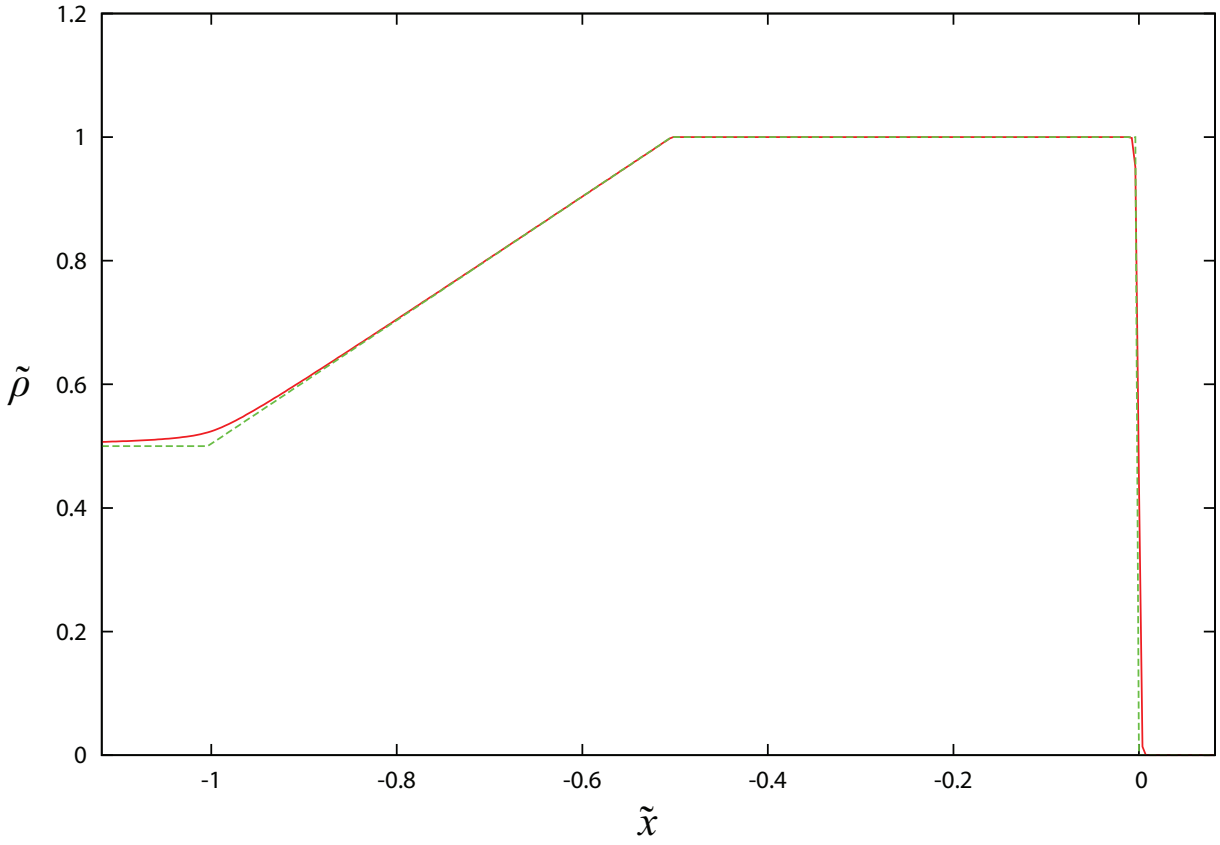

Figure 3.5: The comparison plot of the nondimensional density distribution across the detonations structure. The initial structure is shown in dashed green, while the structure at $\tilde{t} = 2000$ at 256 resolution in solid red has been superimposed over it.

the wave speed measured by the shock front density is captured very well and deviates by only 0.00872%. We also examine the effect of resolution on the stable solution and perform the same long term simulation at an increased resolution of 400 nodes across the detonation structure (Fig. 3.6). We see only minor reduction in the rounding that occurs in the structure at 400 resolution compared with 256, and can conclude that 256 resolution is adequate for reproducing the detonations structure.

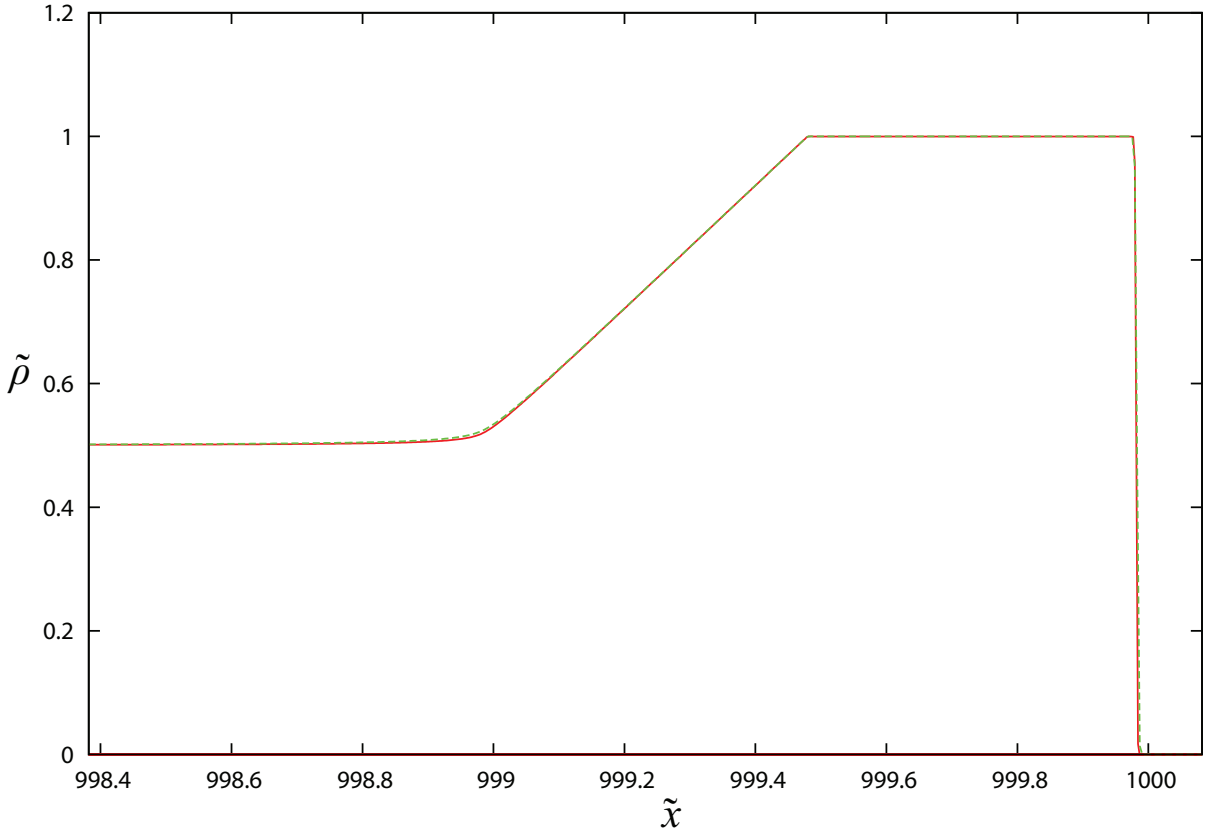

Figure 3.6: The higher resolution comparison plot of the nondimensional density distribution across the detonations structure. The structure at $\tilde{t} = 2000$ at 256 resolution is shown in dashed green, while the structure at $\tilde{t} = 2000$ at 400 resolution is in solid red superimposed over it.

Chapter 4

Pulsating Instability

4.1 Onset of Instability

In this chapter we address the stability of the traveling wave detonation solution. Starting with the analytical steady wave solution as initial conditions, we numerically integrated its evolution by the method discussed in the previous chapter. The undisturbed material in the channel has $\rho = 0, \lambda_r = 0, \lambda_i = 1$. We set the parameters of our simulation at: $Q = 5$, $K_i = 1$, $\nu = 0.5$. We kept a constant density at the start of the domain for our inlet boundary condition. We report our results in this section following the nondimensionalization in Appendix A with respect to the CJ post shock density ($\rho_s = \rho_{s,CJ}$). The position, time, density, and K are nondimensionalized as follows: $\tilde{x} = \frac{xK_i}{\rho_{s,CJ}}$, $\tilde{t} = tK_i$, $\tilde{\rho} = \frac{\rho}{\rho_{s,CJ}}$, and $\tilde{K} = \frac{K_r}{K_i}$.

First we kept $K_r = \tilde{K} = 2$ (with constant $K_i = 1$), and varied the induction rate sensitivity parameter α. For low values of α the detonation front was found to propagate down the channel as a constant velocity given by the steady wave solution. The structure of the wave also retained the structure of the steady wave solution. We label this wave as "stable". However, as we increased α, we found a threshold value after which the detonation strength would no longer remain steady over time, and would begin to regularly oscillate in strength. To measure the change in detonation strength we tracked the front shock density ($\tilde{\rho}_s$) through time as the detonation progressed down the channel.

For α below 5.7 we had a nearly constant front shock density value, implying constant detonation strength. Past an α of 5.7 we had an unstable solution resulting in the shock strength regularly oscillating over time. The stable and unstable solutions are shown in Fig. 4.1. Initially there is some small deviation in the detonation strength caused by start-up errors. The evolution of these initial deviations are affected by α in different ways. In

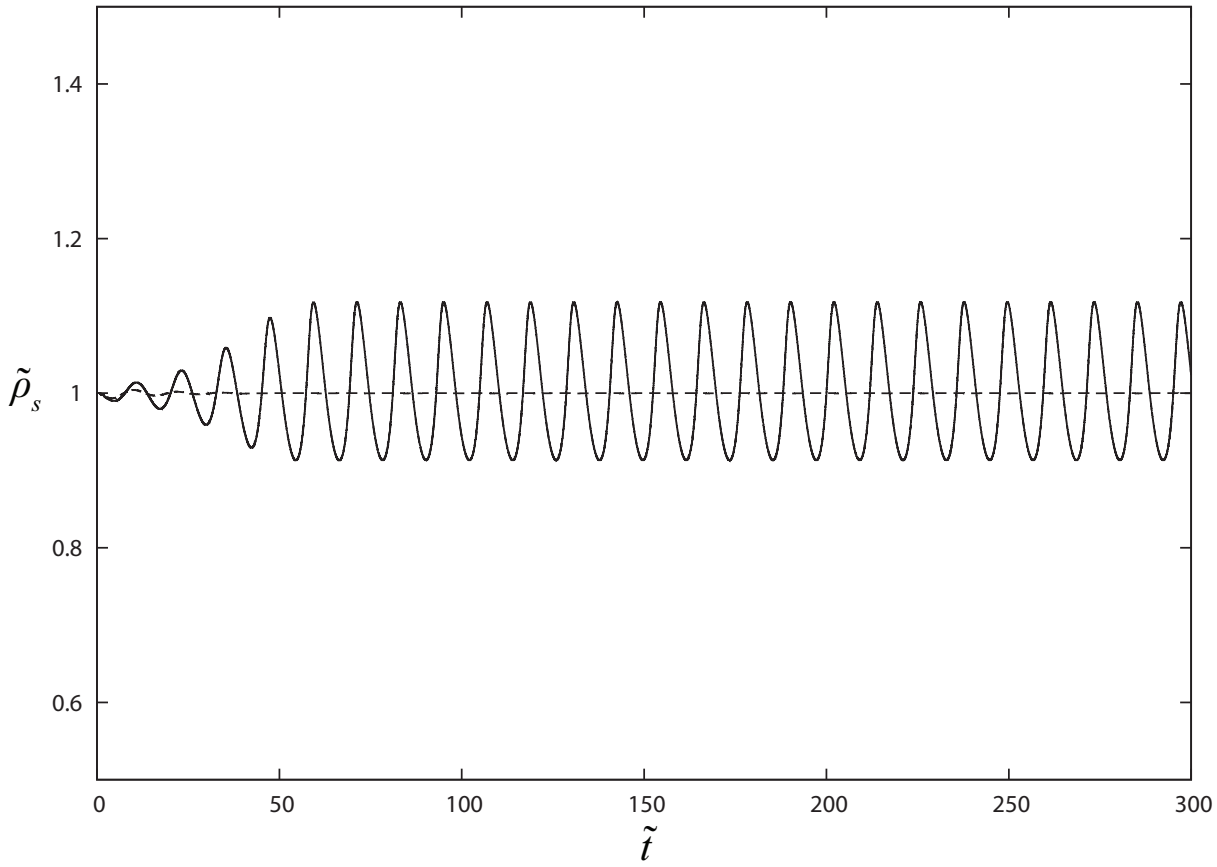

Figure 4.1: Comparison of stable and unstable solutions. This figure plots the nondimensional shock front density variation over time at constant $\tilde{K} = 2$. The stable solution is at $\alpha = 5.2$ and is shown by the dashed line. The unstable solution is at $\alpha = 6.2$ and is shown by the solid line.

the stable solution ($\alpha < 5.7$) these deviations die out and the solution becomes stable with a constant front shock density. In the unstable case ($\alpha > 5.7$), the deviations provide the seed for the physical instability, and grow until the solution oscillates with time. These oscillations are seen to saturate to a limit-cycle, with a fixed oscillation frequency and amplitude.

The unstable detonation behaviour seen in Fig. 4.1 at $\alpha = 6.2$ follows a regular oscillation, implying a series of accelerations and decelerations of the propagating detonation. This follows the 1D pulsating instability seen in detonations modeled with the more complex reactive Euler equations. Thus, Fickett's model with 2-step reaction model does admit both the stable and pulsating instability solutions as seen in more complex systems.

Additionally, we explored the effect of $\tilde{K}$ on stability. We were also able to find that a threshold value of $\tilde{K}$ exists (at constant α) which controls the onset of stability. As seen

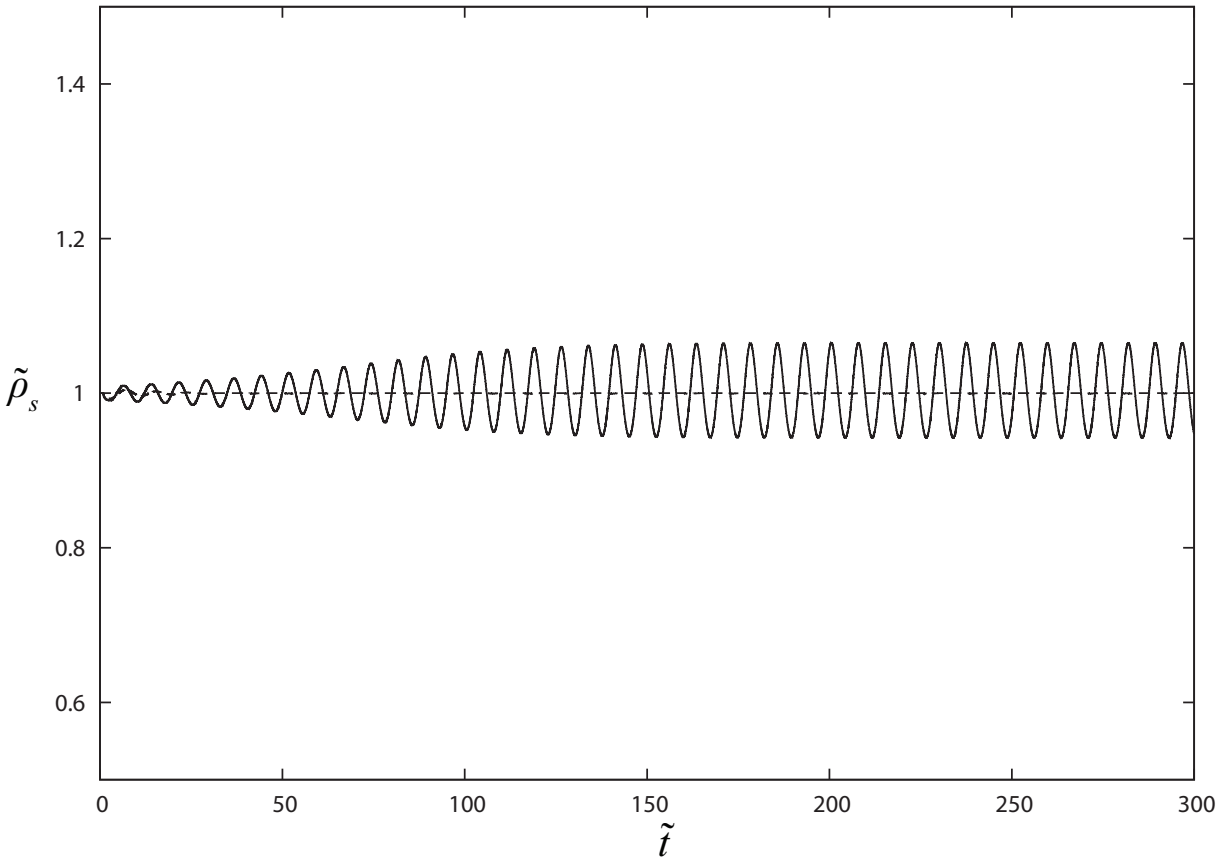

Figure 4.2: Comparison of stable and unstable solutions when varying $\tilde{K}$. The nondimensional front shock density variation with time is shown for constant $\alpha = 4.0$. The stable solution is shown with $\tilde{K} = 4.0$ in the dashed line. The unstable solution is at $\tilde{K} = 5.5$ in the solid line.

in Fig. 4.2 at constant $\alpha = 4.0$, a stable solution occurred for $\tilde{K}$ less than 5.0, while higher values ($\tilde{K} > 5.0$) resulted in unstable oscillation.

Both of these parameters can be related together to show their effect on stability. In Fig. 4.3 we have a diagram in which we varied $\tilde{K}$, and at each value found the α value at which the onset of instability occurred. Two limits appear from our results. For $\tilde{K} << 1$ the neutral stability limit is well approximated by a line with a slope related to the product of α and $\tilde{K}$. For $\tilde{K} >> 1$, the neutral stability boundary asymptotes to a line given by a constant α. Interestingly, the analog system recovers very well the previous results obtained from the reactive Euler equations. In the limit of slow reactions, Short & Sharpe (2003) have found that the product of activation energy and induction to reaction time ratio (given by $\tilde{K}$) controls the stability. In the limit of high $\tilde{K}$, the wave structure approaches the square wave structure, where the vanishing reaction time

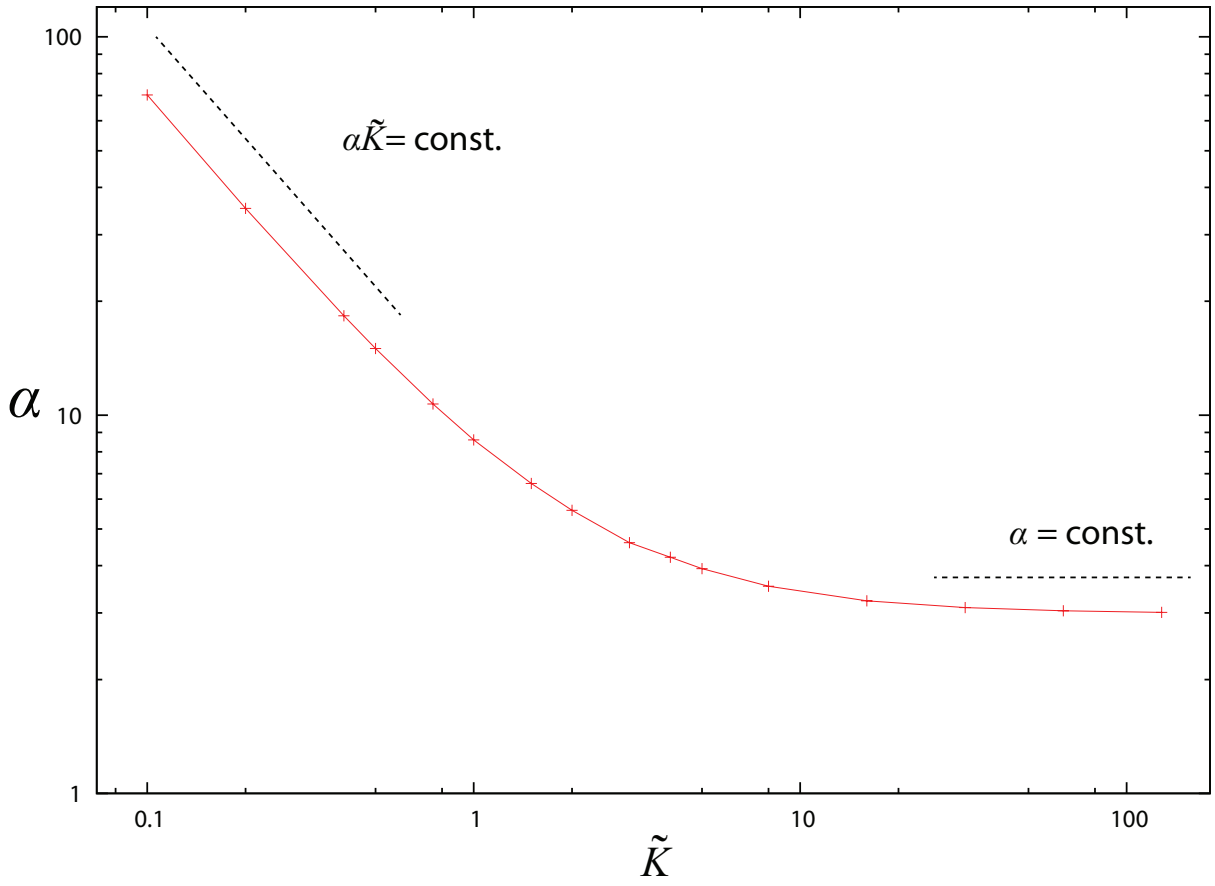

Figure 4.3: Diagram of detonation stability as a function of $\tilde{K}$ and α on a log-log scale. Along the x-axis are values of $\tilde{K}$, while along the y-axis are the values of α at which the onset of instability occurred at those values of $\tilde{K}$.

no longer becomes a relevant time scale in the phenomenon. It is thus not surprising that the activation parameter α uniquely governs the stability in this case. A stability analysis of this interesting observation is left for future study. In the remainder, we focus on the regime close to the neutral stability boundary where $\alpha\tilde{K} = const.$

4.2 Governing Mechanism of the Pulsations

We use a characteristic analysis to clarify the instability mechanism controlling the pulsations in detonation strength. Our model describes the detonation dynamics as the coupling of the compression waves (Equation 2.8) and chemical energy release along the particle paths (Equation 2.9).

To study the nonlinear instability mechanism we take the case of the single period

oscillatory solution at $\alpha = 6.2$ and $\tilde{K} = 2$. Figure 4.4 shows the space-time characteristic diagram of the wave structure for approximately two oscillation cycles in the frame of reference of the steady traveling wave solution (ζ). For reference, the variation in front shock strength is shown in Fig. 4.5, where the times of the strongest (S) and weakest (W) shock strength are labeled by dashed lines. We have also included in Fig. 4.6 a series of detonation profiles showing the density across the reaction zone at snapshots in time over the oscillation cycle. In this figure, profile 1 is taken near the time when the detonation strength is the strongest (S). Profile 2 shows the detonation during the deceleration phase, as it weakens. Profile 3 is taken near the time when the detonation is weakest (W). Profile 4 is taken as the detonation accelerates and strengthens. Profile 5 is taken when the detonation is near its strongest (S), completing the oscillation cycle.

Note that in our characteristic diagram (Fig. 4.4) the pressure wave characteristics travel at the speed of sound in our model, which is equal to the local density $\tilde{\rho}$, and that in the characteristic $\tilde{t} - \zeta$ diagram their linear paths have a slope equal to the inverse of density. As the pressure waves become amplified by the reaction their density increases and their paths slope forward in acceleration. The lead shock front of the detonation in Fig. 4.4 is the locus of where the pressure waves coalesce, and is the initiating point of the chemical reaction. The whole detonation structure is composed of the oscillating lead shock, the following induction zone, and then the reaction zone.

Of note regarding the tail of the detonation is that at this discontinuity at the rear of the reaction zone a finite (numerical) dissipation occurs which makes the characteristics bend somewhat towards the reaction zone in a very narrow region. The growth of this numerical diffusion is minimal over long periods of time. Away from this region our characteristics describe pressure waves of constant strength and speed throughout the system, except in the reaction zone where they accelerate due to the heat release. It is the coupling of these pressure waves and the reaction occurring along the particle path characteristics which describes the dynamics of the detonation. The pressure waves amplify through the reaction zone and propagate forward through the induction zone, where they alter the induction times of subsequently shocked particles.

The instability mechanism can be described through the characteristic diagram in Fig. 4.4. First we note that the oscillation in the lead shock modulates the duration of the induction zone and the onset of the reaction zone. As each particle (along particle path ("P") as indicated in Fig. 4.4) is shocked it undergoes an induction delay period, followed by a reaction period where energy release occurs. The induction zone's duration is dependent on the shocked state, and its sensitivity is controlled by α (Equation 2.10). The reaction zone follows after the induction zone and proceeds for a constant duration.

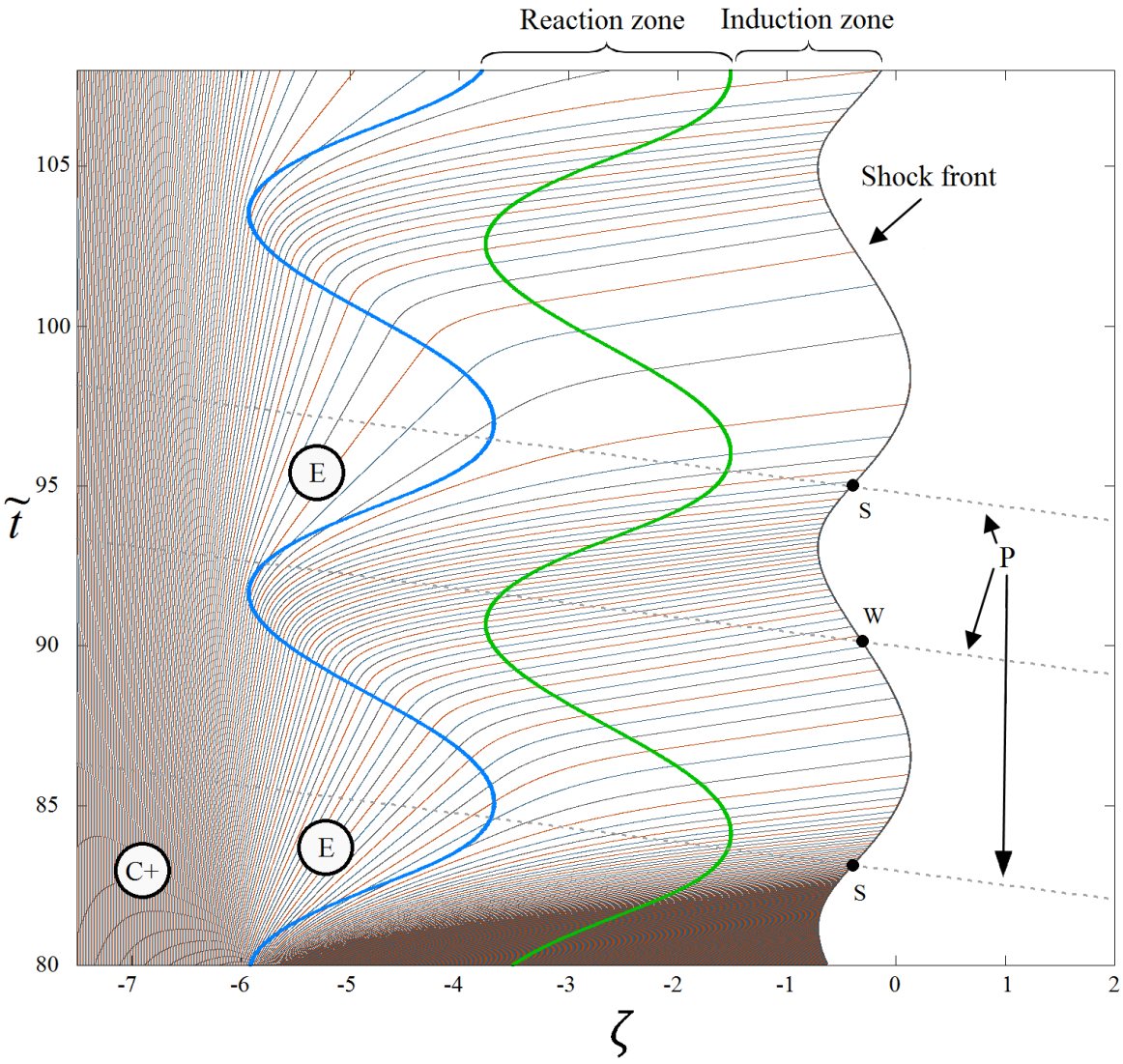

Figure 4.4: A space-time characteristic diagram in the frame of reference of a steady detonation (ζ) showing the interaction between the forward characteristics (C+) and the particle path characteristics (P) during two oscillation periods at $\alpha = 6.2$ and $\tilde{K} = 2$. Additionally, the position of the onset of the reaction zone is shown in thick green, and the end of the reaction zone is shown in thick blue.

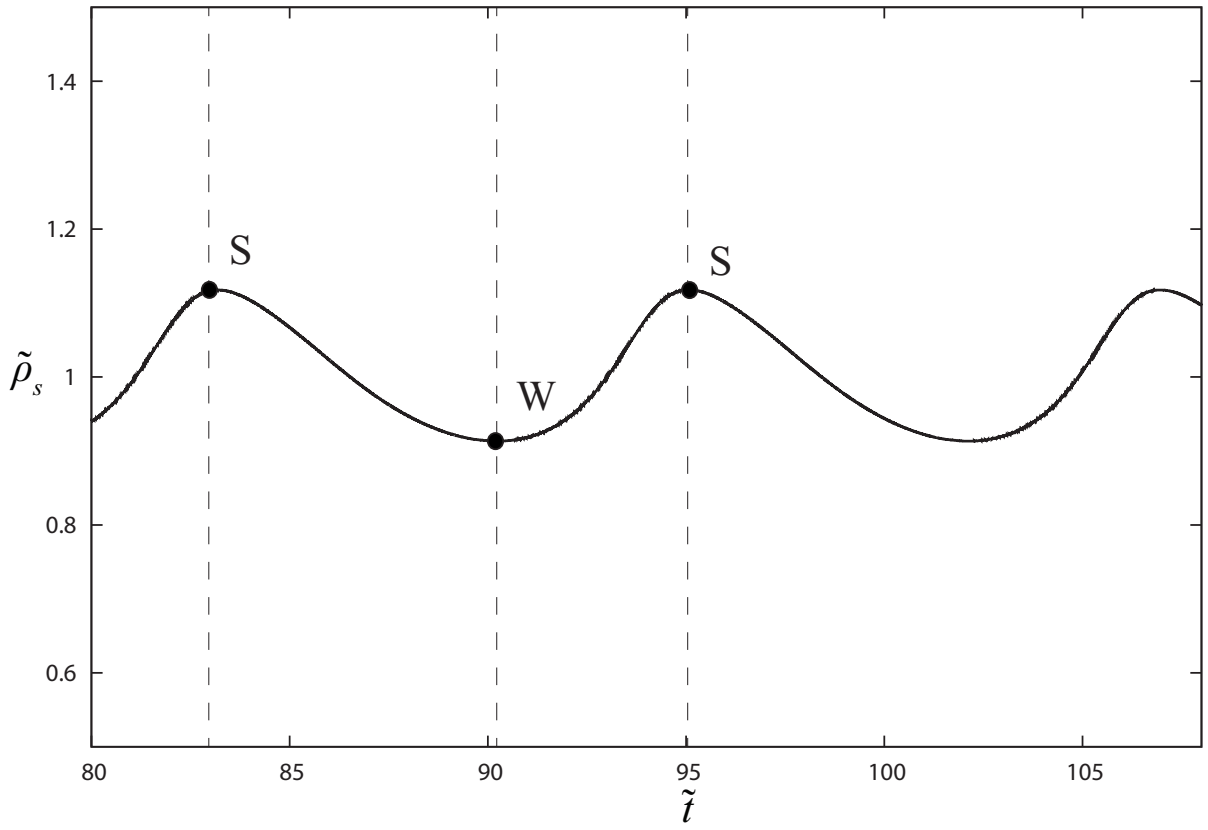

Figure 4.5: Plot of the nondimensional shock stength over time for the oscillation cycle shown in Fig. 4.4. The points of the strongest shock (S) and weakest shock (W) are indicated by the dashed lines.

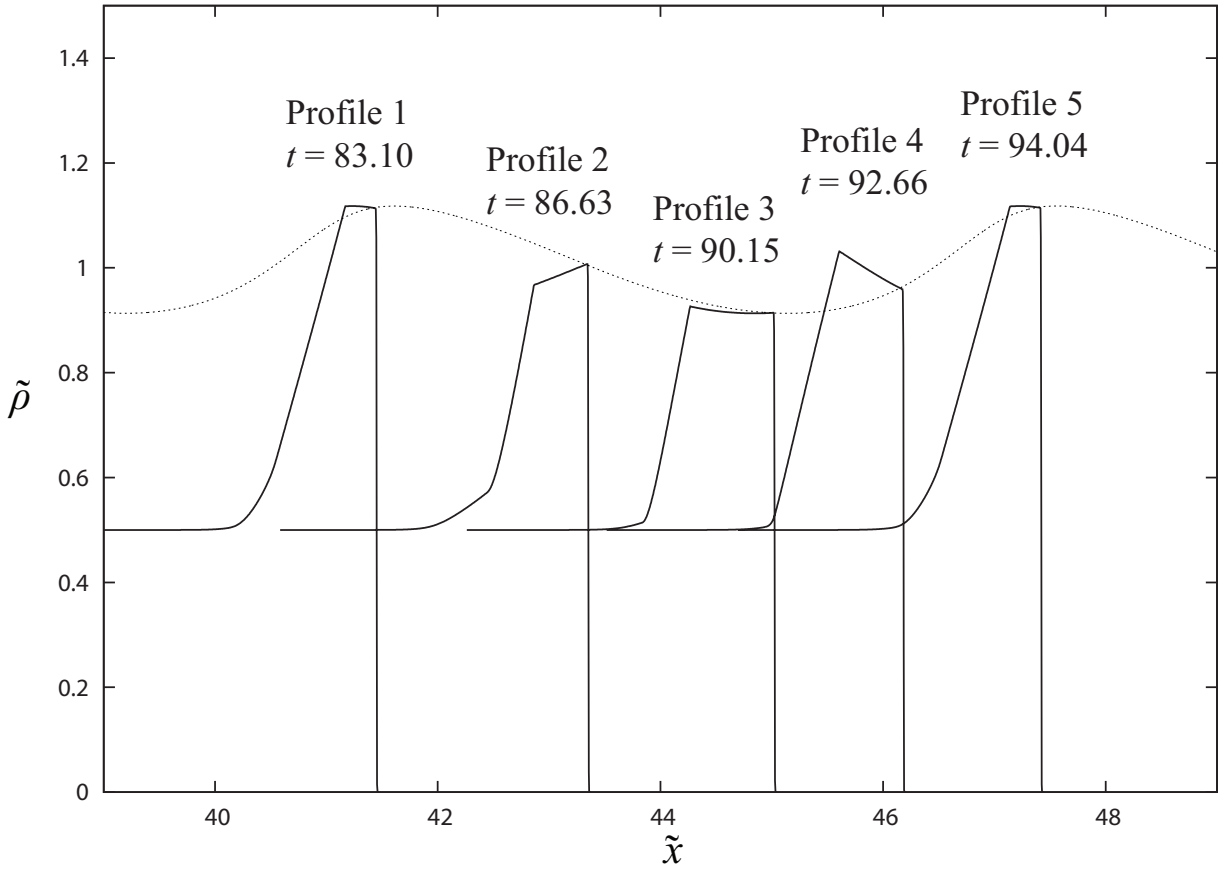

Figure 4.6: The density across the detonation structure is shown plotted at five snapshot (1-5) in time as it propagates down the 1D channel during the oscillation cycle seen in Figs. 4.4 and 4.5. The dashed line is a trace of the path of the front shock density during oscillation as the detonation propagates through the channel.

The modulation of the induction time by the shocked state can be seen from Fig. 4.4. At points where the shock is the strongest ("S") the induction times described along the particle paths ("P") are the shortest. Likewise, the weakest shocks ("W") yield the longest induction times. This modulation of the induction times and subsequent energy release in the reaction zone are what affects the acceleration and deceleration of the lead shock during the unstable pulsations.

The amplification stage of the lead shock corresponds to the arrival of pressure waves that have traveled in phase with the energy release reaction zone, where the pressure wave characteristics are almost parallel to the reaction zone band. Likewise, the deceleration phase corresponds to when the less amplified pressure waves, which have traveled out of phase with the energy release, reach the lead shock. Waves which travel in phase with the reaction zone amplify more from their longer exposure to the energy release, and communicate an acceleration to the lead shock. Since this occurs during the lead shock amplification stage, the feedback accentuates the amplification. Similarly, a decelerating shock provides a feedback between the forward pressure waves and energy release which continues to weaken the front shock. In our system, the pressure wave amplification can be obtained by integrating Equation 2.8 at a constant reaction rate r, which shows that the amplification of a pressure wave is proportional to the residence time of the wave in the energy release zone. The induction zone duration controlling the onset of the reaction and energy release is seen to be affected by the local density (Equation 2.10). Thus, the amplified pressure waves from the reaction zone travel forward through the induction zone to amplify the shock front, and reduce the induction time altering the motion of the reaction zone in or out of phase with future pressure waves. So, during the amplification stage, it is the coupling of the pressure waves becoming amplified, and their subsequent modification of the induction time and reaction zone phase, which causes the acceleration of the shock front and detonation. This feedback mechanism is what causes the detonation to be drawn away from stability, either in acceleration or in deceleration.

The overall pulsating dynamic, of regular acceleration and deceleration, can be seen by linking the feedback amplification with a restoring mechanism. Following an acceleration stage (Fig. 4.4), the forward characteristics emanating from the rear of the reaction zone just clip the reaction zone. They obtain some small amplification and form an expansion wave ("E"), shown in the characteristic diagram as a diverging fan of forward characteristics. The expansion wave immediately following the compression waves weaken the shock front and provide the restoring mechanism for the instability. In this way the pulsations are caused by a series of compression and expansion waves.

Chapter 5

Acceleration Phase

The acceleration phase of the pulsations take place when the shock front starts to get reinforced by the amplified waves emanating from the reaction zone, and the whole detonation structure accelerates forward. This behaviour is clarified through examining the case of piston-initiated shock-induced ignition. In this case an inert shock causes a fluid to react, and is then accelerated by the energy release to eventually amplify into a detonation.

In the study of this problem we nondimensionalize our system in the manner shown in Appendix A, where density is scaled by the initial shocked density, and the time and position are scaled by the induction time to ignition. Quantities with tildes are nondimensional quantities. We study the effect of the two factors: the ratio of induction to reaction time $\tilde{K}$ which sets the energy release rate in relation to the induction time, and the inverse activation energy $\tilde{\epsilon}$ which controls the sensitivity of the induction time to density. We keep the other parameters constant at $\tilde{Q}$=1, ν=0.5. These factors have been seen to play an important role in controlling the unstable detonation dynamics (Short & Sharpe, 2003; Ng *et al.*, 2005*b*; Leung *et al.*, 2010), and we hope to clarify how they affect the amplification behaviour of detonations.

We numerically model our shock-induced ignition problem by a 1D channel of unreacted material ($\lambda_i = 1, \lambda_r = 0, \tilde{\rho} = 0$) into which a piston located at the entrance of the channel sends an inert shock with $\tilde{\rho} = 1, \lambda_i = 1, \lambda_r = 0$. The piston travels at constant velocity and its path is fixed at $\tilde{x} = 0$ in the Lagrangian frame of reference. This corresponds to a shock of speed $\frac{1}{2}$ propagating into the channel followed by a constant state of $\tilde{\rho} = 1$. We used a grid resolution of 1600 points per unit length.

The acceleration behaviour is described in the characteristic diagram in Fig. 5.1 for $\tilde{K} = 0.2, \tilde{\epsilon} = 0.2$. This diagram is not taken in the same frame of reference as our previous characteristic figure following a stable detonation. Figure 5.1 follows our model's

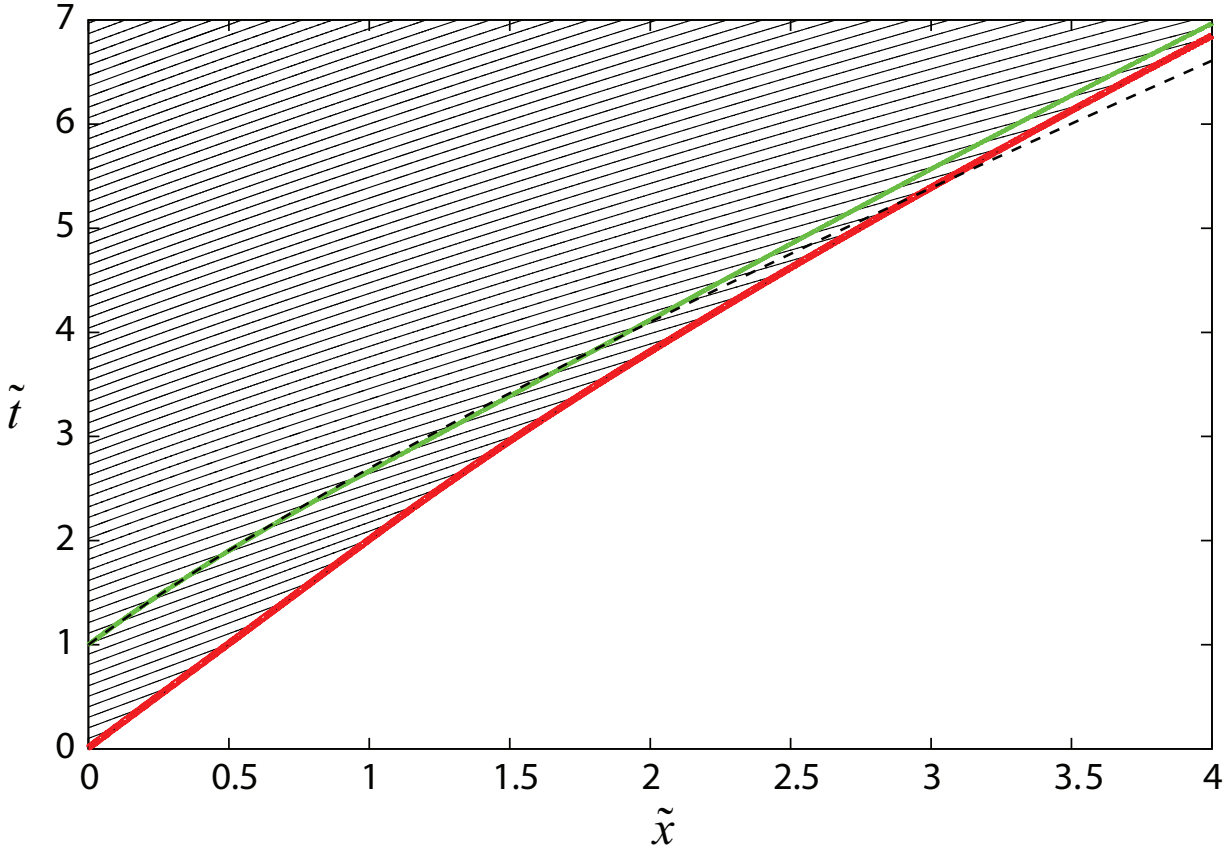

Figure 5.1: Characteristic $\tilde{t} - \tilde{x}$ plot of the acceleration process for $\tilde{K} = 0.2, \tilde{\epsilon} = 0.2$; the red line represents the main shock front $\tilde{t}_s(x)$, the green line represents the fire trajectory $\tilde{t}^*(x)$; the solid lines are $C+$ pressure wave characteristics; the broken line is the analytical prediction for the fire trajectory given by Equation 5.18

Lagrangian frame of reference in which the particle paths are stationary vertical lines (not shown in figure). The trajectories of the leading shock, the onset of energy release (henceforth called 'fire'), and the internal pressure waves are shown in the $\tilde{t} - \tilde{x}$ characteristic diagram. Initially, an inert shock propagates through the channel, then the fire occurs at $\tilde{t} = 1$ and the first pressure waves are emitted from the reaction zone. The subsequent solution consists of an accelerating shock and fire, which provide an amplification to the leading shock.

5.1 Amplification mechanism

The amplification behaviour during this acceleration phase can be clarified through the simplified characteristic sketch in Fig. 5.2 showing the early transient dynamics.

The pressure waves become amplified though the reaction zone and travel forward through the induction zone to reach and accelerate the shock front. However, as the pressure waves transition through the induction zone, they compress the post-shock material and reduce the induction delay along subsequent particle paths. This accelerates the path of the fire to be in phase with future pressure waves and increases the pressure wave's residence time in the reaction zone. These more amplified pressure waves then propagate forward to further alter the induction delay time and fire to be in phase with the pressure waves, eventually meeting with and amplifying the shock front. It is this feedback between the pressure waves propagating forward and the modification of the induction delay which modulates the amount of amplification.

5.2 Influence of $\tilde{\epsilon}$ and $\tilde{K}$ on Detonation Dynamics

We examine the effect of the reaction parameters $\tilde{\epsilon}$ and $\tilde{K}$ on the amplification process and detonation dynamics. The parameter $\tilde{\epsilon}$ is the inverse activation energy controlling the sensitivity of the induction reaction rate to density, given by Equation A.12. $\tilde{K}$ is the ratio of induction to reaction times and controls the rate of energy release from the reaction zone in relation to the induction rate as given by Equation A.13. We vary both these parameters in our numerical piston-initiated shock-induced ignition simulation and examine the amplification behaviour.

When $\tilde{K}$ is increased the energy release occurs faster and there is a more coherent amplification of the pressure waves residing in the reaction zone. So, keeping $\tilde{\epsilon} = 0.2$ as above and increasing $\tilde{K}$ to a value of 2 provides a more rapid amplification, as shown in Fig. 5.3, where we can see the path of the fire is more quickly accelerated from the stronger feedback occurring. We can as well see that the shock front becomes more strongly amplified by the pressure waves once they reach the shock front and more strongly alter its path, signifying a sudden acceleration. Additionally, the internal dynamics have changed such that the stronger amplification has caused an internal shock to form inside the induction zone. We can see the pressure waves converge more strongly and meet up, signifying the formation of an internal shock. The subsequent motion of the internal shock and fire are now in phase, and propagate quasi-steadily. The model thus recovers the internal reaction wave dynamics observed experimentally (Strehlow, 1968) and for the reactive Euler equations

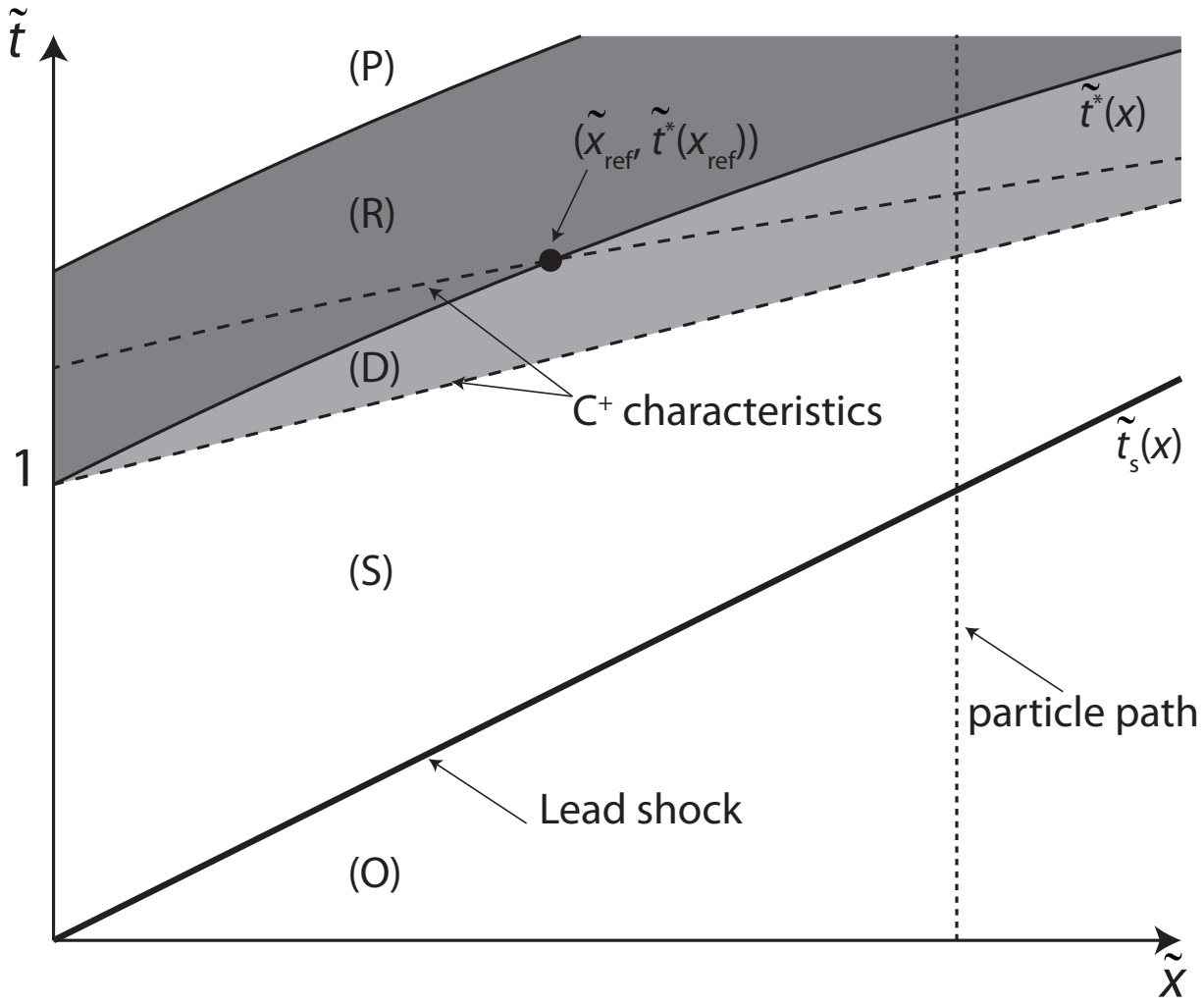

Figure 5.2: Space-time diagram illustrating the run-away process at early times. A $C+$ pressure wave originating at the piston ($\tilde{x} = 0$) amplifies while traveling through the reaction zone (R). Its emergence into the induction zone modifies the post shock state from (S) to a (D). This shortens the ignition delay ($\tilde{t}^* - \tilde{t}_s$). The shorter ignition delay in turn provides a more coherent amplification of $C+$ pressure waves in the reaction zone. Zones (O) and (P) denote the initial and product states, respectively.

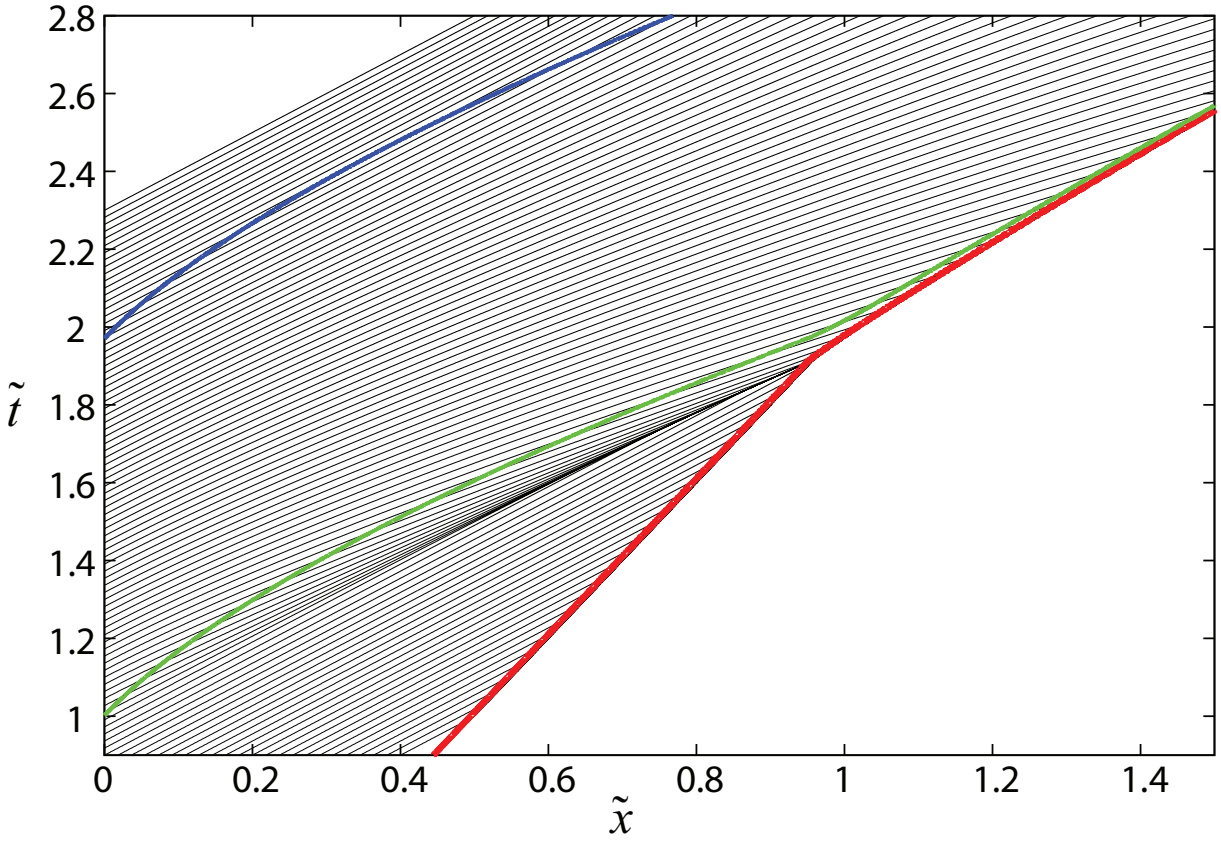

Figure 5.3: Characteristic $\tilde{t} - \tilde{x}$ plot of acceleration process for $\tilde{K}$=2, $\tilde{\epsilon}$=0.2; same legend as with Fig. 5.1, additionally with blue line representing the end of the reaction layer.

(Sharpe, 2002), where both subsonic and supersonic waves can be established internally. The supersonic waves occur when the initial acceleration of the fire is sufficiently large.

A further increase in the rate of energy release rate $\tilde{K}$ leads to a more prompt amplification of the pressure waves. In Fig. 5.4 $\tilde{K}$ is increased to 5. The internal shock wave now forms earlier. The stronger compression brought by the pressure waves through the induction zone now gives rise to a significant reduction in the induction delay. Note that, though the induction zone appears to be reduced to zero length and that the path of the fire appears to intersect with the shock front, this is only an artifact of the resolution of the plot, and there is actually a finite induction zone length. From the increased induction zone alteration, the fire now becomes more in phase with the internal shock motion and the two slowly accelerate. The internal wave that is produced takes the form of a quasi-stable weak internal detonation. It is not self-sustaining as its trajectory is set by the completion of the induction delay. For reference, a CJ internal wave propagating into the induction

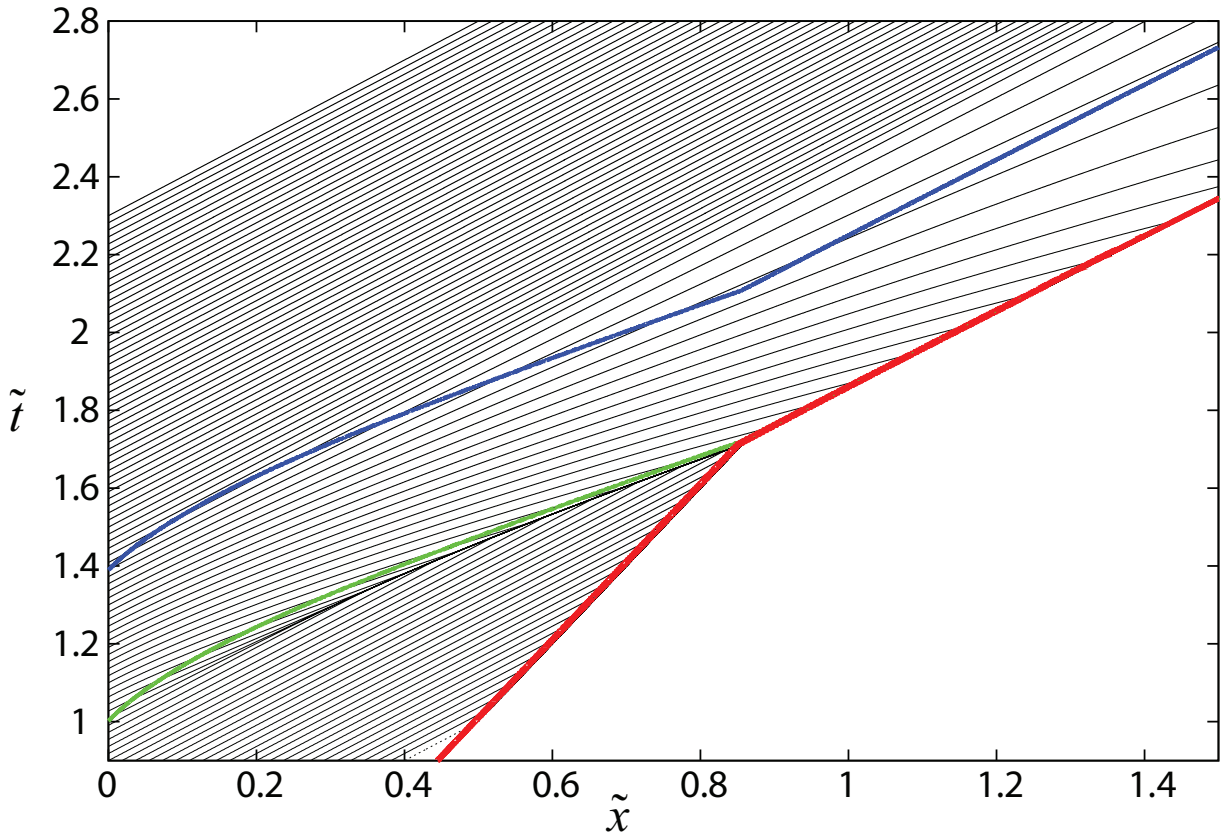

Figure 5.4: Characteristic $\tilde{t} - \tilde{x}$ plot of acceleration process for $\tilde{K}$=5, $\tilde{\epsilon}$=0.2; same legend as for Fig. 5.3.

zone material (with $\tilde{\rho} = 1$) would have a speed of 2 (Fickett, 1985b). Instead, we find that the speed of this internal detonation wave is approximately 1.5 when it encounters the leading shock. For even larger values of $\tilde{K}$, we see the same evolution, where the internal weak detonations take on velocities higher than the corresponding CJ values. Increasing the value of $\tilde{K}$ augments the reaction rate in relation to the induction rate to directly cause stronger compression waves to form. Higher $\tilde{K}$ also increases the role that feedback amplification plays, and we see faster acceleration of the fire and stronger internal shocks develop.

We also examine the effect of $\tilde{\epsilon}$ on the dynamics. Lower values of $\tilde{\epsilon}$ makes the induction delay time become more affected by the pressure waves traversing the induction zone and compressing the material there. For low $\tilde{\epsilon}$ (i.e., high activation energy), the induction delay can be significantly reduced.

We examine the case for $\tilde{K} = 2$ (refer to Fig. 5.3 for comparison) but reduce $\tilde{\epsilon}$ by half to $\tilde{\epsilon} = 0.1$ as seen in Fig. 5.5. We can see that the induction delay is reduced more by the pressure waves traversing into the induction zone, and that the path of the fire accelerates to a greater degree. This indicates a stronger amplification, and we see the formation of a stronger internal shock. The lowering of the induction delay puts the fire more in phase with the pressure waves and serves to increase the amount of feedback between them. For higher values of $\tilde{\epsilon}$, the opposite occurs, and we see a reduced alteration to the induction delay time, and a weaker acceleration of the fire (Fig. 5.6). Thus, lower $\tilde{\epsilon}$ increases the feedback mechanism and strengthens the amplification that occurs, while higher $\tilde{\epsilon}$ weakens the feedback and reduces the amplification.

Both of these factors $\tilde{K}$ and $\tilde{\epsilon}$ are shown to play an important part in the amplification process which affects the stability of detonations, as clearly demonstrated through our simple model based on Fickett's detonation analogue.

5.3 Analytical solution

Using our simplified model we are able to describe an analytical solution by using a high activation energy analysis to predict the path of the fire representing the amount of amplification occurring (this analysis has now also been published (Tang & Radulescu, 2012)). A larger acceleration of the onset of reaction means that it is drawn more in phase with the pressure waves, and a stronger feedback amplification occurs. We can use this approach to show more definitively the effect of both $\tilde{\epsilon}$ and $\tilde{K}$ on the amplification process and dynamics of detonations.

We can approach our system mathematically and apply an asymptotic analysis to

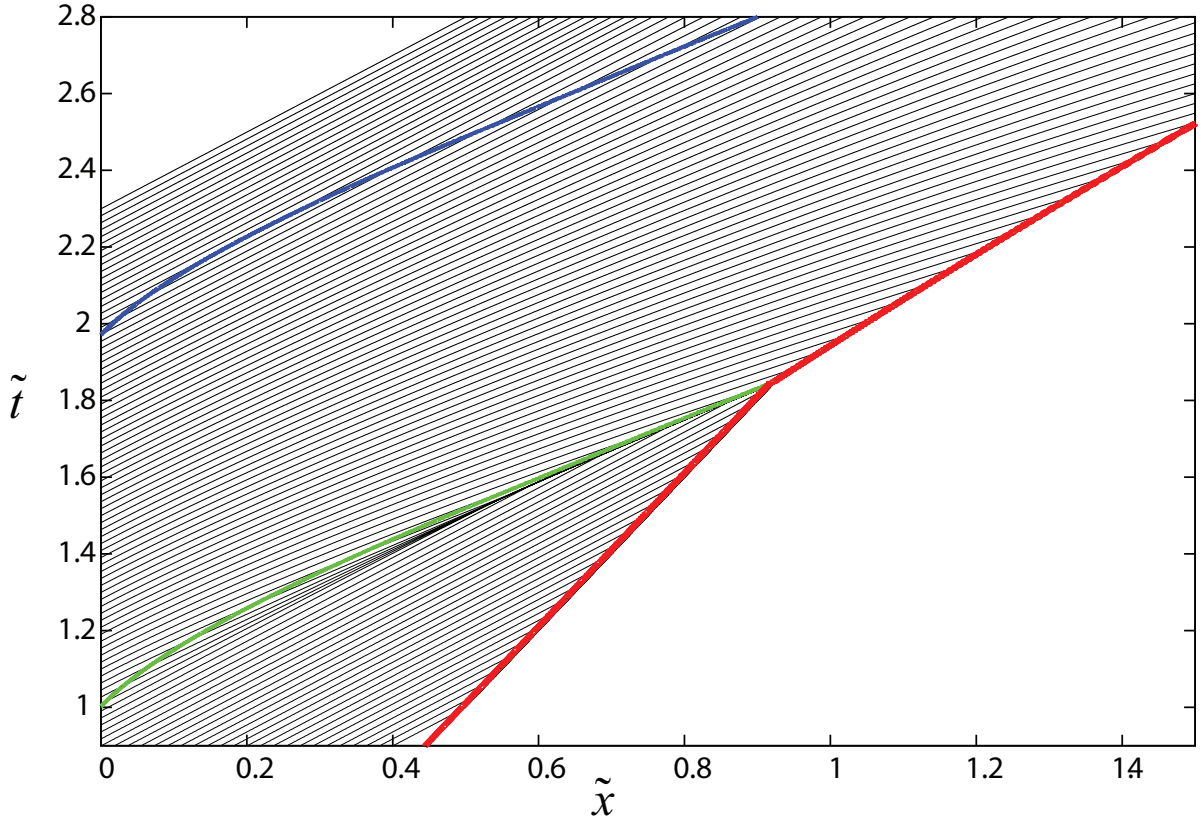

Figure 5.5: Characteristic $\tilde{t} - \tilde{x}$ plot of acceleration process for $\tilde{K} = 2$, $\tilde{\epsilon}$=0.1; same legend as for Fig. 5.3.

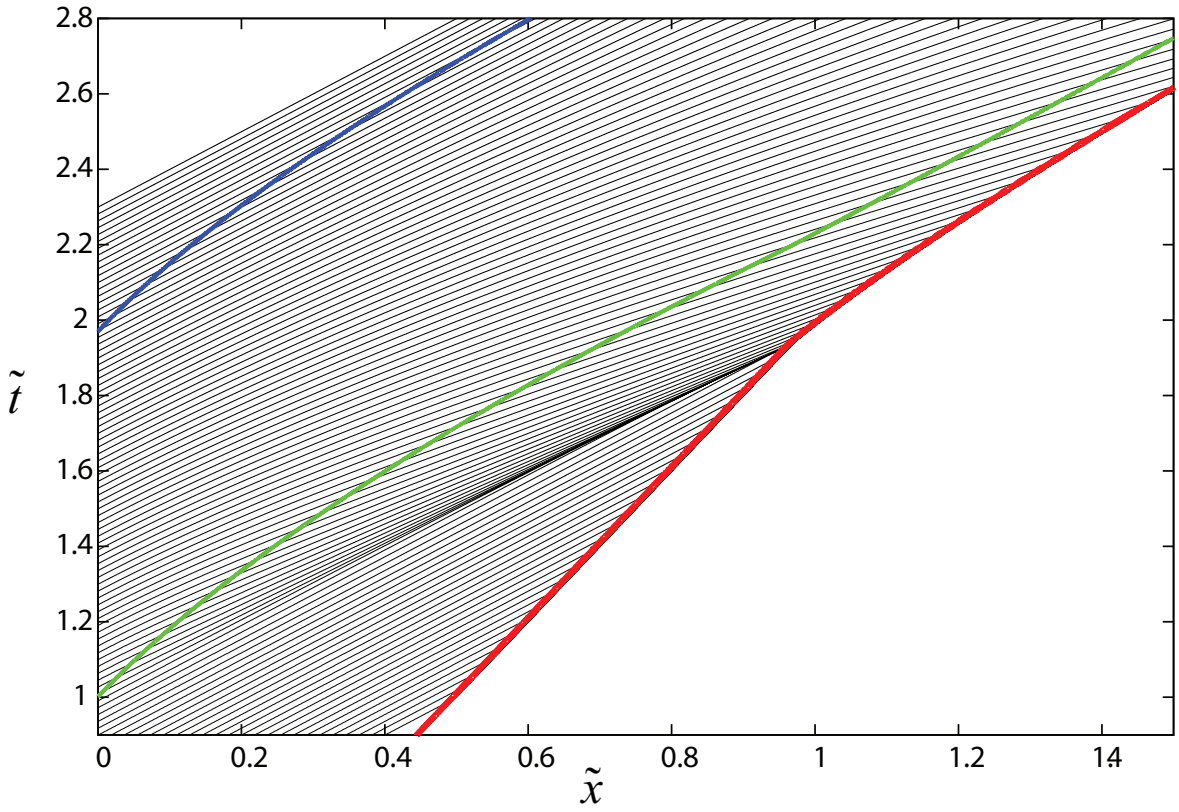

Figure 5.6: Characteristic $\tilde{t} - \tilde{x}$ plot of shock initiation for $\tilde{K} = 2$, $\tilde{\epsilon}$=0.4; same legend as for Fig. 5.3.

the early transient dynamics (before the first pressure waves from the reaction zone alter the shock front). We are interested in describing the path of the fire which represents the amount of amplification occurring, which we now denote as $\tilde{t}^*(\tilde{x})$. The asymptotic analysis assumes a large activation energy (i.e., $\tilde{\epsilon} << 1$). The framework is similar to that used by Sharpe (2002) for the reactive Euler equations.

We assume that the energy release rate is slow, i.e.,

$$\beta \equiv \frac{\tilde{K}}{\tilde{\epsilon}} = O(1) \tag{5.1}$$

This makes the solution accurate on time scales of order unity (i.e., induction time scales). We expand the density, reaction progress variable, and fire path in the form:

$$\tilde{\rho}(\tilde{x},\tilde{t}) = \tilde{\rho}_1(\tilde{x},\tilde{t}) + \tilde{\epsilon}\tilde{\rho}_2(\tilde{x},\tilde{t}) + O(\tilde{\epsilon}^2) \tag{5.2}$$

$$\lambda_r(\tilde{x},\tilde{t}) = \lambda_{r1}(\tilde{x},\tilde{t}) + \tilde{\epsilon}\lambda_{r2}(\tilde{x},\tilde{t}) + O(\tilde{\epsilon}^2) \tag{5.3}$$

$$\tilde{t}^*(\tilde{x}) = \tilde{t}_1^*(\tilde{x}) + O(\tilde{\epsilon}) \tag{5.4}$$

We substitute these expansions (Equations 5.2, 5.3, 5.4) into the governing equations (Equations A.11, A.13, A.12) and into the boundary conditions (channel is initially at $\tilde{\rho}(\tilde{x},\tilde{t}=0) = 0, \lambda_r(\tilde{x},\tilde{t}=0) = 0, \lambda_i(\tilde{x},\tilde{t}=0) = 1$. Inlet wall boundary condition set to constant velocity piston at $\tilde{\rho}(\tilde{x}=0,\tilde{t}) = 1$). We can then solve for our leading order solution:

$$\tilde{\rho}_1(\tilde{x},\tilde{t}) = 1 \tag{5.5}$$

$$\lambda_{r1}(\tilde{x},\tilde{t}) = 0 \tag{5.6}$$

$$\tilde{t}_1^*(\tilde{x}) = 1 + 2\tilde{x} \tag{5.7}$$

This solution corresponds to the inert solution of a piston driven shock wave.

With the $O(1)$ solution obtained, the $O(\tilde{\epsilon})$ problem to be solved is:

$$\frac{d}{d\tilde{t}}\left(\tilde{\rho}_2 + \lambda_{r2}\frac{\tilde{Q}}{2}\right) = \frac{1}{2}\beta\tilde{Q} \quad \text{along} \quad \frac{d\tilde{x}}{d\tilde{t}} = 1 \tag{5.8}$$

$$\frac{d\lambda_{r2}}{d\tilde{t}} = \beta \quad \text{along} \quad \frac{d\tilde{x}}{d\tilde{t}} = 0 \tag{5.9}$$

$$\tilde{\rho}_2(\tilde{x} = 0, \tilde{t}) = 0 \tag{5.10}$$

$$\lambda_{r2}(\tilde{x}, \tilde{t} < \tilde{t}^*) = 0 \tag{5.11}$$

$$\int_{\tilde{t}_s(\tilde{x})}^{\tilde{t}^*(\tilde{x})} e^{\tilde{\rho}_2} d\tilde{t} = 1 \tag{5.12}$$

The resulting problem is one of linear acoustics. According to Equation 5.8, the forward facing pressure waves all propagate at the constant speed (of unity), but amplify at constant rate in the reaction zone due to energy release. The solution can be obtained by the method of characteristics. In the reaction zone, for $\tilde{t} > \tilde{t}^*$ (zone R in Fig. 5.2), the reaction progress variable can be immediately obtained.

$$\lambda_{r2}(\tilde{x}, \tilde{t} > \tilde{t}^*) = \beta\left(\tilde{t} - \tilde{t}^*(\tilde{x})\right) \tag{5.13}$$

Substituting Equation 5.13 into Equation 5.8 and using the order $\tilde{\epsilon}$ boundary condition (Equation 5.10), we obtain the variation of density in the reaction zone:

$$\tilde{\rho}_2 = \frac{\beta\tilde{Q}}{2}\left(\tilde{t}^*(\tilde{x}) - 1\right) \tag{5.14}$$

Once the density is known in the reaction zone, the value of density in the disturbed region D (refer to Fig. 5.2) can be found by extending the C+ characteristics into this region. In region D, $\lambda_2 = 0$ and the C+ characteristic relation (Equation 5.8) requires that density is constant along a characteristic. The constant is evaluated using Equation 5.14 at the intersection of the C+ characteristic with the path $\tilde{t} = \tilde{t}^*(\tilde{x})$. Denoting this reference position $\tilde{x}_{ref}(\tilde{x}, \tilde{t})$ (refer to Fig. 5.2), we get:

$$\tilde{\rho}_2(\tilde{x}, \tilde{t}) = \frac{\beta\tilde{Q}}{2}\left(\tilde{t}^*(\tilde{x}_{ref}(\tilde{x}, \tilde{t}) - 1\right) \tag{5.15}$$

with $\tilde{x}_{ref}$ given implicitly from the trajectory of the C+ characteristic, i.e.

$$\frac{\tilde{x} - \tilde{x}_{ref}}{\tilde{t} - \tilde{t}^*(\tilde{x}_{ref})} = 1 \tag{5.16}$$

The undisturbed post-shock zone, Region S, is bounded by the shock $\tilde{t}_s(\tilde{x}) = 2\tilde{x}$ and the first C+ disturbance originating at $(\tilde{x} = 0, \tilde{t} = 1)$, given by $\tilde{t} = 1 + \tilde{x}$. In this region, using the method of characteristics, we get $\tilde{\rho}_2(\tilde{x}, \tilde{t}) = \lambda_2(\tilde{x}, \tilde{t}) = 0$. The solution is now complete, and the integral relation (Equation 5.12) can now be written as

$$\int_{1+\tilde{x}}^{1+2\tilde{x}+\tilde{\epsilon}\tilde{t}_2*(\tilde{x})} e^{\frac{\tilde{Q}\beta}{2}\left(\tilde{t}_1^*(\tilde{x}_{ref}(\tilde{x},\tilde{t})-1\right)} d\tilde{t} - \tilde{x} = 0 \tag{5.17}$$

This expression, along with Equation 5.16, gives the trajectory of the fire $\tilde{t}^*(\tilde{x})$ implicitly. Adopting Sharpe's iterative strategy (Sharpe, 2002) to find $\tilde{t}^*(\tilde{x})$, we substitute the first order approximation $\tilde{t}_1^*(\tilde{x})$ in the integrand and solve for the correction appearing in the integral's upper bound. From the first iteration, we find the following approximation:

$$\tilde{t}^*(\tilde{x}) \approx 1 + \tilde{x} + \frac{\tilde{\epsilon}}{\tilde{Q}\tilde{K}} \ln\left(1 + \tilde{Q}\frac{\tilde{K}}{\tilde{\epsilon}}\tilde{x}\right) \tag{5.18}$$

This expression is shown plotted in Fig. 5.1. It reproduces quite accurately the acceleration of the reaction path. We can more clearly describe the acceleration if we differentiate Equation 5.18 with respect to time and evaluate it at the origin ($\tilde{x} = 0$):

$$a = \frac{1}{8}\frac{\tilde{K}}{\tilde{\epsilon}}\tilde{Q} \tag{5.19}$$

This shows us that the initial acceleration of the fire (Equation 5.19), representing the strength of the amplification, is directly related to the parameters $\tilde{K}$ and $\tilde{\epsilon}$, and as well $\tilde{Q}$. This shows how the amplification process of a detonation can be described by $\tilde{K}$ and $\tilde{\epsilon}$ together to control the detonation dynamics.

Chapter 6

Instability Modes

6.1 Period Doubling Bifurcations and Route to Chaos

We return now to our formulation from Chapter 4 modeling an initial CJ detonation propagating down a 1D channel. We increase α (at constant $\tilde{K} = 2$) further into the unstable range ($\alpha > 5.7$) to observe the change in dynamics and the existence of other oscillatory modes. We track the change in the dynamics by plotting the strength of the detonation, in terms of the nondimensional shock front density $\tilde{\rho}_s$, over time.

With increasing α the amplitude of oscillation in the shock density increases regularly as well. However, when α reaches 6.9 a period doubling bifurcation occurres and another oscillation mode is seen. This double-period solution is seen in Fig. 6.1. The peak amplitude is seen to have two values (as shown in the dashed lines) instead of having a single amplitude of oscillation. The period now includes two amplitudes instead of a single amplitude. Further increases to α lead to another bifurcation and the quadruple period solution shown in Fig. 6.2. We can see four distinct amplitudes as shown by the dashed lines in the figure.

These bifurcations continue to occur in smaller and smaller increments of α until the solution becomes chaotic and there is no longer any discernible regular period of oscillation. Evidence of true chaos, as opposed to very long periods oscillations, is due to the existence of an odd period-numbered solution (Ng *et al.*, 2005*a*) as seen in Fig. 6.3, which is regained after the even-numbered period-doubling had transitioned to chaos.

These results can be compiled into a single bifurcation diagram showing the peak amplitudes in shock density oscillation ρ_{max} (as indicated by the dashed lines in Figs. 6.1-6.3) with increasing α as shown in Fig. 6.4. The peak amplitudes are nondimensionalized ($\tilde{\rho}_{max}$) in terms of the CJ front shock density $\rho_{s,CJ}$. The bifurcation diagram created from

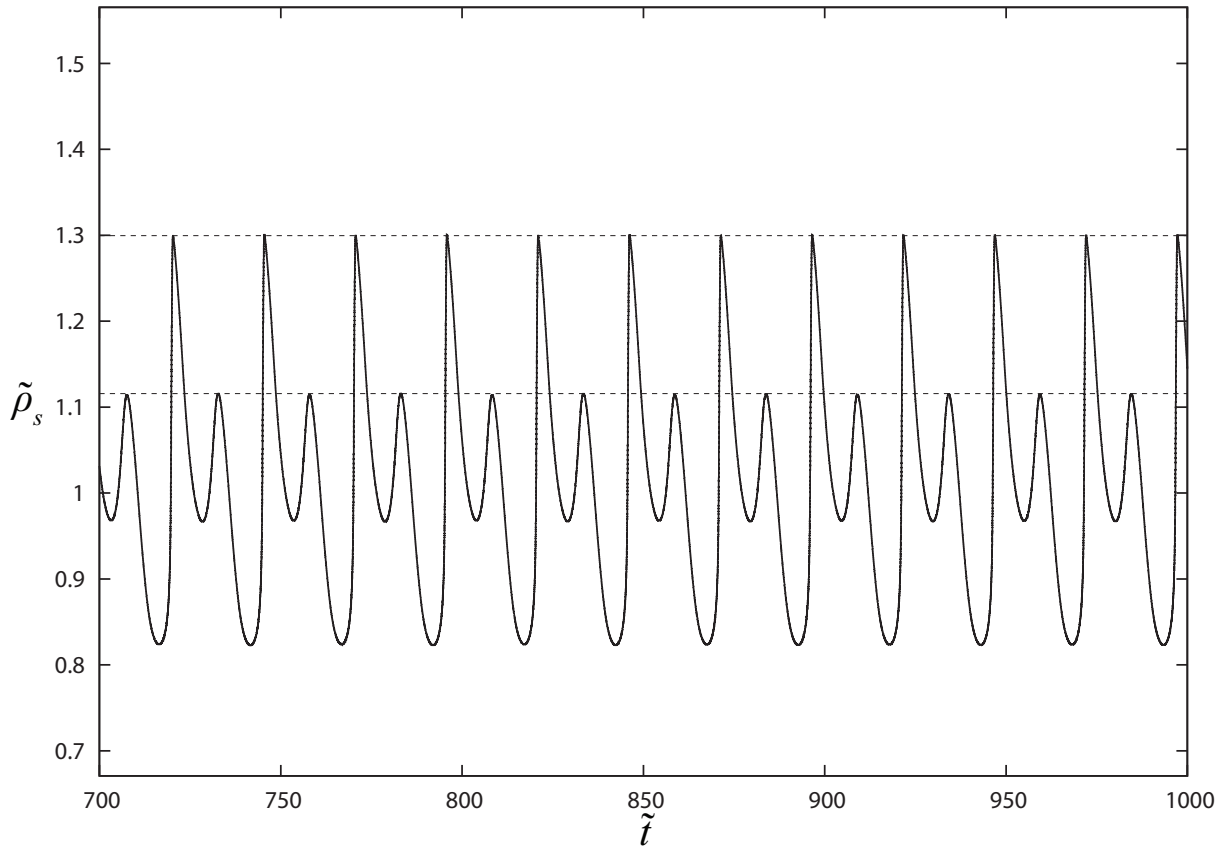

Figure 6.1: Detonation strength evolution at $\alpha = 7.6$ representing a double-period oscillatory solution as shown by the nondimensional shock peak density variation over time. The peak amplitudes that are reached are shown in dashed lines.

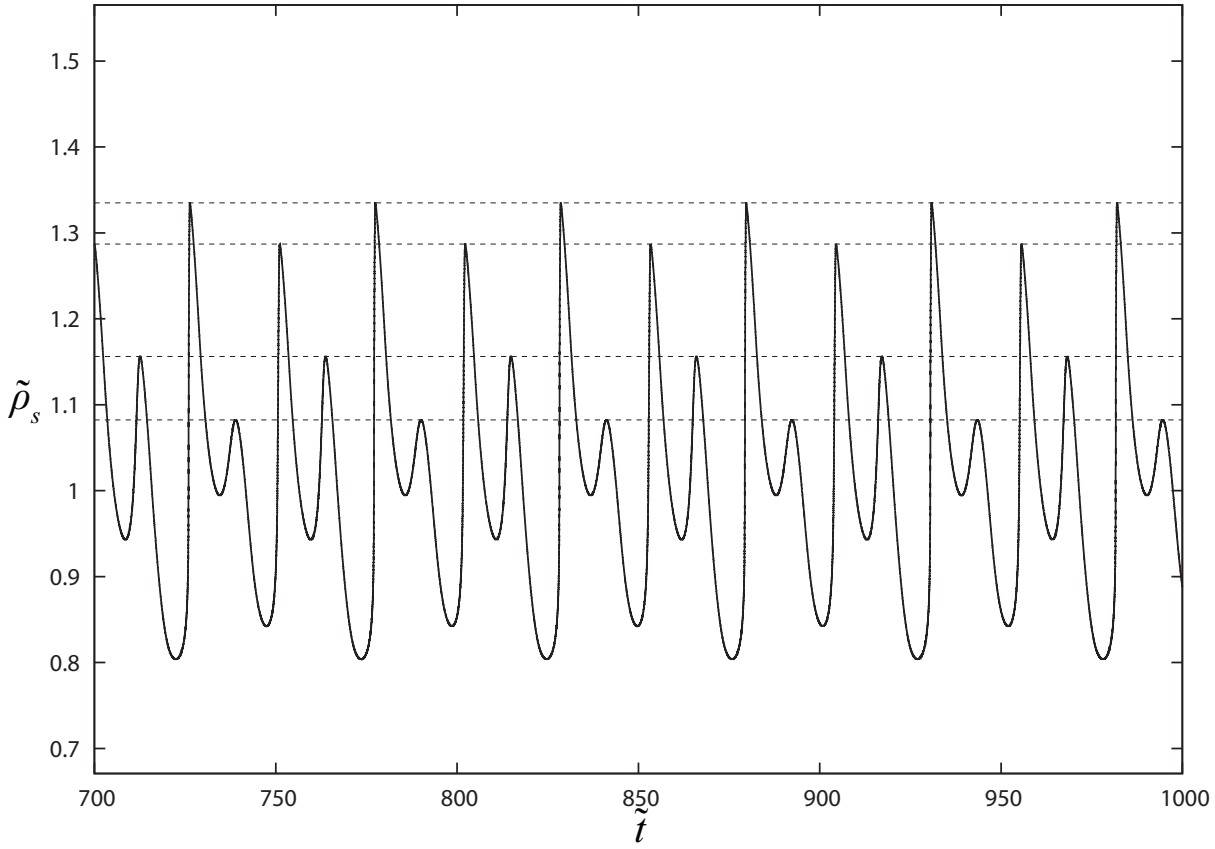

Figure 6.2: Detonation strength evolution at $\alpha = 7.8$ representing a quadruple period oscillatory solution as shown by the nondimensional shock peak density variation over time. The peak amplitudes that are reached are shown in dashed lines.

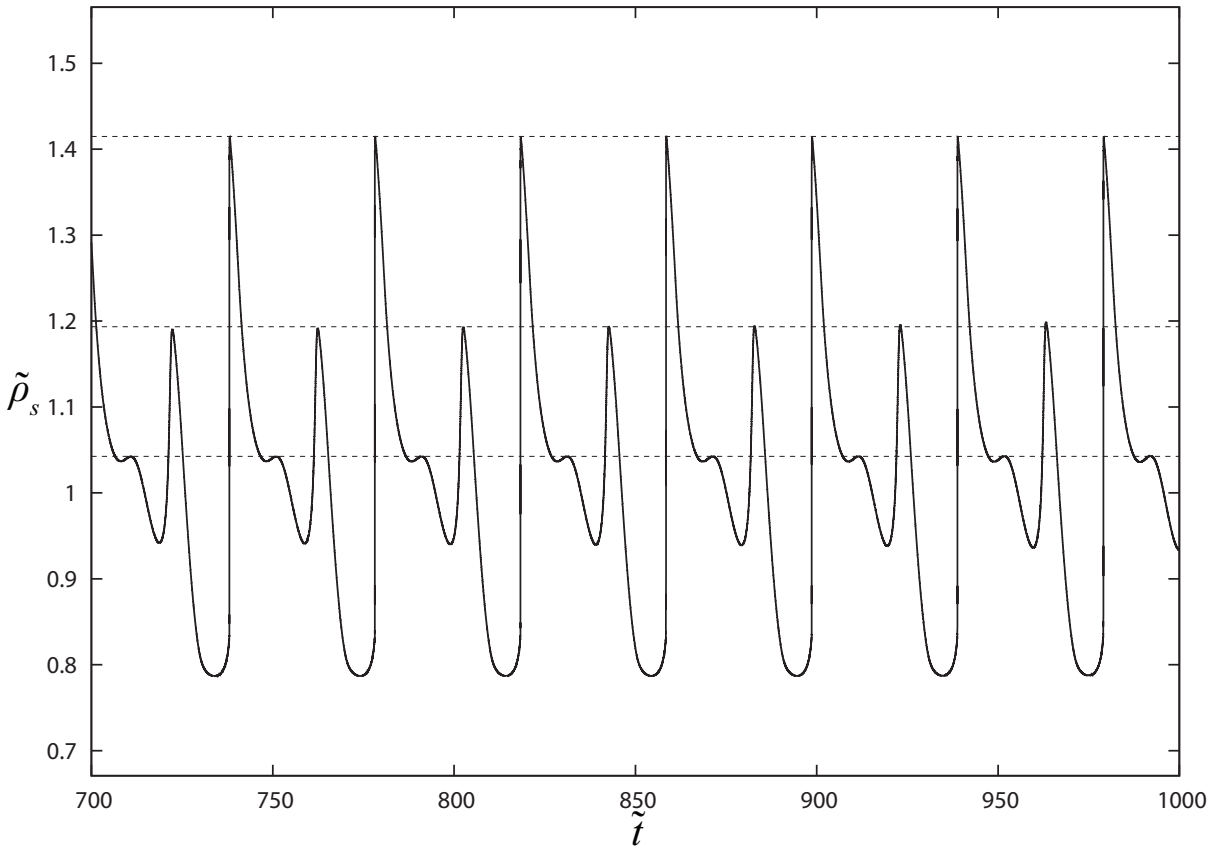

Figure 6.3: Detonation strength evolution at $\alpha = 8.72$ representing an odd numbered three period oscillatory solution as shown by the nondimensional shock peak density variation over time. The peak amplitudes that are reached are shown in dashed lines.

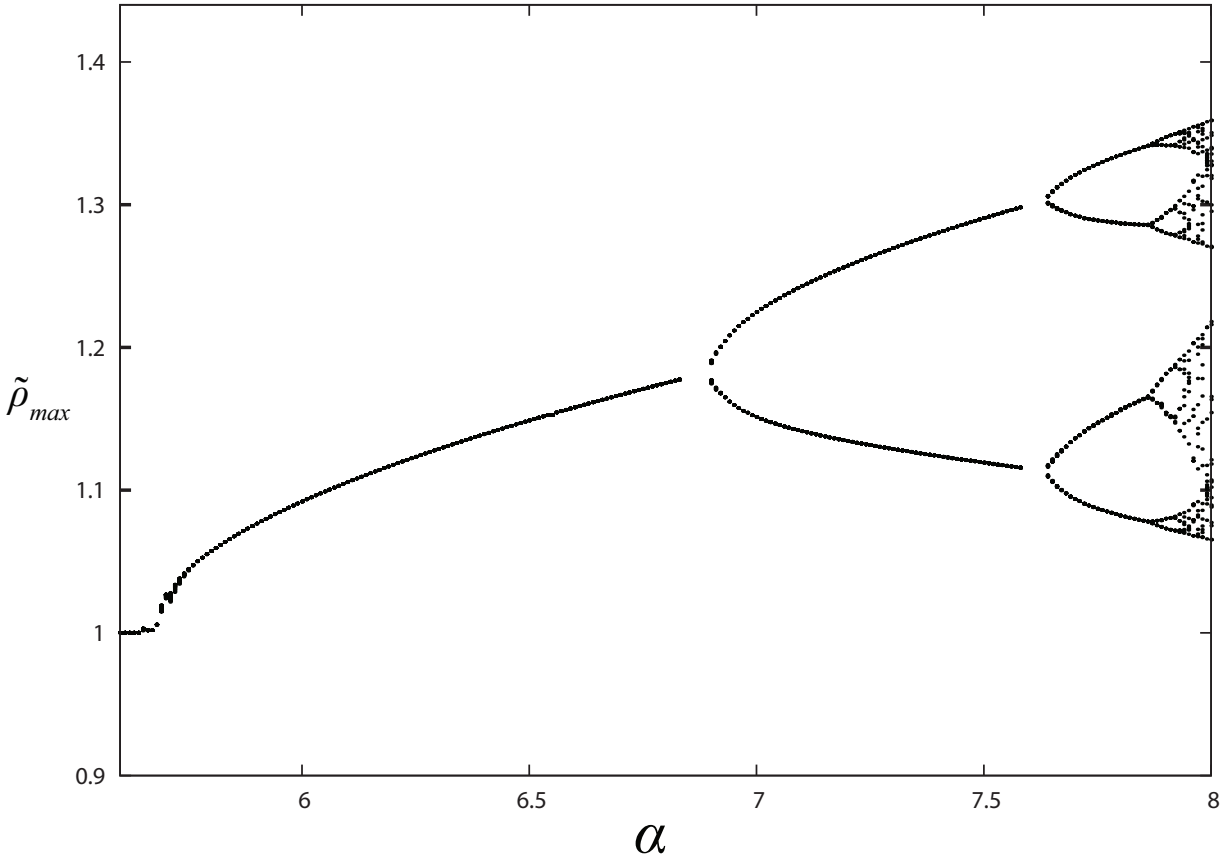

Figure 6.4: Bifurcation diagram showing the peak amplitudes in detonation strength with increasing α

our model closely resembles that obtained from the Euler equations (Fig. 1.4) where we see a similar sharp transition from stability, multiple period doubling bifurcations, and the transition to chaos with the existence of an odd-numbered solution (Fig. 6.3). The sequence of period doubling bifurcations and onset of chaos appears to follow Feigenbaum's route to chaos, which is very similar to the nonlinear dynamics of chemical detonations (Ng *et al.*, 2005*a*) and many other nonlinear systems. This clearly shows that our simple detonation model can capture this universality which is observed in the nonlinear dynamics of complex systems.

Chaos Analysis: Lorenz Map

An interesting pattern has been documented from the chaotic solution seen at higher values of α. When the peak shock densities are plotted against subsequent peak density values (i.e., for a set α, the density for an arbitrary peak (u_n) is plotted against the density

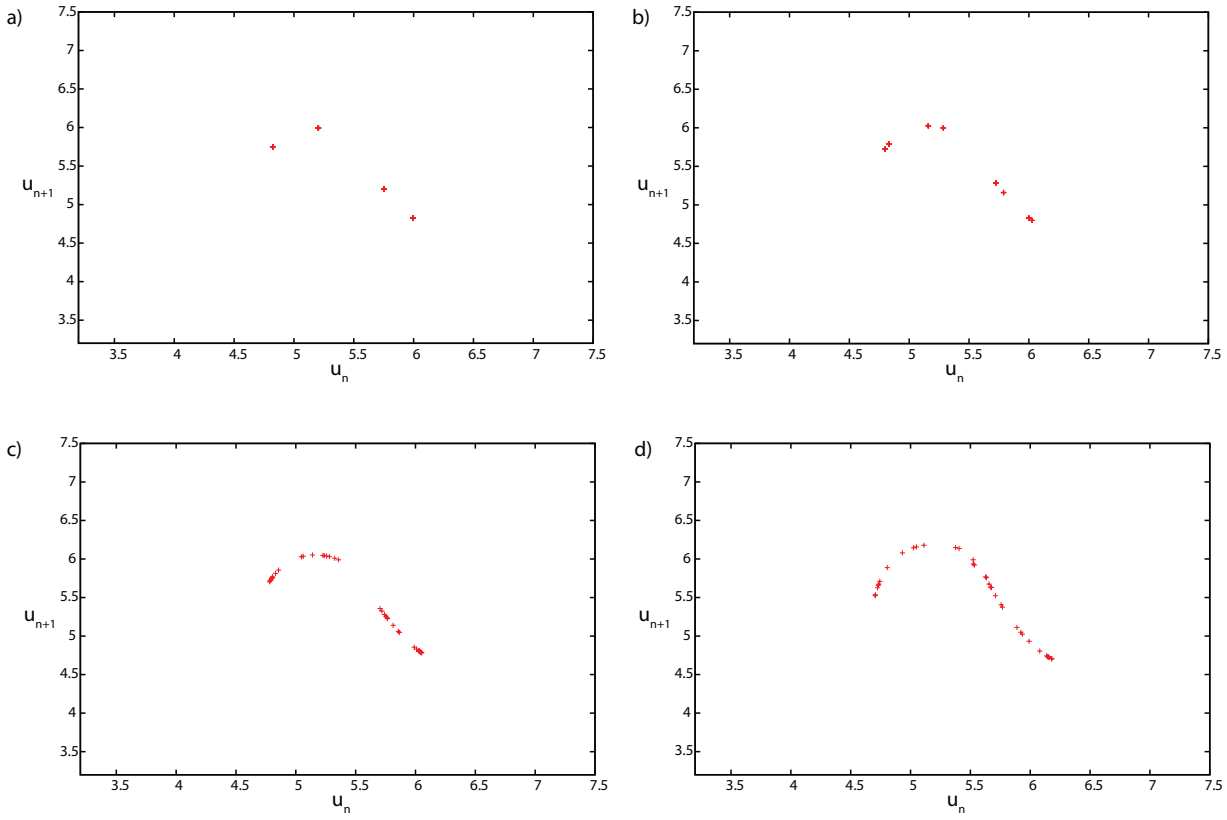

Figure 6.5: Lorenz map of successive peaks plotting for a range of alpha values from $\tilde{t} = 1000$ to $\tilde{t} = 1500$. a) Map for the 4-period solution at $\alpha = 7.85$. b) Map for 8-period solution at $\alpha = 7.90$. c) Map for chaotic solution at $\alpha = 7.95$ d) Map for chaotic solution at $\alpha = 8.20$

for the next peak (u_{n+1})) a pattern appears to form in the chaotic region. This mapping is similar to the Lorenz map for a system.

For a regular oscillation period the Lorenz map has only a set number of concentrated points following a repeating period. Seen in Fig. 6.5 a) & b) are the Lorenz maps for regular oscillation at $\alpha = 7.85$ and $\alpha = 7.90$ respectively, showing the 4 and 8 period solutions in which there are only a cluster of 4 or 8 points. As we increase α into the chaotic region, the regularity of the peaks decreases and their amplitude becomes seemingly random, and the Lorenz map begins to show a scatter of points (Fig. 6.5 c)). However, as we plot the peak-to-peak values in a Lorenz map for higher values of α further into the chaotic region, we can see a trend start to occur, (Fig. 6.5 d)) where a bell shaped curve appears. Whether this suggests that the chaotic region follows some predictable trend and what governs such a trend is left for future study.

6.2 Galloping Mode

With further increases of α past the chaotic region we reached another mode of propagation in which the detonation strength is seen to suddenly spike then die off, and the time between peaks becomes longer and irregular. This behaviour resembles the "galloping mode" seen experimentally and from the reactive Euler equations (He & Lee, 1995). This galloping mode occurs when internal shocks start to form from the rapid amplification of compression waves that occurs from the increased sensitivity of the induction zone. These internal shocks eventually meet up with and intensely amplify the detonation. The formation of an internal shock is seen in Fig. 6.6, which shows the nondimensional density distribution in the domain across the detonations structure. The variation in nondimensional front shock density over time is shown in Fig. 6.7 for this galloping mode. The galloping mode is characterized by large dips in detonation strength followed by a sudden increase in strength when the internal shock meets up with the front shock.

6.3 Quenching

As α is increased even further, another threshold value is reached in which the detonation appears to quench and a stable inert shock propagates forward propelled only by the piston boundary conditions. Figure 6.8 shows the nondimensional front shock density development at $\alpha = 50$. We can see the front shock density quickly diminishes and remains constant for long times at an apparent "quenched" state. Figure 6.9 shows the detonation density profile at the initial and quenched states. Initially we have the stable CJ solution, but the detonation strength quickly dies out into an inert piston-supported shock traveling into unreacted material.

To demonstrate that the quenched inert shock speed is decoupled from the reaction, we can evaluate the Riemann problem for burnt material traveling into unburnt material and derive the speed of the shock that would develop (Fig. 6.10). We find that the inert shock density would be $\tilde{\rho}_{ishock} = 0.71$ which is what we numerically find from our simulations.

Mathematically, we assume reignition to occur at some point, though essentially the detonation has "quenched" and there is no reaction and energy release for a very long time. We can determine the time for reignition by evaluating the induction time for our model. By integrating Equation 2.10 at the constant density of the inert shock, we can solve for the induction time:

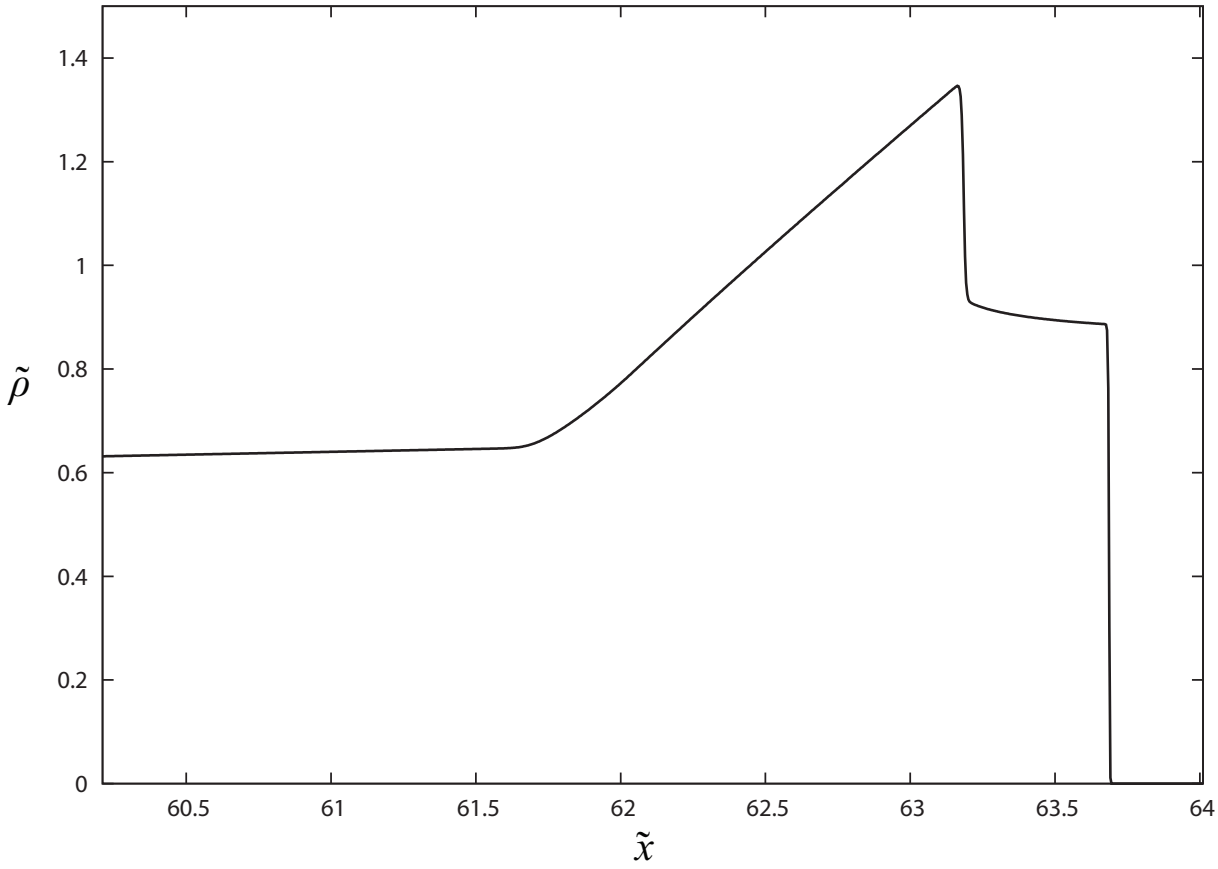

Figure 6.6: Plot of the nondimensional density across the detonation structure during the galloping mode of instability at $\tilde{K} = 2.0, \alpha = 13.0$ showing the formation of an internal shock.

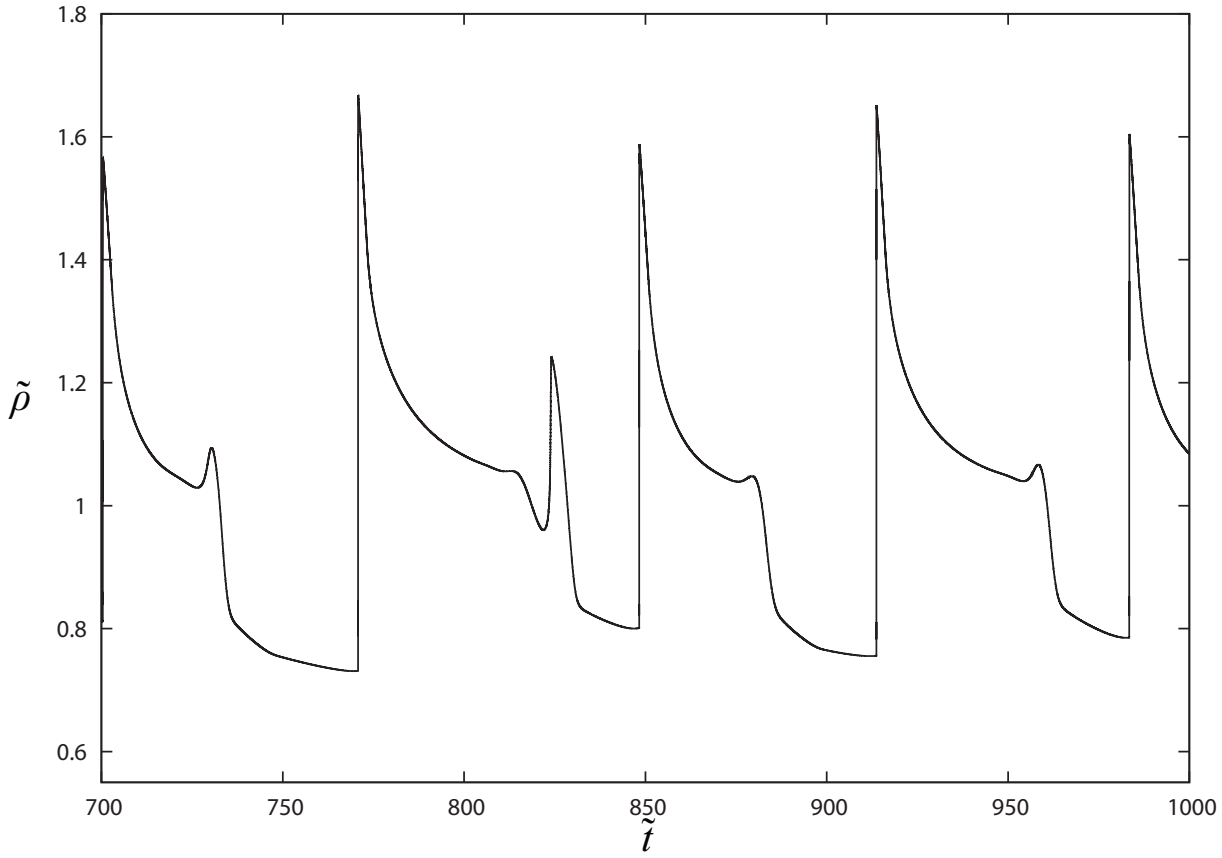

Figure 6.7: Plot of the nondimensional front shock density over time showing the galloping mode of unstable oscillation at $\alpha = 13.0$.

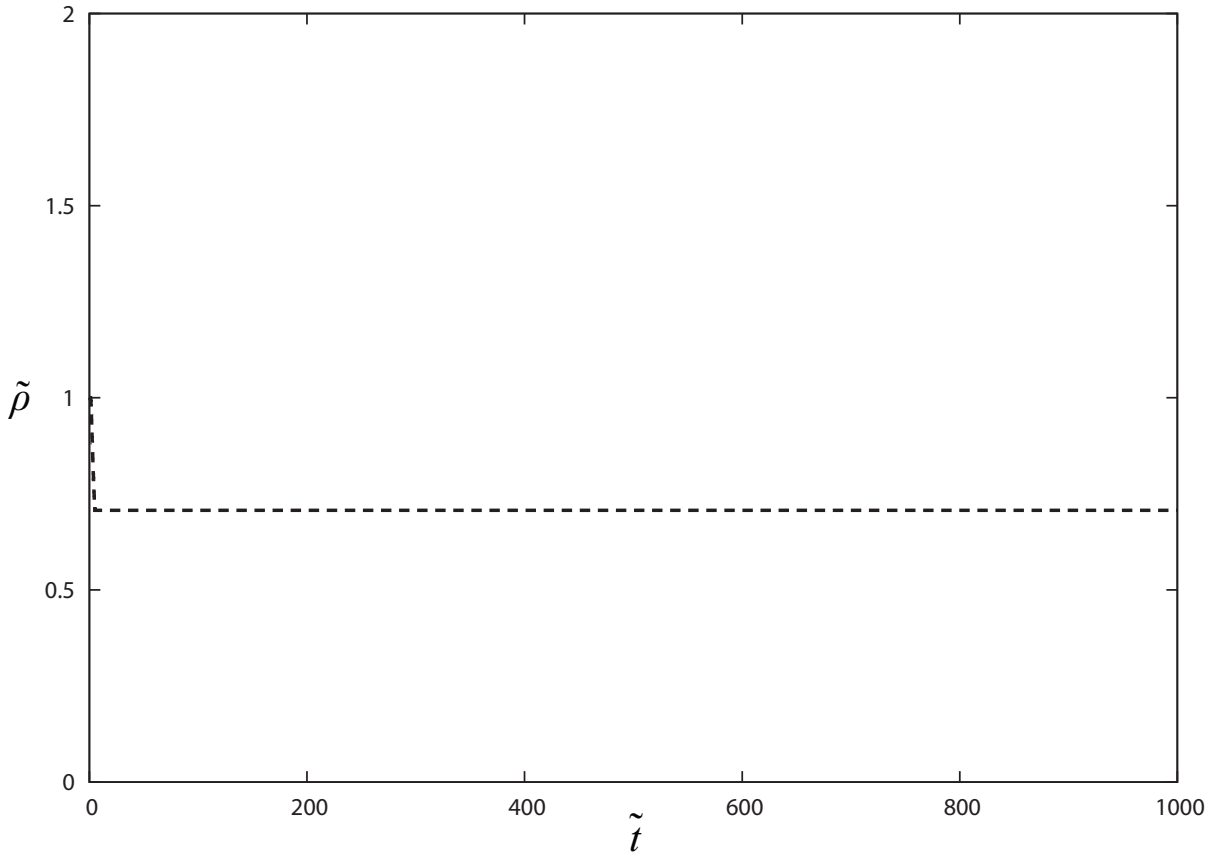

Figure 6.8: Plot of the nondimensional front shock density over time showing quenching behaviour at $\alpha = 50.0$, $\tilde{K} = 2.0$.

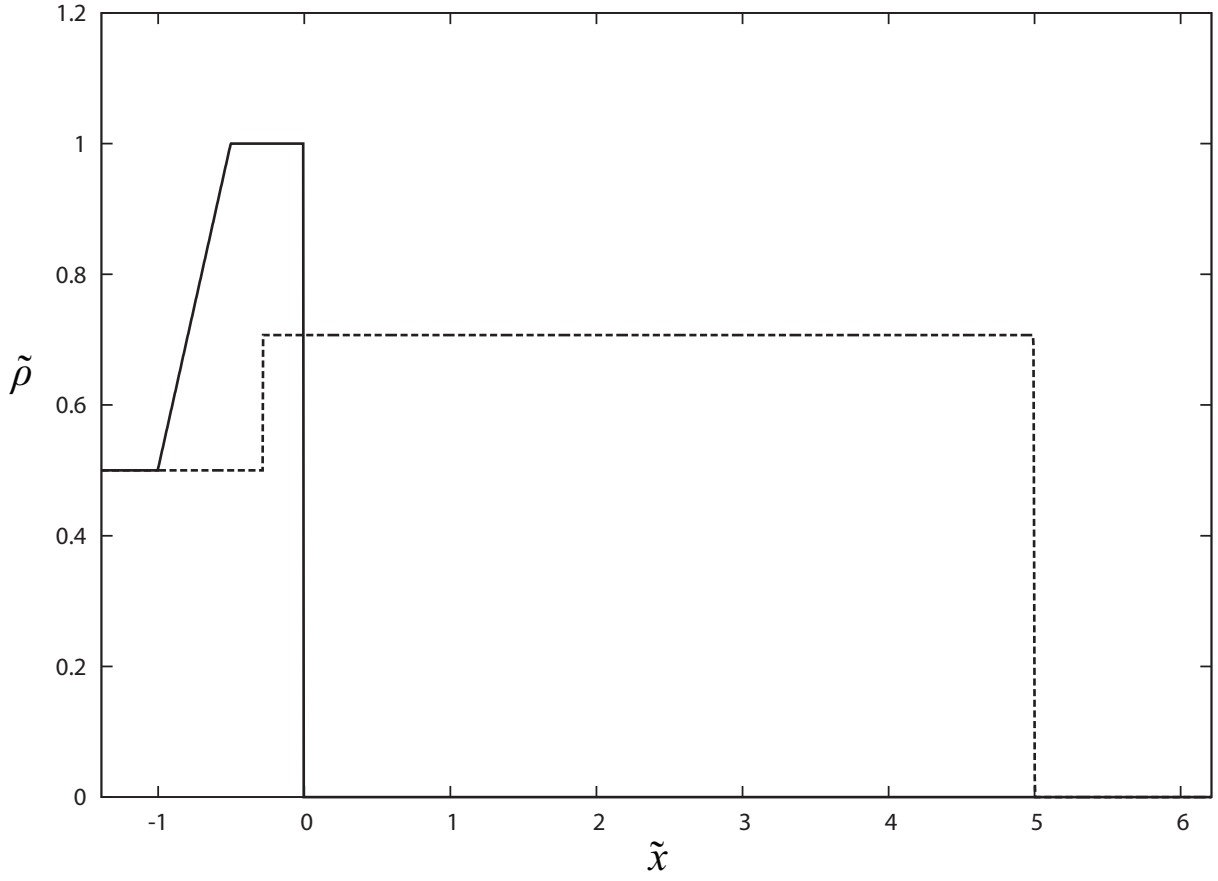

Figure 6.9: A plot of the nondimensional density distribution across the domain at two times taken at $\alpha = 50.0, \tilde{K} = 2.0$. The initial CJ detonation density profile is shown by the solid line and the quenched detonation profile at a later time is in the dashed line.

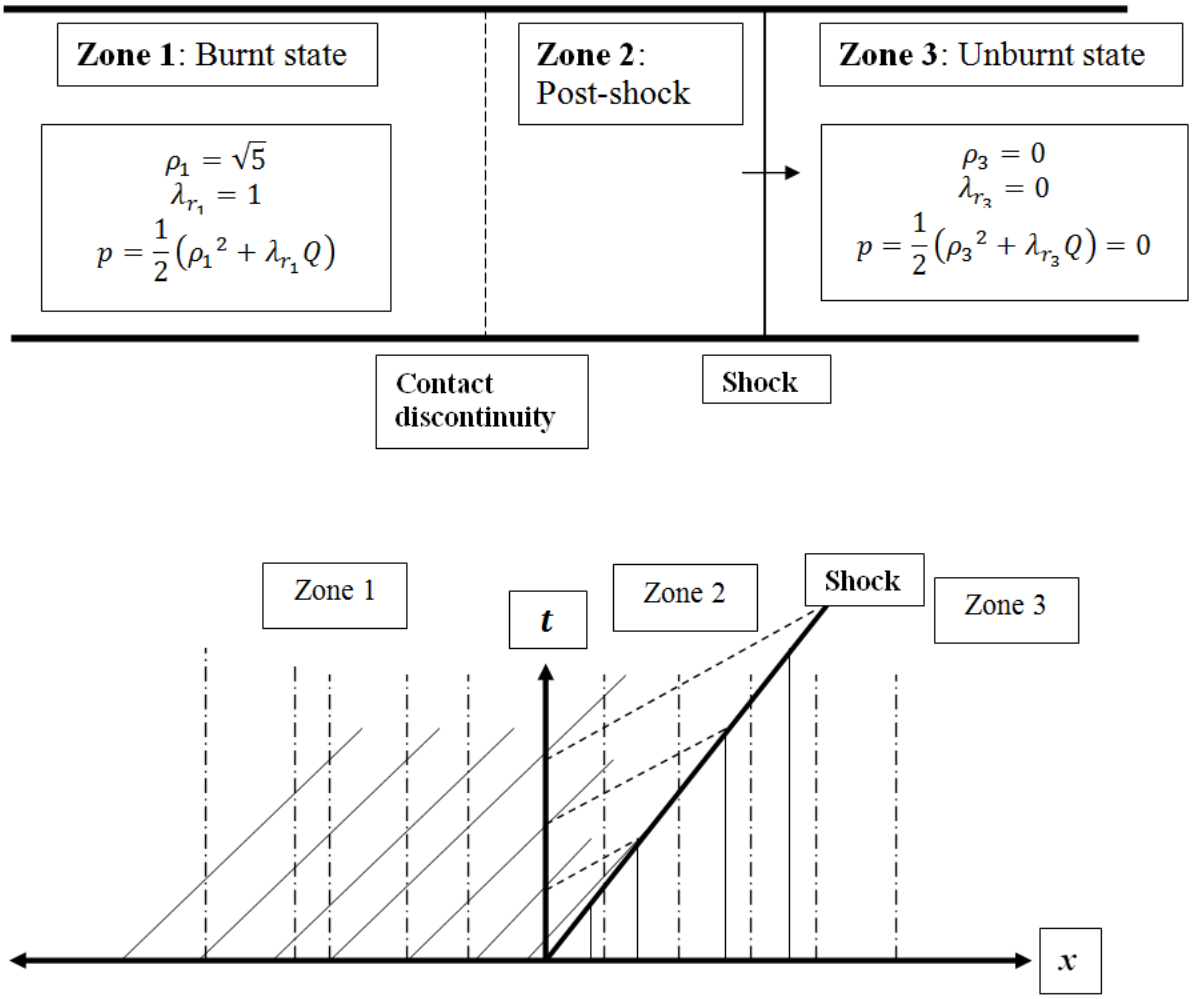

Figure 6.10: A sketch of the Riemann problem for evaluating the strength of the inert shock that would develop from our burnt material traveling into unburnt material. The top sketch shows a 1D channel of burnt and unburnt material separated by a contact discontinuity, with a shock propagating into the unburnt material. The bottom sketch shows a characteristic diagram for this case. Solid lines are C+ characteristics, dash-dot are particle paths. The dashed lines show the altered post-shock C+ paths.

$$t_i = \frac{1}{e^{\alpha(\frac{1}{\sqrt{2}}-1)}} \tag{6.1}$$

Evaluating t_i at $\alpha = 50$, we can see that we would have an induction time of $t_i = \tilde{t}_i = 2.3e6$ (with $K_i = 1$) representing a very long reignition time. To show that reignition can occur, we look at a shorter induction time case, as seen in Fig. 6.12 with $\alpha = 22.0$ and $\tilde{K} = 2.0$. For this value of α we would have a reignition time of 629; however, due to the extra time it would take for the reaction wave to catch up to the shock front, we would expect to see amplification of the shock front after reignition to occur at a later time. Considering the distance traveled by the inert shock during the induction time, and assuming the internal reaction wave travels at constant CJ conditions within the shock (Fig. 6.11), we expect the amplification of the front shock to occur at time $\tilde{t} = 890$, which is close to what we see in Fig. 6.12, where the shock front amplifies at $\tilde{t} = 875$.

In the characteristic diagram at early times (Fig. 6.13) we can see the reaction zone quickly diminishes and disappears while the induction zone continues to grow. In the longer-time characteristic diagram (Fig. 6.14) we can see the reaction zone has completed and is stationary. The induction zone continues to grow as the inert shock (bold red) continues to diverge from the end of induction and reaction zones (green and blue). The inert shock travels at a constant velocity into the unreacted material propelled only by the piston induced conditions of the following flow. With the lack of reaction zone to amplify the pressure waves, the pressure characteristics simple travel at constant velocity through either the fully reacted, or unreacted states.

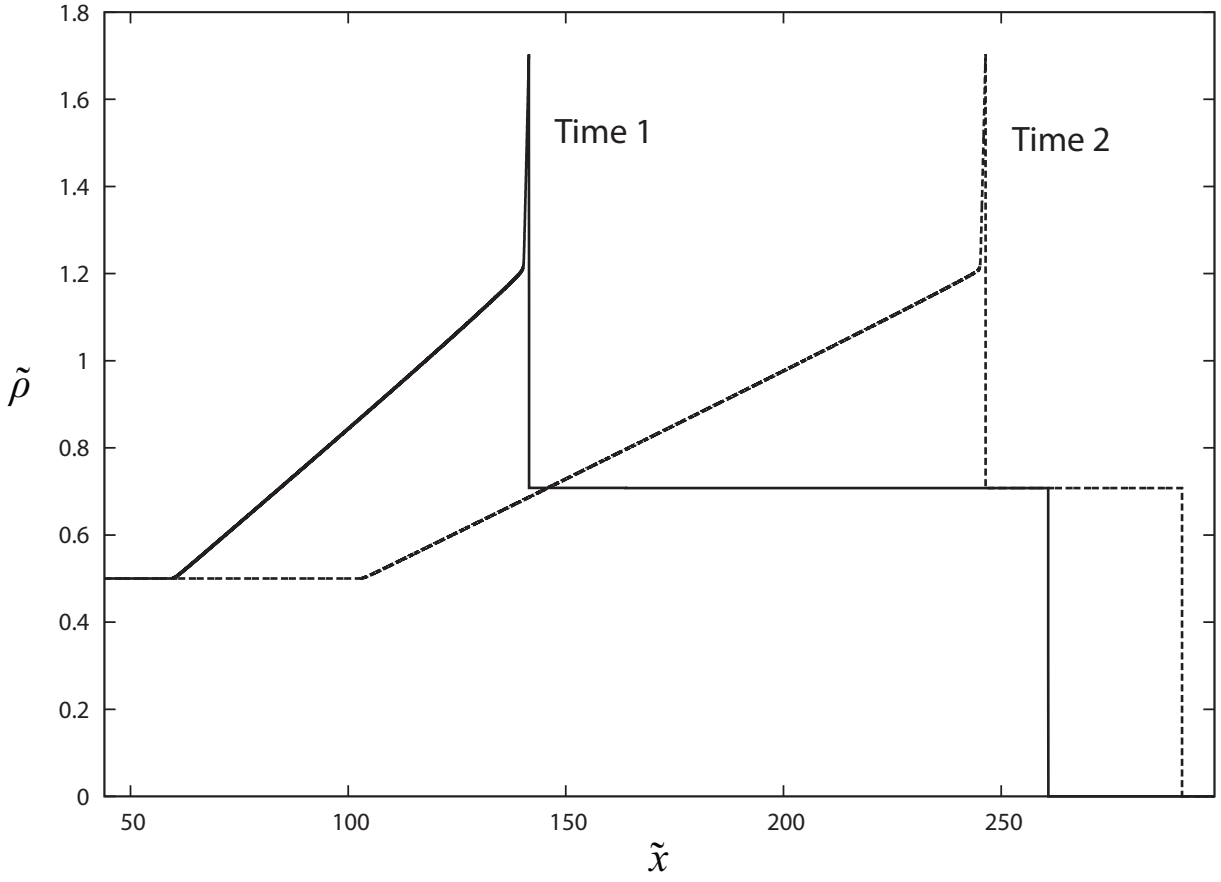

Figure 6.11: The detonation density profile taken at two times at $\alpha = 22.0$ and $\tilde{K} = 2.0$. The internal wave appears to travel at constant CJ conditions during reignition as seen by the constant density peak.

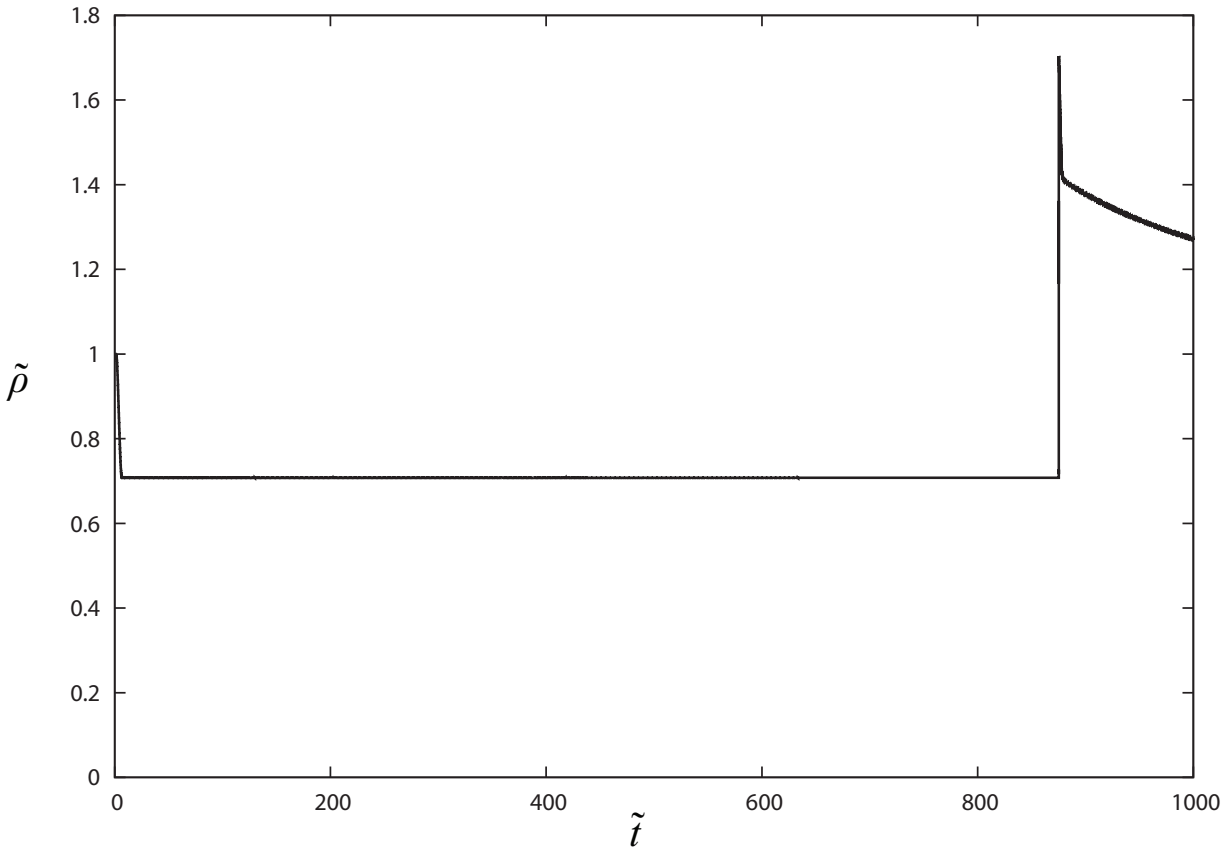

Figure 6.12: The change in nondimensional shock front density over time at $\alpha = 22.0$ and $\tilde{K} = 2.0$ showing quenching, then reignition at a later time.

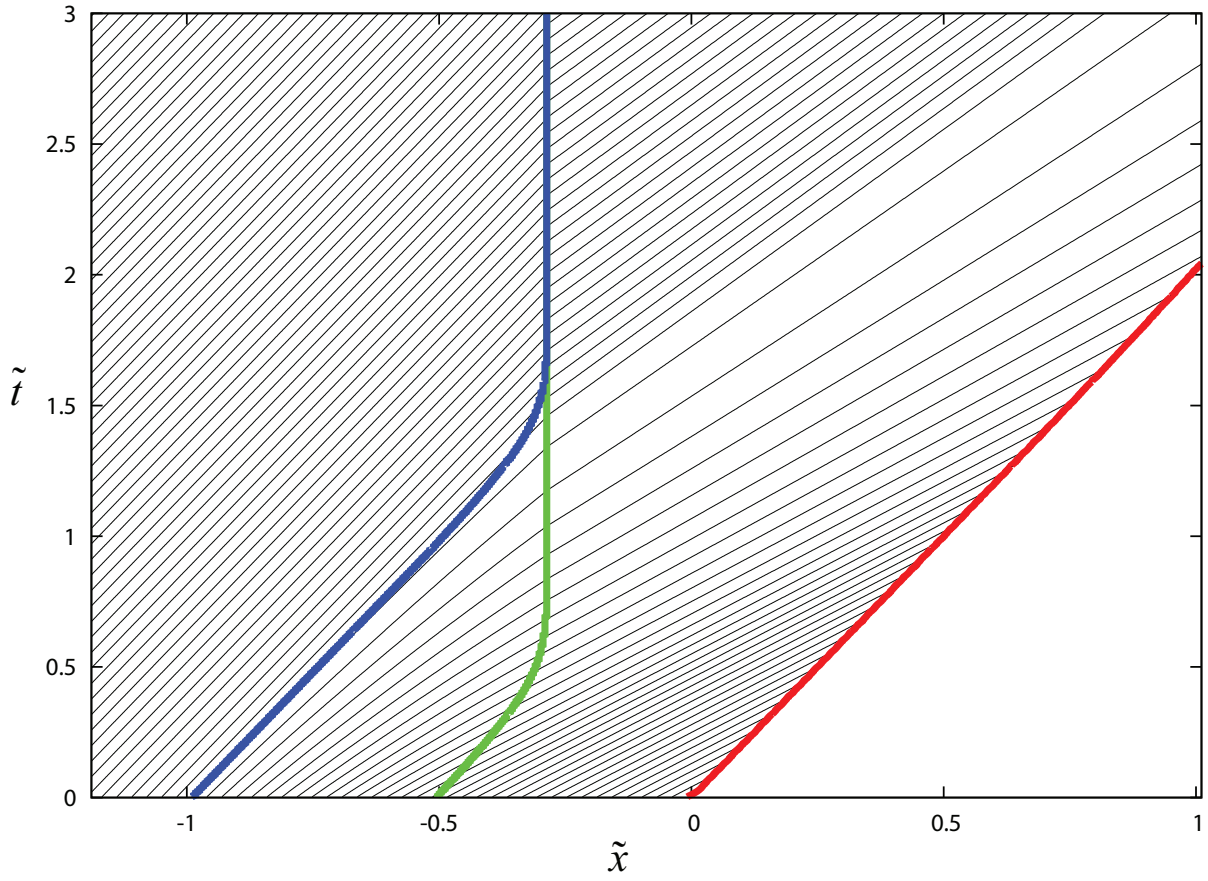

Figure 6.13: Characteristic diagram for quenched behaviour at $\alpha = 50.0, \tilde{K} = 2.0$ up to time $\tilde{t} = 3$ taken in the absolute frame of reference. The shock wave position is shown in bold red. The line in bold green is the end of the induction zone, while the line in bold blue is the end of the reaction zone. The forward sloping black lines are the pressure wave characteristics.

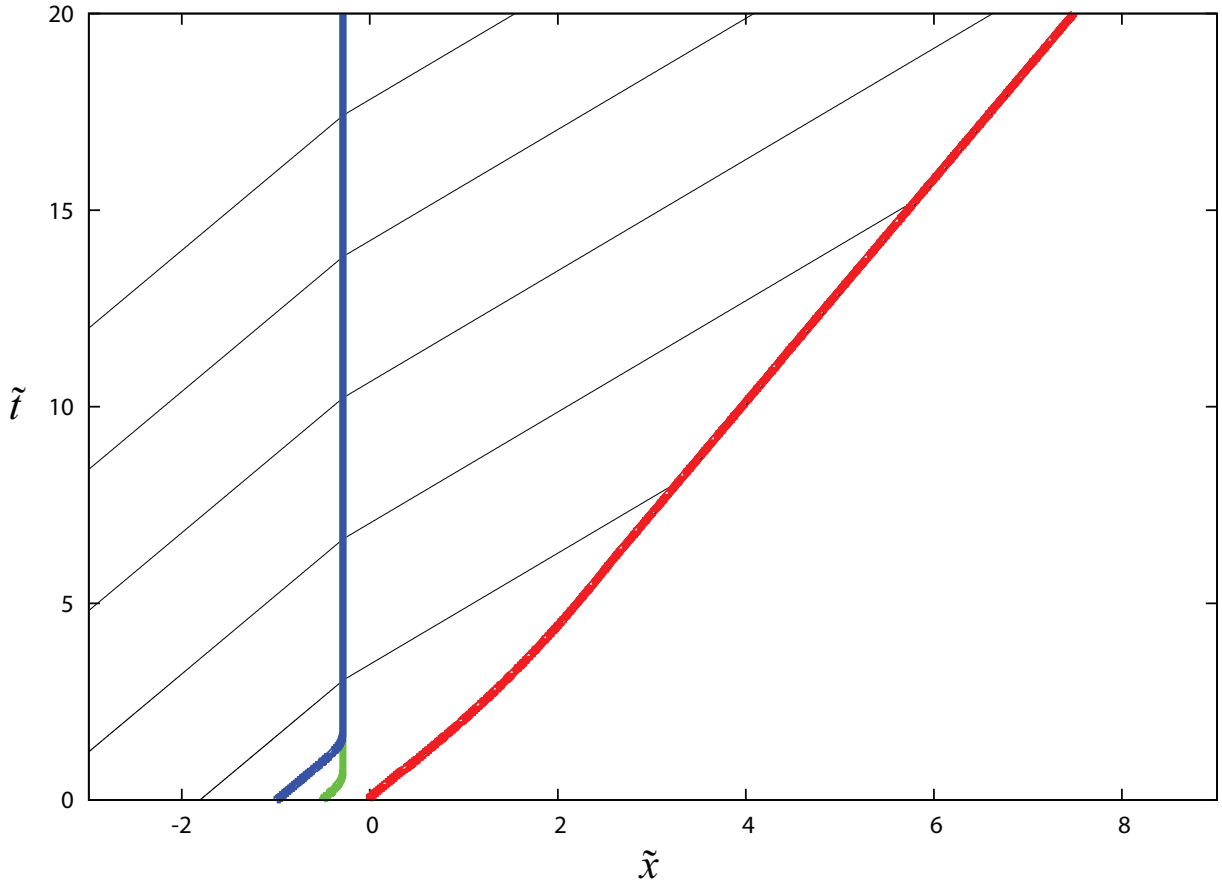

Figure 6.14: Characteristic diagram for quenched behaviour at $\alpha = 50.0, \tilde{K} = 2.00$ up to time $\tilde{t} = 20$ taken in the absolute frame of reference. The shock wave position is shown in bold red. The line in bold green is the end of the induction zone, while the line in bold blue is the end of the reaction zone. The forward sloping black lines are the pressure wave characteristics.

Chapter 7

Discussion

We have used a simplified detonation analogue in order to gain a more transparent description of the dynamics in supersonic reactive fluid flow pertaining to detonations. A main simplification in our model is the reduction in characteristics compared with the Euler equations, allowing us to describe the wave dynamics more clearly. We have described the 1D pulsating instability of detonations as a series of compression waves and expansion rarefactions through characteristic analysis. This wave description follows the 1D wave-interaction model suggested to be at play behind chemical detonations, as seen by McVey & Toong (1971) and later by Leung *et al.* (2010). Toong's 1D wave-interaction model was used to describe the hydrodynamic and chemical kinetic coupling in unstable reactive flows, such as in exothermic hypersonic flow about blunt projectiles, and in numerical piston-supported detonations (Toong, 1974). However the complexity of the governing equations has not permitted the isolation of the controlling mechanism. We were able to clearly describe the instability through the coupling of pressure waves amplifying through the reaction zone, and their effect on the induction delay timing. Both the acceleration and deceleration away from stability are produced by a feedback coupling which shifted the pressure waves in- or out-of-phase with the reaction zone resulting in feedback amplification or attenuation. This process of amplification is similar to the SWACER mechanism of "shock wave amplification by coherent energy release" (Yoshikawa, 1980). It entails a similar process in which a reaction energy-release gradient in phase with pressure waves causes an overall coherent amplification effect. The SWACER mechanism describes a shock wave traveling through a reaction gradient of nearly reacted material, speeding up the reaction and coherently amplifying the shock wave faster as it progresses, speeding up the reaction and being sped up in turn by the completing reactions. With our simplified model we were able to clearly show the relationship that develops between the compres-

sion waves generated from the chemical reaction and the change to the induction delay gradient through a characteristic analysis. The complex dynamics seen experimentally and in the Euler equations are shown to be reproducible by our simple wave-interaction model, which reinforces and clarifies how the detonation dynamics can reduce primarily to the coherent coupling of waves and reactions.

To further investigate the coherent coupling we used our 2-step reaction model to study the effect of the two reaction parameters: $\tilde{K}$, the ratio of induction to reaction time controlling the relative rate of energy release, and $\tilde{\epsilon}$, the inverse activation energy controlling the sensitivity of the induction rate to changes in $\tilde{\rho}$. Altering the inverse activation energy changed the sensitivity of the induction delay to $\tilde{\rho}$ and changed the acceleration of the onset of the reaction zone and its coupling with the pressure waves. This resulted in an increase to the amplification process for low $\tilde{\epsilon}$, and decreased amplification for high $\tilde{\epsilon}$. Similarly, a higher $\tilde{K}$ increased the amount of amplification pressure waves received for the same residence time in the reaction zone, and thus higher $\tilde{K}$ led to stronger amplification while lower $\tilde{K}$ caused weaker amplification. In this way we were able to clearly show the effect of each of these parameters on the amplification behaviour, an important process in unstable detonation initiation and propagation.

In our analytical description of the amplification process we were able to describe the acceleration of the onset of the reaction zone as the relation between the ratio of induction to reaction time $\tilde{K}$, the inverse activation energy $\tilde{\epsilon}$, and the heat of release $\tilde{Q}$ (Equation 5.19). This relation is relatable to the nondimensional parameter $\chi = \frac{t_i}{t_r}\frac{E_a}{RT}$ (where $\frac{t_i}{t_e}$ is the ratio of induction to reaction time, $\frac{E_a}{RT}$ is the nondimensional activation energy) which has been identified in recent studies to correlate with a number of different detonation behaviours. For example χ has been seen to affect 1D detonation stability (Short & Sharpe, 2003; Ng *et al.*, 2005*b*; Leung *et al.*, 2010), and also to affect the propensity for hotspots in reactive material to amplify into detonations (Bradley, 2012). Though the development of hotspots can be analyzed in 1D, globally, multiple hotspots were seen to have a coherent amplification effect. The χ parameter can also be used to correlate multidimensional detonation effects, and has been used in predicting cellular detonation regularity as well (Radulescu, 2003). Our asymptotic analysis was able to derive χ from our simple model (as the acceleration of the fire in Equation 5.19) and clarify the mechanism by which it controls amplification. The main dynamic was between the pressure wave amplification and coherent energy release which caused a feedback behaviour dependent on $\tilde{K}$ and $\tilde{\epsilon}$.

Fickett's model was also shown to demonstrate the same period doubling bifurcation behaviour and route to chaos with increasing α as seen in the Euler equations (Ng *et al.*,

2005*a*; Henrick *et al.*, 2006). We were able to build a bifurcation diagram and reproduce the characteristic odd numbered period-3 solution implying transition to chaos. Our model was very simple, yet retained the same nonlinear behaviour seen in the full reactive Euler equations.

Following our documentation of the Feigenbaum-type instability in Fickett's model (Radulescu & Tang, 2011), Kasimov *et al.* (2013) were also able to document numerical results for the same type of instability in a different model, though they did not address the physical mechanism of instability.

With further increases to α in our simulations we found a "galloping mode" of instability in which internal shocks form and cause the detonation to transition from periods of low strength to sudden amplification. Upon reaching a threshold value in α the feedback coupling reaches a state in which rapid amplification led to the formation of internal shocks.

Additionally, at α values past the galloping mode region, we were able to model quenching-like behaviour, in which the detonation would die off in strength and develop into a propagating unreacted shock maintained only by the piston induced flow from behind. The reactions behind the initial CJ detonation are seen to decoupled from the shock front and complete, while an inert shock propagates forward. We were able to show that for our system, reignition does occur at some finite time after the quenching. Both the galloping mode and quenching behaviour have been documented to occur from the Euler equations as well (He & Lee, 1995).

Chapter 8

Conclusion and Future Study

In our study we were able to clarify the dynamics of 1D detonations and to describe the governing mechanism behind the unstable behaviour through a characteristic analysis and by analytically solving our simplified system: Fickett's model with 2-step reaction. Fickett's model was seen to admit an unstable, pulsating instability solution. The simplicity of the model allowed us to describe the pulsating behaviour by the interaction between only two characteristics for the reaction along the particle paths, and the propagation and amplification of compression waves. We found that the unstable pulsations were caused by a feedback mechanism between the amplification of pressure waves passing in phase through the reaction zone and their modification of the induction zone and onset of reactions. This feedback mechanism reinforced the acceleration or deceleration of the detonation drawing it away from stability.

We then examined the unstable acceleration of a detonation by modeling shock induced ignition. We were able to describe the effect of the inverse activation energy ($\tilde{\epsilon}$) and the ratio of the induction to reaction time ($\tilde{K}$) on the amplification behaviour of the detonation. Changing $\tilde{\epsilon}$ alters the induction zone sensitivity to changes in density, which alters the path of the onset of the reaction zone changing the amount of time pressure waves are in phase with the reaction zone, and the strength of the feedback mechanism. Thus, lower values of $\tilde{\epsilon}$ increased the feedback and amplification process, while higher values decreased the amplification. Changing $\tilde{K}$ increased the rate of energy release and amplification in the reaction zone, which means stronger pressure waves emanating from the reaction zone, and a stronger alteration of the induction zone timing. Higher values of $\tilde{K}$ meant stronger amplification, while lower values meant weaker amplification. We were able to analytically solve our simple system in order to demonstrate mathematically the effect of both $\tilde{\epsilon}$ and $\tilde{K}$ on the acceleration of the onset of the reaction zone, representing

the strength of the feedback and amplification.

Fickett's model was also shown to reproduce similar behaviour to those found in the more complex Euler equations, such the period doubling bifurcation route to chaos, and the galloping mode and quenching. Chaos was seen to occur by the presence of the odd numbered period-3 oscillatory solution.

It is recommended that future studies address the stability limits in our model analytically. The $\tilde{K} - \alpha$ stability trends seen in Section 4.1 can be further extended. The bifurcation behaviour can be examined to determine the mechanism governing its occurrence as well. The chaos study can be extended to try to describe the cause of the trend seen in the Lorenz map. The galloping mode and quenching behaviour are also open to exploration. A further refinement of the analytical study could be conducted to describe the later time path of the onset of reaction, after the shock front has been perturbed by the compression waves from the reaction zone.

Bibliography

Bdzil, John B. & Stewart, D. Scott 2007 The dynamics of detonation in explosive systems. *Annual Review of Fluid Mechanics* **39**, 263–292.

Bradley, D. 2012 Autoignitions and detonations in engines and ducts. *Philosophical Transactions of the Royal Society a-Mathematical Physical and Engineering Sciences* **370**, 689–714.

Chapman, D.L. 1889 On the rate of explosion in gases. *Phil. Mag.* **47**, 90–104.

Edwards, D. H. & Morgan, J. M. 1977 Instabilities in detonation waves near the limits of propagation. *J. Phys. D* **10**, 2377–87.

Feigenbaum, M. J. 1983 Universal behavior in nonlinear systems. *Physica D: Nonlinear Phenomena* **7** (13), 16 – 39.

Fickett, W. 1979 Detonation in miniature. *American Journal of Physics* **47** (12), 1050–1059.

Fickett, Wildon 1985*a* *Introduction to Detonation Theory*. Berkeley: University of California Press.

Fickett, Wildon 1985*b* Stability of the square-wave detonation in a model system. *Physica 16D* pp. 358–370.

Fickett, Wildon & Davis, William Chester 2000 *Detonation: Theory and Experiment*. Mineola, N.Y.: Dover Publications.

Flynn, M. R., Kasimov, A. R., Nave, J.-C., Rosales, R. R. & Seibold, B. 2009 Self-sustained nonlinear waves in traffic flow. *Phys. Rev. E* **79**, 056113.

Hall, F. S. & Ludford, G. S. S. 1987 Stability of a detonation wave. *Physica D* **28**, 1–17.

He, L. & Lee, J. H. S 1995 The dynamical limit of one-dimensional detonations. *Phys. Fluids* **7**, 1151–1168.

Henrick, A. K, Aslam, T. D. & Powers, J. M. 2006 Simulations of pulsating one-dimensional detonations with true fifth order accuracy. *Journal of Computational Physics* **213**, 311–329.

Jouguet, E. 1904 Sur l'onde explosive. *C. R. Acad. Sci. Paris* **140**, 1211.

Jouguet, E. 1905 On the propagation of chemical reaction in gases. *J. Math Pures Appl. 6th Seri.* **1**, 347.

Kasimov, A. R. 2008 A stationary circular hydraulic jump, the limits of its existence and its gasdynamic analogue. *J. of Fluid Mech.* **601**, 189–198.

Kasimov, A. R., Faria, L. M. & Rosales, R. R. 2013 Model for Shock Wave Chaos. *Physical Review Letters* **110** (10), 104104.

Lee, J.H.S 1984 Dynamic parameters of gaseous detonations. *Ann. Rev. Fluid Mech.* **16**, 311–36.

Lee, J.H.S. 2008 *The Detonation Phenomenon*. Cambridge: Cambridge University Press.

Leung, C., Radulescu, M. I. & Sharpe, G. J. 2010 Characteristics analysis of the one-dimensional pulsating dynamics of chain-branching detonations. *Physics of Fluids* **22** (12), 126101.

McVey, J. B. & Toong, T. Y. 1971 Mechanism of instability of exothermic hypersonic blunt-body flows. *Combustion Science and Technology* **3**, 63–76.

Ng, H. D., Higgins, A. J., Kiyanda, C. B., Radulescu, M. I., Lee, J. H. S., Bates, K. R. & Nikiforakis, N. 2005*a* Nonlinear dynamics and chaos analysis of one-dimensional pulsating detonations. *Combust. Theory and Modelling* **9**, 159–170.

Ng, H. D., Radulescu, M. I., Higgins, A. J., Nikiforakis, N. & Lee, J. H. S. 2005*b* Numerical investigation of the instability for one-dimensional Chapman-Jouguet detonations with chain-branching kinetics. *Combustion Theory and Modelling* **9** (3), 385–401.

Radulescu, Matei Ioan 2003 The propagation and failure mechanism of gaseous detonations : experiments in porous-walled tubes. PhD thesis, McGill University.

Radulescu, M. I. & Tang, J. 2011 Nonlinear dynamics of self-sustained supersonic reaction waves: Fickett's detonation analogue. *Physical Review Letters* **107** (16), 164503.

Sharpe, G. J. 2002 Shock-induced ignition for a two-step chain-branching kinetics model. *Physics of Fluids* **14** (12), 4372–4388.

Sharpe, G. J. & Falle, S. A. E. G. 2000 Numerical simulations of pulsating detonations: I. Nonlinear stability of steady detonations. *Combust. Theory and Modelling* **4**, 557–574.

Sharpe, G. J. & Short, M. 2003 Detonation ignition from a temperature gradient for a two-step chain-branching kinetics model. *J. Fluid Mech.* **476**, 267–292.

Shepherd, J. E. 2012 Detonation in gases. *Proceedings of the Combustion Institute* **32**, 83–98.

Short, M. & Sharpe, G. J. 2003 Pulsating instability of detonations with a two-step chain-branching reaction model: theory and numerics. *Combustion Theory and Modelling* **7** (2), 401–416.

Strehlow, Roger A. 1968 *Fundamentals of Combustion*. Scranton, Pennsylvania: International Textbook Company.

Tang, J. & Radulescu, M. I. 2012 Dynamics of shock induced ignition in Fickett's model: influence of χ. *Proceedings of the Combustion Institute* **34**, 2035–2041.

Toong, Tau-Yi 1974 Instabilities in reacting flows. *Acta Astronautica* **1**, 317–344.

Whitham, G. B. 1974 *Linear and Nonlinear Waves*. New York: Wiley.

Yoshikawa, N 1980 Coherent shock wave amplification in photochemical initation of gaseous detonations. PhD thesis, McGill University.

Zhang, F. 2009 *Shock Wave Science and Technology Reference Library, Vol.4: Heterogeneous Detonation*. Berlin: Springer.

Appendix A

Nondimensionalization

The nondimensionalization used for our results is shown below. Variables with a tilde represent the nondimensional quantities. Our initial governing equations for the conservation and reaction are:

$$\frac{\partial \rho}{\partial t} + \frac{\partial}{\partial x}(\frac{1}{2}\rho^2 + \frac{1}{2}\lambda_r Q) = 0 \tag{A.1}$$

$$\frac{\partial \lambda_i}{\partial t} = -K_i H(\lambda_i) e^{\alpha(\frac{\rho}{2\rho_{CJ}} - 1)} \tag{A.2}$$

$$\frac{\partial \lambda_r}{\partial t} = K_r[1 - H(\lambda_i)]H(1 - \lambda_r)(1 - \lambda_r)^\nu \tag{A.3}$$

We nondimensionalize our density with respect to the post shock state ρ_s, and nondimensionalize time with the ignition time to reaction, which is our induction delay time. Density and time are nondimensionalized as follows:

$$\tilde{\rho} = \frac{\rho}{\rho_s} \tag{A.4}$$

$$\tilde{t} = \frac{t}{t_{igs}} \tag{A.5}$$

where t_{igs} is the ignition time for the initially shocked material (ρ_s) to react. The ignition time is determined by the induction reaction equation (Equation 2.10) which is integrated from $\lambda_i = 1$ to $\lambda_i = 0$:

$$t_{igs} = \frac{1}{K_i e^{\alpha(\frac{\rho_s}{2\rho_{CJ}} - 1)}} \tag{A.6}$$

The space coordinate, heat release parameter, and reaction zone constant are nondimensionalized as follows:

$$\tilde{x} = \frac{x}{\rho_s t_{igs}} \tag{A.7}$$

$$\tilde{Q} = \frac{Q}{\rho_s^2} \tag{A.8}$$

$$\tilde{K} = K_r t_{igs} \tag{A.9}$$

We define a new parameter $\tilde{\epsilon}$, which we call the inverse activation energy in analogue to the physical quantity by the same name which controls the sensitivity of the reaction rates:

$$\tilde{\epsilon} = \frac{2\rho_{CJ}}{\alpha \rho_s} \tag{A.10}$$

We can now nondimensionalize the governing equations. Our new set of equations for the conservation, induction, and reaction rate are:

$$\frac{\partial \tilde{\rho}}{\partial \tilde{t}} + \frac{\partial}{\partial \tilde{x}}(\frac{1}{2}\tilde{\rho}^2 + \frac{1}{2}\lambda_r \tilde{Q}) = 0 \tag{A.11}$$

$$\frac{\partial \lambda_i}{\partial \tilde{t}} = -H(\lambda_i) e^{\frac{\tilde{\rho}-1}{\tilde{\epsilon}}} \tag{A.12}$$

$$\frac{\partial \lambda_r}{\partial \tilde{t}} = \tilde{K}[1 - H(\lambda_i)]H(1-\lambda_r)(1-\lambda_r)^{\nu} \tag{A.13}$$

A.1 Numerical Discretization

The numerical discretization of the nondimensional form of the governing equations follows the same discretization scheme seen in Chapter 3. The conservation, induction and reaction rate equations are discretized as follows:

$$\tilde{\rho}_i^{n+1} = \tilde{\rho}_i^n + \frac{\Delta \tilde{t}}{2\Delta \tilde{x}}((\tilde{\rho}_{i-1}^n)^2 - (\tilde{\rho}_i^n)^2 + \tilde{Q}(\lambda_{r_{i-1}}^n - \lambda_{r_i}^n)) \tag{A.14}$$

$$\lambda_i^{n+1} = \lambda_i^n - H(\lambda_i)H(\tilde{\rho}_i - \tilde{\rho}_{act}) e^{\frac{\tilde{\rho}_i - 1}{\tilde{\epsilon}}} \Delta \tilde{t} \tag{A.15}$$

$$\lambda_r^{n+1} = 1 - [(1-\lambda_r^n)^{1-\nu} - (1-\nu)[1 - H(\lambda_i)]H(1-\lambda_r)\tilde{K}\Delta \tilde{t}]^{\frac{1}{1-\nu}} \tag{A.16}$$

Appendix B

Programming code

The C++ code used for the numerical simulations is contained here. The follow script requires an input file ("fickettinput.txt") for the parameters values and simulation settings, and outputs three separate data files ("fickettdata-XX.txt") for the shock front density values over time, the density variation over the domain at snapshots at time, and characteristic data.

The script used for the dimensional simulations varying α and K_r is listed below:

```
/*----------------LIBRARIES----------------------*/
#include <stdio.h>
#include <stdlib.h>
#include <math.h>
#include <string.h>
#include <string>

#include <iostream>
#include <fstream>
#include <sstream>
using namespace std;

/*-----------------------------------------------*/


/*----------------PROTOTYPES---------------------*/
double hydrodynamicstep (double density, double densityprev, double massfraction,
    double massfractionprev);
double reactivestep (double density, double massfractioni, double massfractionr, int
    zone);
```

```
double H (double valueone);    //heavyside func.
double maximum (double *arrayonep ); //for finding the maximum value from a set
double startpeak (double *arraytwop ); //for finding the shock density peak

/*-------------------------------------------------*/
                 /**/
/*-----------------SYMBOLIC CONSTANTS--------------*/
# define PI 3.1415926535

/*-------------------------------------------------*/
                /**/
/*----------------GLOBAL VARIABLES--------------*/

int counter, countertwo, counterthree,counterfour;   //Counters
double x, xend, deltax=0, xd, zeta, zetacj, zetaind;  //Position variables
int Ng;                          //Nodes
double t, tend, deltat=0;              //Time variables
double Q, Ki, Kr,nu,Dcj,activation,cfl, Krend=-99, Qend=-99;  // Constants
double alpha,alphaend=-99;         //Reaction rate sensitivity parameter
char alphastring[20];

/*-------------------------------------------------*/

int main()
{

//DECLARATION OF VARIABLES

int numofsteps;   //variable to keep track of the total number of timesteps
int resolution;   //the number of nodes used to describe the entire detonation
    structure
int arraysize=123;  //the size of the density and progress variable arrays. Initial
    value is arbitrary.

ofstream filea,filep; //the output file stream variable for the amplitude, and density
    profile
ifstream filei;   //the input file stream variable for the input file
string fileamplitude, fileprofile; //the name of the file to be created (amp, or
    profile)
string holder;    //a place-holder string
char holder2[90]="0", stringholder[25];
```

```
ofstream filec;
string filecharacteristics;
double shock, ctstart, ctend, cpstart, cpend; //the value of the shock, the
    charateristic starting and ending time and position
int find, search, check;   //loop variables
int shockposition, endofind, endofreact, cend; //
double wavec[1000];   //wave characteristic. It holds the x-pos of each # of char

int icchoice,savechoice,paramchoice=1,countertwostart=1,Ngend;
double xpulse,tstart=0;
ifstream fileicp;
char fileinitialconditionprofile[90];


//INTRODUCTION

cout<<"-----Welcome to the Detonation modeller using Fickett's Analogue. Ver.12.2 with
    parameter variation"<<endl<<endl;

//Read all the parameter values in from the data input file "fickettinput.txt"
filei.open( "fickettinput.txt" ); //open input file

getline (filei, holder);   //skip line in fickettinput file

filei>>holder2;
resolution=strtol(holder2,NULL,0); //The number of nodes describing the detonation

getline(filei, holder);
getline (filei, holder);

filei>>holder2;
tend=strtod(holder2,0);   //End time for simulation

getline(filei, holder);
getline (filei, holder);
getline (filei, holder);

filei>>holder2;
alpha=strtod(holder2,0);  //alpha

getline(filei, holder);
getline (filei, holder);
```

```
filei>>holder2;
Kr=strtod(holder2,0);  //Reaction zone constant

getline(filei, holder);
getline (filei, holder);

filei>>holder2;
Ki=strtod(holder2,0);  //Induction zone constant

getline(filei, holder);
getline (filei, holder);

filei>>holder2;
Q=strtod(holder2,0);  //Heat of release

getline(filei, holder);
getline (filei, holder);

filei>>holder2;
cfl=strtod(holder2,0);  //CFL number, the stability criterion

getline(filei, holder);
getline (filei, holder);

filei>>holder2;
nu=strtod(holder2,0);  //constant of reaction formulation

getline(filei, holder);
getline (filei, holder);

filei>>holder2;
activation=strtod(holder2,0); //the activation energy

getline(filei, holder);
getline (filei, holder);
getline (filei, holder);

filei>>holder2;
icchoice=strtol(holder2,NULL,0); //the initial condition choice

getline(filei, holder);
getline (filei, holder);
```

```
filei>>holder2;
savechoice=strtol(holder2,NULL,0); //save profile or not choice

getline(filei, holder);
getline (filei, holder);

filei>>fileinitialconditionprofile; //profile ic file-name

getline(filei, holder);
getline (filei, holder);
getline (filei, holder);

filei>>holder2;
cend=strtol(holder2,NULL,0); //the number of characteristics

getline(filei, holder);
getline (filei, holder);

filei>>holder2;
ctstart=strtod(holder2,0); //the characteristic start time

getline(filei, holder);
getline (filei, holder);

filei>>holder2;
ctend=strtod(holder2,0); //the characteristic end time

getline(filei, holder);
getline (filei, holder);

filei>>holder2;
cpstart=strtod(holder2,0); //the characteristics start position

getline(filei, holder);
getline (filei, holder);

filei>>holder2;
cpend=strtod(holder2,0); //the characteristics end position

getline(filei, holder);
getline (filei, holder);
getline (filei, holder);
```

```
filei>>holder2;
paramchoice=strtol(holder2,NULL,0); //choice of which parameter to vary

getline(filei, holder);
getline (filei, holder);

filei>>holder2;
if (paramchoice==1)//the last parameter value at which to stop the program
  alphaend=strtod(holder2,0);
else if (paramchoice==2)
  Krend=strtod(holder2,0);
else if (paramchoice==3)
  Qend=strtod(holder2,0);

getline(filei, holder);
getline (filei, holder);


//PROGRAM BEGINS
do  //start of do-loop to process over different parameter values
{
if (paramchoice==1)
{
  filei>>alphastring;     //read in value of alpha as string
  alpha=strtod(alphastring,0); //store alpha value as a double
  getline(filei, holder);   //skip to next line in fickettinput
}
else if (paramchoice==2)
{
  filei>>alphastring;     //read in value of kr as string (it says 'alphastring' but
      that's just a placeholder)
  Kr=strtod(alphastring,0); //store kr value as a double
  getline(filei, holder);   //skip to next line in fickettinput
}
else if (paramchoice==3)
{
  filei>>alphastring;     //read in value of Q as string (it says 'alphastring' but that
      's just a placeholder)
  Q=strtod(alphastring,0);  //store alpha value as a double
  getline(filei, holder);   //skip to next line in fickettinput
}
```

```
//INITIALIZATION OF VARIABLES

xd=5*(pow(Kr,-1.0)+0.5)+5.2;    //Initial position of detonation
Dcj=pow(Q,0.5);         //The CJ detonation velocity
xend=tend*(Dcj+1.1)+xd;    //Total domain length (based on speed of wave plus starting
    point of detonation)

deltax=(Dcj/Kr/(1.0-nu))/(resolution-1.0);  //Distance between nodes

if ( (Dcj/Ki/deltax+1.0)<128 ) //[if the nodes of the induction zone are too small]in
    case the reaction zone to induction zone ratio is too large so that the resolution
    of the induction zone is too small, we set the induction zone res to a minimum
  deltax=Dcj/Ki/(128.0-1.0);

Ng=int(xend/deltax+1.0); //Number of nodes in the domain

arraysize=Ng+2;       //The array sizes are equal to the number of nodes plus small
    leeway
double *density = new double [arraysize]; //Density variable vector array
double *newdensity = new double [arraysize]; //Density-place-holder vector
double *lambdai = new double [arraysize]; //Progress variable for induction zone vector
double *newlambdai = new double [arraysize]; //Progress variable for induction zone
    place-holder vector
double *lambdar = new double [arraysize]; //Progress variable for reaction zone vector
double *newlambdar = new double [arraysize]; //Progress variable for reaction zone
    place-holder vector


zetaind=-Dcj/Ki;  //Zeta is the position coordinate in the frame of the shock
zetacj=zetaind-Dcj/Kr/(1-nu);


for (int a=0; a<cend; a++)
{
  wavec[a]=cpstart+(cpend-cpstart)/(cend-1.0)*a;
}

for (int i=0; i<Ng; i++) //initialize the density and lambda arrays with arbitrary
    values before initial conditions
{
  density[i]=1.23;
  lambdai[i]=0.987;
  lambdar[i]=0.123;
```

```
}


//INITIAL CONDITIONS

//Initial Condition Choices:
//1. Steady CJ solution
//2. Density impulse function
//3. Large initial step
//4. Previous Save

if (icchoice==1) //Steady solution
{
  for (zeta=-xd,counter=0; counter<Ng; zeta=zeta+deltax, counter++) //zeta is position
      relative to shock
  {
    if (zeta<zetacj) //CJ state
    {
      density[counter]=Dcj;
      lambdai[counter]=0;
      lambdar[counter]=1;
    }
    else if (zeta>=zetacj && zeta<zetaind) //soln in the reaction zone
    {
      density[counter]=Dcj*(1+pow((1+(1-nu)*Kr/Dcj*(zeta-zetaind)),(1.0/2.0/(1-nu))));
      lambdai[counter]=0;
      lambdar[counter]=1-pow((1+(1-nu)*Kr/Dcj*(zeta-zetaind)),(1.0/(1-nu)));
    }
    else if (zeta>=zetaind && zeta<0) //soln in the induction zone
    {
      density[counter]=2.0*Dcj;
      lambdai[counter]=1+Ki/Dcj*zeta;
      lambdar[counter]=0;
    }
    else if (zeta>=0) //soln ahead of the shock
    {
      density[counter]=0;
      lambdai[counter]=1;
      lambdar[counter]=0;
    }
  }
}
else if (icchoice==2) //Density impulse
```

```
{
  xpulse=xd*-0.01; //The x position in shock frame of the end of the pulse in terms of
      xd. Should not be made larger than xd or it could go over the domain size.

  for (zeta=-xd,counter=0; counter<Ng; zeta=zeta+deltax, counter++) //loop through
      entire domain
  {
    if (zeta<xpulse) //ic behind the pulse
    {
      density[counter]=0;
      lambdai[counter]=1;
      lambdar[counter]=0;
    }
    else if (zeta>=xpulse && zeta<0) //ic in the pulse
    {
      density[counter]=90;
      /*if (zeta<0.5*xpulse)
        density[counter]=20.0*(xpulse-zeta)/xpulse;
      else
        density[counter]=20.0*zeta/xpulse;*/
      lambdai[counter]=1;
      lambdar[counter]=0;
    }
    else if (zeta>=0) //ic ahead of the pulse
    {
      density[counter]=0;
      lambdai[counter]=1;
      lambdar[counter]=0;
    }
  }
}
else if (icchoice==3) //Large initial step
{

  for (zeta=-xd,counter=0; counter<Ng; zeta=zeta+deltax, counter++) //loop through
      entire domain
  {
    if (zeta<xd) //ic behind step at x=xd
    {
      density[counter]=pow(5,0.5);
      lambdai[counter]=0;
      lambdar[counter]=1;
    }
```

```
    else if (zeta>=xd) //ic ahead of the pulse
    {
      density[counter]=0;
      lambdai[counter]=1;
      lambdar[counter]=0;
    }
  }

}
else if (icchoice==4) //Previous save file
{
  fileicp.open( fileinitialconditionprofile ); //open previous profile data file

  getline (fileicp, holder);  //skip lines
  getline (fileicp, holder);
  getline (fileicp, holder);

  fileicp>>holder2;
  tstart=strtod(holder2,0);   //starting time to resume simulation at

  getline (fileicp, holder);
  getline (fileicp, holder);

  fileicp>>holder2;
  countertwostart=strtol(holder2,NULL,0); //the starting point for the countertwo

  getline (fileicp, holder);
  getline (fileicp, holder);

  fileicp>>holder2;
  Ngend=strtol(holder2,NULL,0); //the starting point for the countertwo

  getline (fileicp, holder);
  getline (fileicp, holder);
  getline (fileicp, holder);

  for (int i=0; i<Ng; i++) //initialize the density and lambda arrays with the ic from
      the file
  {
    if (i<Ngend)
    {
      fileicp>>holder2;  //skip node #
      fileicp>>density[i]; //read in density
```

```
      fileicp>>lambdar[i]; //read in lambda r
      fileicp>>lambdai[i]; //read in lambda i
    }
    else
    {
      density[i]=0;
      lambdai[i]=1;
      lambdar[i]=0;
    }
  }

  fileicp.close();

}
else
{
  cout<<"There was an ic choice error"<<endl;
  exit (1);
}


//FILE MANAGEMENT

fileamplitude="fickettdata-amplitude-Kr="; //set the amplitude file name
sprintf(stringholder,"%.2f",Kr);
fileamplitude+=stringholder;  //append Kr to the file name
fileamplitude+="-alpha=";
sprintf(stringholder,"%.2f",alpha);
fileamplitude+=stringholder;  //append the alpha value to the file name
fileamplitude+="-Q=";
sprintf(stringholder,"%.2f",Q);
fileamplitude+=stringholder;  //append the Q value to the file name
fileamplitude+="-time=(";
sprintf(stringholder,"%.1f",tstart);
fileamplitude+=stringholder;
fileamplitude+="-";
sprintf(stringholder,"%.0f",tend);
fileamplitude+=stringholder;
fileamplitude+=")-char#=";
sprintf(stringholder,"%d",cend);
fileamplitude+=stringholder;  //append # of characteristics to file name
fileamplitude+=".txt";
```

```
filecharacteristics="fickettdata-char-Kr=";
sprintf(stringholder,"%.2f",Kr);
filecharacteristics+=stringholder;  //append Kr to the file name
filecharacteristics+="-alpha=";
sprintf(stringholder,"%.2f",alpha);
filecharacteristics+=stringholder;  //append the alpha value to the file name
filecharacteristics+="-Q=";
sprintf(stringholder,"%.2f",Q);
filecharacteristics+=stringholder;  //append the Q value to the file
    namefilecharacteristics+="-time=(";
sprintf(stringholder,"%.1f",tstart);
filecharacteristics+=stringholder;
filecharacteristics+="-";
sprintf(stringholder,"%.0f",tend);
filecharacteristics+=stringholder;
filecharacteristics+=")-char#=";
sprintf(stringholder,"%d",cend);
filecharacteristics+=stringholder;
filecharacteristics+=".txt";

filea.open( fileamplitude.c_str() ); //open separate files for writing (amp, and
    profile) ...
filec.open( filecharacteristics.c_str() );

//Density Profile Initial Conditions
//Write density profile heading, and initial values to file

fileprofile="fickettdata-profile-Kr="; //set the density profile file name
sprintf(stringholder,"%.2f",Kr);
fileprofile+=stringholder;  //append Kr to the file name
fileprofile+="-alpha=";
sprintf(stringholder,"%.2f",alpha);
fileprofile+=stringholder;  //append the alpha value to the file name
fileprofile+="-Q=";
sprintf(stringholder,"%.2f",Q);
fileprofile+=stringholder;  //append the Q value to the file name
fileprofile+="-time=(";
sprintf(stringholder,"%.1f",tstart);
fileprofile+=stringholder;
fileprofile+="-";
sprintf(stringholder,"%.0f",tend);
fileprofile+=stringholder;
fileprofile+=")-char#=";
```

```
sprintf(stringholder,"%d",cend);
fileprofile+=stringholder;
fileprofile+=".txt";
filep.open( fileprofile.c_str() );

filep<<"Density Profile over x"<<endl;
filep<<"Node\t\t\tDensity"<<"\t\t\tLambda r\t\t\tLambda i\t\t\t";
filep<<"Alpha="<<alpha<<",\tEnd time="<<tend<<",\tNumber of grid points="<<Ng<<",\
    tChannel length="<<xend<<",\tKr="<<Kr<<",\tKi="<<Ki<<",\tCFL#="<<cfl<<",\tNu="<<nu
    <<",\tQ="<<Q<<",\tActivation Energy="<<activation<<",\tResolution="<<resolution;
filep<<",\t# Char="<<cend<<",\tStart time for char="<<ctstart<<",\tEnd time for char="
    <<ctend<<",\tStart position of char="<<cpstart<<",\tEnd position of char="<<cpend<<
    endl;

filep<<"Time= "<<tstart<<endl; //writing time at which density is taken at

for ( counter=0; counter<Ng; counter++ ) //Writing density ic to file
  filep<<(counter)<<"\t\t\t"<<density[counter] <<"\t\t\t"<<lambdar[counter]<<"\t\t\t"<<
      lambdai[counter]<<endl;
filep<<endl;

filep.close();

//Write amplitude peak heading, and initial values to file

filea<<endl<<"Time\t\tPeaks\t\t";
filea<<"Alpha="<<alpha<<",\tEnd time="<<tend<<",\tNumber of grid points="<<Ng<<",\
    tChannel length="<<xend<<",\tKr="<<Kr<<",\tKi="<<Ki<<",\tCFL#="<<cfl<<",\tNu="<<nu
    <<",\tQ="<<Q<<",\tActivation Energy="<<activation<<",\tResolution="<<resolution;
filea<<",\t# Char="<<cend<<",\tStart time for char="<<ctstart<<",\tEnd time for char="
    <<ctend<<",\tStart position of char="<<cpstart<<",\tEnd position of char="<<cpend<<
    endl;
filea<<endl;

filea<<tstart;        //initial starting time
filea<<"\t\t";
filea<<startpeak(density);  //initial density
filea<<endl;


//Write characteristic headings
filec<<"Characteristic Data"<<endl<<endl;
filec<<"Alpha="<<alpha<<",\tEnd time="<<tend<<",\tNumber of grid points="<<Ng<<",\
```

```
    tChannel length="<<xend<<",\tKr="<<Kr<<",\tKi="<<Ki<<",\tCFL#="<<cfl<<",\tNu="<<nu
    <<",\tQ="<<Q<<",\tActivation Energy="<<activation<<",\tResolution="<<resolution;
filec<<",\t# Char="<<cend<<",\tStart time for char="<<ctstart<<",\tEnd time for char="
    <<ctend<<",\tStart position of char="<<cpstart<<",\tEnd position of char="<<cpend<<
    endl;
filec<<endl;
filec<<"Time\t\tShock Front\tEnd of Induction Zone\t\tEnd of Reaction zone\t\tWave
    Characteristics"<<endl;




//UNSTEADY SOLUTION
deltat=cfl*deltax/( maximum(density) );  //Time steps
numofsteps=int(tend/deltat);

for ( (t=tstart+deltat, countertwo=countertwostart); t<=tend ; (t=t+deltat, countertwo
    ++) ) //cycle through timesteps
{
  //Hydrodynamic step
  for (counter=0; counter<Ng ; counter++) //Go through nodes and update the density
  {
    //Boundary conditions of the channel
    if (counter==0) //at first node
    {
      newdensity[0]=density[0];
      newlambdai[0]=lambdai[0];
      newlambdar[0]=lambdar[0];
    }
    else //evaluate density through channel
    {
      newdensity[counter]=hydrodynamicstep( density[counter], density[counter-1],
          lambdar[counter],lambdar[counter-1]);
      newlambdai[counter]=lambdai[counter];
      newlambdar[counter]=lambdar[counter];
    }
  }

  //Reactive step
  for (counter=0; counter<Ng ; counter++) //Go through nodes and update the reaction
      rates
  {
    //Boundary conditions of the channel
```

```
  if (counter==0) //at first node
  {
    density[0]=newdensity[0];
    lambdai[0]=newlambdai[0];
    lambdar[0]=newlambdar[0];
  }
  else //evaluate density through channel
  {
    density[counter]=newdensity[counter];
    lambdai[counter]=reactivestep( newdensity[counter], newlambdai[counter],
        newlambdar[counter], 1 );
    lambdar[counter]=reactivestep( newdensity[counter], newlambdai[counter],
        newlambdar[counter], 2 );
  }
}


//WRITE NEW DENSITY VALUES TO FILE
//if (  (countertwo==int(numofsteps*2.0/10.0) ) || (countertwo==int(numofsteps
    *(4.0/10.0))) || (countertwo==int(numofsteps*(6.0/10.0)) ) || (countertwo==int(
    numofsteps*(8.0/10.0)) ) || (countertwo==int(numofsteps*9.9/10.0)) ) //only write
     certain timesteps to file
//if (  (countertwo==200 ) || (countertwo==300) || (countertwo==400) || (countertwo
    ==500) || (countertwo==int(numofsteps*9.0/10.0)) ) //only write certain timesteps
     to file
//if ( (div(countertwo,3200).rem==0) ) //only write certain timesteps to file

//{
//  filep<<"Time= "<<t<<"\tCountertwo="<<countertwo<<endl; //writing time at which
    density is taken at
//
//  for ( counter=0; counter<Ng; counter++ ) //Writing densities to file
//    filep<<counter<<"\t\t\t"<<density[counter]<<"\t\t\t"<<lambdar[counter]<<"\t\t\t
    "<<lambdai[counter]<<endl;
//  filep<<endl;
//}

//WRITE NEW AMPLITUDE PEAK VALUES TO FILE
filea<<t;
filea<<"\t\t";
filea<<startpeak(density);
filea<<endl;
```

```
//CALCULATE CHARACTERISTICS

if ( t>ctstart && t<ctend )
{
  //characteristics (density); function

  for (shock=0,check=0,find=(Ng-1); find>=0; find--) //search backwards for first
      point above activation
  {
    if ( density[find]>activation && shock==0) //"shock==0" so this is only activated
        once
    {
      shock=density[find];
      for (search=find; search>=(find-8); search--)
      {
        if (density[search]>shock)
        {
          shock=density[search];
          shockposition=search;
        }
      }
    }

    if (lambdai[find]<=0 && check==0)
    {
      endofind=find;
      check=1;
    }

    if (lambdar[find]>=0.999) //some leeway
    {
      endofreact=find;
      find=-1; //for exiting the search loop
    }
  }

  for (int a=0; a<cend; a++)
  {
    wavec[a]=wavec[a]+deltat*(density[int( (wavec[a]+Dcj*t)/deltax+1.0)]-Dcj); //the
        density has to be evaluated at the x value in the NON-cj frame
  }
```

```
    filec<<t<<"\t\t";
    filec<<( (shockposition-1.0)*deltax-(Dcj*t) )<<"\t\t"; //position and time of shock
         in CJ frame
    filec<<( (endofind-1.0)*deltax-(Dcj*t) )<<"\t\t\t\t"; //position and time of end of
         induction zone in CJ frame
    filec<<( (endofreact-1.0)*deltax-(Dcj*t) )<<"\t\t\t"; //position and time of end of
         reaction zone in CJ frame

    for (int a=0; a<cend; a++)
    {
      filec<<wavec[a]<<"\t\t";
    }

    filec<<endl;

  }


  //Calculate new timestep
  deltat=cfl*deltax/( maximum(density) );  //Time steps


} //end of time loop



//WRITE FINAL POSITION DATA OF DETONATION TO FILE

//this is a backup point so that the simulation can be run again from this point
    onwards.

if (savechoice==1)
{
  fileprofile="profilesave-Kr="; //set the density profile file name
  sprintf(stringholder,"%.2f",Kr);
  fileprofile+=stringholder;  //append Kr to the file name
  fileprofile+="-alpha=";
  fileprofile+=alphastring;  //append the alpha value to the file name
  fileprofile+="-time=(";
  sprintf(stringholder,"%.1f",tstart);
  fileprofile+=stringholder;
  fileprofile+="-";
  sprintf(stringholder,"%.0f",tend);
```

```
  fileprofile+=stringholder;
  fileprofile+=")-char#=";
  sprintf(stringholder,"%d",cend);
  fileprofile+=stringholder;
  fileprofile+=".txt";
  filep.open( fileprofile.c_str() );

  filep<<"Saved Density Profile over x"<<endl<<endl;
  filep<<"At Time:"<<endl<<(t-deltat)<<endl<<"At Countertwo:"<<endl<<(countertwo-1)<<
      endl<<"At Ng:"<<endl<<Ng<<endl<<endl; //the time and countertwo that is output is
       set back by the amount the time loop incremented it by as it exited the loop
  filep<<"Node\t\t\tDensity"<<"\t\t\tLambda r\t\t\tLambda i\t\t\t";
  filep<<"Alpha="<<alpha<<",\tEnd time="<<tend<<",\tNumber of grid points="<<Ng<<",\
      tChannel length="<<xend<<",\tKr="<<Kr<<",\tKi="<<Ki<<",\tCFL#="<<cfl<<",\tNu="<<
      nu<<",\tQ="<<Q<<",\tActivation Energy="<<activation<<",\tResolution="<<resolution
      ;
  filep<<",\t# Char="<<cend<<",\tStart time for char="<<ctstart<<",\tEnd time for char=
      "<<ctend<<",\tStart position of char="<<cpstart<<",\tEnd position of char="<<
      cpend<<endl;


  for ( counter=0; counter<Ng; counter++ ) //Writing densities to file
    filep<<counter<<"\t\t\t"<<density[counter]<<"\t\t\t"<<lambdar[counter]<<"\t\t\t"<<
        lambdai[counter]<<endl;
  filep<<endl;

  filep.close();
}



//FILE CLEANUP
filea.close(); //Close files ...

delete [] density;
delete [] newdensity;
delete [] lambdai;
delete [] newlambdai;
delete [] lambdar;
delete [] newlambdar;

}while (alpha<alphaend || Kr<Krend || Q<Qend); //end of loop to process over alpha
```

```
//END OF PROGRAM


filei.close();

cout<<endl<<"-----Program Ended"<<endl;
system("PAUSE");
return 0;
}



//FUNCTIONS

double hydrodynamicstep (double density, double densityprev, double massfraction,
    double massfractionprev)
{
  double hydrodynamicdensity;

  hydrodynamicdensity=density+deltat/deltax*( pow(densityprev,2)/2-pow(density,2)/2 +Q
      /2.0*(massfractionprev-massfraction) );

  return hydrodynamicdensity;
}


double reactivestep (double density, double massfractioni, double massfractionr, int
    zone)
{
  double massfraction; //the 1st element is the induction m.f., the 2nd element is the
      reactive m.f.

  if (zone==1) //induction zone
    massfraction=massfractioni-H(massfractioni)*H((density-activation))*Ki*exp(alpha*(
        density/Dcj/2.0-1.0))*deltat;
  else if (zone==2) //reaction zone
    massfraction=1-pow( (pow((1-massfractionr),(1-nu))-(1-nu)*Kr*(1-H(massfractioni))*H
        ((1-massfractionr))*deltat), (1.0/(1-nu)) );

  return massfraction;
}
```

```
double H (double valueone) //heavyside func.
{
  double heaviside;

  if (valueone<=0)
    heaviside=0;
  else if (valueone>0)
    heaviside=1;
  else
  {
    heaviside=0;
    cout<<"There was an error with the heaviside func"<<endl<<endl;
    cout<<"The value that the function tried to evaluate was:"<<valueone<<endl;
    system("PAUSE");
    exit(1);
  }

  return heaviside;
}


double maximum (double *arrayonep )
{
  double max;

  //max=arrayone[0];
  max=*arrayonep; //set max a initially the first element in the density array

  for (counterthree=1; counterthree<Ng; counterthree++)
  {
    if (*(arrayonep+counterthree)>max)
      max=*(arrayonep+counterthree);
  }

  return max;
}


double startpeak (double *arraytwop )
{
  double maxpeak=0;
```

```
  int search;


  for (counterthree=(Ng-1); counterthree>=0; counterthree--) //search backwards for
      first point above activation
  {
    if ( *(arraytwop+counterthree)>activation)
    {
      maxpeak=*(arraytwop+counterthree);
      for (search=counterthree; search>=(counterthree-8); search--)
      {
        if (*(arraytwop+search)>maxpeak)
          maxpeak=*(arraytwop+search);
      }
      counterthree=-1;
    }
  }

  return maxpeak;
}
```